EUROPEAN ORGANIZATION FOR NUCLEAR RESEARCH (CERN)

CERN-EP-2025-202
2026/01/06

CMS-HIG-24-018

# Simultaneous probe of the charm and bottom quark Yukawa couplings using $t\bar{t}H$ events

The CMS Collaboration*

arXiv:2509.22535v2 [hep-ex] 5 Jan 2026

## Abstract

A search for the standard model Higgs boson decaying to a charm quark-antiquark pair, $H\to c\bar{c}$, produced in association with a top quark-antiquark pair ($t\bar{t}H$) is presented. The search is performed with data from proton-proton collisions at $\sqrt{s} = 13\,\text{TeV}$, corresponding to an integrated luminosity of $138\,\text{fb}^{-1}$. Advanced machine learning techniques are employed for jet flavor identification and event classification. The Higgs boson decay to a bottom quark-antiquark pair is measured simultaneously and the observed $t\bar{t}H(H\to b\bar{b})$ event rate relative to the standard model expectation is $0.91^{+0.26}_{-0.22}$. The observed (expected) upper limit on the product of production cross section and branching fraction $\sigma(t\bar{t}H)\mathcal{B}(H\to c\bar{c})$ is 0.11 (0.13) pb at 95% confidence level, corresponding to 7.8 (8.7) times the standard model prediction. When combined with the previous search for $H\to c\bar{c}$ via associated production with a W or Z boson, the observed (expected) 95% confidence interval on the Higgs-charm Yukawa coupling modifier, $\kappa_c$, is $|\kappa_c| < 3.5$ (2.7), the most stringent constraint to date.

*Published in Physical Review Letters as* doi:10.1103/9nwb-splk.

© 2026 CERN for the benefit of the CMS Collaboration. CC-BY-4.0 license

*See Appendix C for the list of collaboration members

The discovery of a Higgs boson (H) by the ATLAS [1] and CMS [2, 3] experiments was a landmark achievement in understanding electroweak (EW) symmetry breaking. With a measured mass of $125.38 \pm 0.14$ GeV [4], the Higgs boson's observed interactions with gauge bosons and third-generation fermions [5–15], as well as all its measured properties [16–24], align with the standard model (SM) predictions. Following the first evidence of Higgs boson decays to muons, i.e., second-generation leptons [25], another important milestone is to observe its couplings to second-generation quarks.

The charm quark Yukawa coupling, $y_c$, can be significantly modified in the presence of physics beyond the SM [26–34]. Searches for Higgs boson decays to a charm quark-antiquark pair, $c\bar{c}$, provide direct access to $y_c$. To date, the most sensitive approach at the LHC exploits associated production of a Higgs boson with a V (W or Z) boson. Using proton-proton (pp) collision data at 13 TeV, corresponding to an integrated luminosity of about 140 $fb^{-1}$, the ATLAS [35] and CMS [36] Collaborations reported observed (expected) 95% confidence level (CL) intervals on $\kappa_c = y_c / y_c^{SM}$ of $|\kappa_c| < 4.2$ (4.1) and $1.1 < |\kappa_c| < 5.5$ ($|\kappa_c| < 3.4$), respectively. The search in the dominant gluon fusion production mode yields lower sensitivity because of the overwhelming $c\bar{c}$ background from quantum chromodynamics (QCD) multijet production [37]. Despite these advancements, projections for the High-Luminosity LHC [38] indicate that current approaches may prove insufficient to achieve evidence of $H \to c\bar{c}$ decay within the experiment's lifetime.

In this Letter, we present a new approach: to search for $H \to c\bar{c}$ via associated production of a Higgs boson with a top quark-antiquark pair ($t\bar{t}H$) and to measure simultaneously the $H \to b\bar{b}$ decay. We use pp collision data at $\sqrt{s} = 13$ TeV, collected with the CMS detector in 2016–2018, and corresponding to an integrated luminosity of 138 $fb^{-1}$ [39–41]. The analogous processes $t\bar{t}Z(Z \to c\bar{c})$ and $t\bar{t}Z(Z \to b\bar{b})$ are measured to validate the analysis strategy. For $t\bar{t}H(H \to c\bar{c})$ and $t\bar{t}H(H \to b\bar{b})$, the presence of multiple jets, including several b and c jets, poses significant challenges in identifying the jet origins and in reconstructing the top quark and Higgs boson decays. To address this, we employ advanced machine learning algorithms, PARTICLENET [42] for jet flavor identification and PARTICLE TRANSFORMER (PART) [43] for event classification. The resulting sensitivity is comparable to the best achieved in the VH channel [36].

The CMS apparatus [44, 45] is a multipurpose, nearly hermetic detector, designed to trigger on [46–48] and identify electrons, muons, photons, and hadrons [49–51]. A global "particle-flow" algorithm [52] aims to reconstruct all individual particles in an event, combining information provided by the all-silicon inner tracker and by the crystal electromagnetic and brass-scintillator hadron calorimeters, operating inside a 3.8 T superconducting solenoid, with data from the gas-ionization muon detectors embedded in the flux-return yoke outside the solenoid. The reconstructed particles are used to build jets, employing the anti-$k_T$ algorithm [53, 54] with a distance parameter $R = 0.4$, and to compute missing transverse momentum [55, 56].

Signal and background processes are simulated using various Monte Carlo event generators. The $t\bar{t}H$ signal process is generated at next-to-leading order (NLO) accuracy in QCD using POWHEG v2 [57–59], with the Higgs boson and top quark masses set to 125 and 172.5 GeV, respectively. The main background is $t\bar{t}$ production with additional jets ($t\bar{t}$+jets), particularly when these additional jets originate from the hadronization of b or c quarks, as such events closely resemble the signal topology. This background is categorized based on the flavor of the additional jets, i.e., those that do not originate from top quark decays. Jets containing at least one b hadron (at least one c hadron and no b hadron) are defined as b (c) jets, following the ghost association procedure [60]. The remaining jets are labeled as light jets. Events containing one extra b jet are labeled as $t\bar{t}$+b, while those with two or more are labeled as $t\bar{t}$+$\geq$2b. Similarly, events with no b jets but one (two or more) extra c jet are labeled as $t\bar{t}$+c ($t\bar{t}$+$\geq$2c).

The remaining $t\bar{t}$+jets events, containing no b or c jets other than those from top quark decays, are labeled $t\bar{t}$+light. To achieve the highest available accuracy in modeling the $t\bar{t}$+jets components, a dedicated $t\bar{t}b\bar{b}$ sample is used to predict the $t\bar{t}$+b and $t\bar{t}+\geq$2b backgrounds. This sample is generated at NLO in QCD in the four-flavor scheme using POWHEG-BOX-RES [61, 62] and OPENLOOPS [63], explicitly including additional b quarks in the matrix element calculation. Contributions to $t\bar{t}$+b and $t\bar{t}+\geq$2b from double parton scattering—amounting to ≈15% of the $t\bar{t}b\bar{b}$ production cross section—are not included in the $t\bar{t}b\bar{b}$ sample and are modeled separately. The remaining components, $t\bar{t}$+c, $t\bar{t}+\geq$2c, and $t\bar{t}$+light, are modeled using an inclusive $t\bar{t}$ sample simulated with POWHEG v2 at NLO in QCD in the five-flavor scheme [64]. Measurements of $t\bar{t}+\geq$1b and $t\bar{t}+\geq$1c production [65–68] indicate moderate mismodeling in simulation, necessitating corrections of the background estimates based on control samples in data.

Single top quark production in the $t$ channel ($s$ channel) and in association with a W boson is simulated at NLO accuracy with POWHEG v2 [69–71] (MADGRAPH5_aMC@NLO v2.6.5 [72]). The production cross sections for the $t\bar{t}$ and single top quark samples are computed at next-to-NLO (NNLO) [73, 74]. For $t\bar{t}$, the differential cross section as a function of top quark $p_T$ is corrected to the NNLO QCD + NLO EW prediction [75]. The $t\bar{t}W$ and $t\bar{t}Z$ (tWZ) processes are simulated at NLO (leading order, LO) accuracy in QCD using MADGRAPH5_aMC@NLO. The matching of jets from matrix element calculations and those from parton showers is done with the FxFx [76] (MLM [77]) prescription for NLO (LO) samples. For all samples, the proton structure is described by the NNLO NNPDF3.1 parton distribution function (PDF) set [78]. Parton showering and hadronization are handled by PYTHIA v8.240 [79] with the CP5 underlying event tune [80]. Additional pp interactions within the same or nearby bunch crossings (pileup) are simulated with PYTHIA and added to the hard-scattering process, with events reweighted to match the pileup profile observed in data. The detector response is modeled with GEANT4 [81].

The analysis is carried out in three mutually exclusive channels targeting the fully hadronic (0L), single-lepton (1L), and dilepton (2L) decays of the top quark-antiquark pair. Events are collected using triggers based on high jet and b jet multiplicities, or on the presence of one or two well-identified and isolated leptons (electrons or muons). In the offline selection, only jets with transverse momentum $p_T > 25\,\text{GeV}$ and pseudorapidity $|\eta| < 2.4$ are considered. In the 0L channel, events must contain at least seven jets, of which at least six have $p_T > 40\,\text{GeV}$, and have a jet $p_T$ scalar sum exceeding 500 GeV to satisfy trigger requirements. The 1L channel selects events with one isolated electron or muon with a minimum $p_T$ of 26 to 30 GeV, depending on the lepton flavor and the trigger requirements in each data-taking year, along with at least five jets. The 2L channel selects events with two oppositely charged leptons, at least one with $p_T > 25\,\text{GeV}$, and at least four jets. To suppress the Drell–Yan background, events with a dielectron or dimuon invariant mass below 20 GeV or within the Z boson mass window (76–106 GeV) are excluded. Across all channels, events must contain at least three jets tagged as either b or c jets, with at least one tagged as a b jet, using criteria corresponding to tagging efficiencies of approximately 70% (50%) for b (c) jets. Additional details of the event selection criteria are provided in Supplemental Material (Section B.3).

A key challenge in this analysis is accurately identifying jet flavor—not only efficiently tagging heavy-flavor jets initiated by b or c quarks but also distinguishing between them. To address this, PARTICLENET [42], a dynamic graph convolutional neural network [83], is employed to classify jet flavors by leveraging spatial and kinematic correlations of individual particles and secondary vertices associated with the jets. Two discriminants are constructed from the PARTICLENET outputs: $p_{B+C}$, which differentiates heavy-flavor from light jets, and $p_{BvsC}$, which distinguishes b from c jets. Based on these, 11 mutually exclusive tagging categories are de-

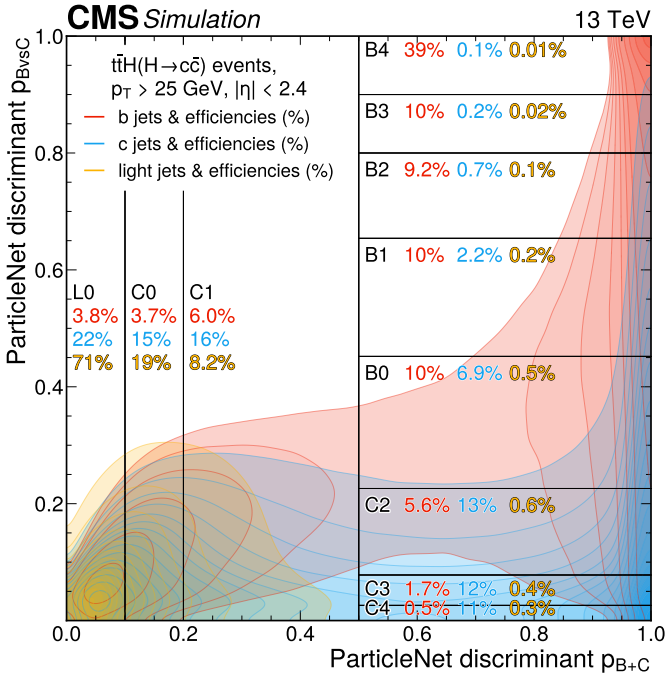


Figure 1: Distribution of b, c, and light jets in the two-dimensional PARTICLENET discriminant plane. The vertical and horizontal lines correspond to the edges of the tagging categories. The numbers in each bin correspond to the tagging efficiencies for b (red), c (blue), and light (yellow) jets, evaluated on a sample of simulated $\mathrm{t\bar{t}H(H{\to}c\bar{c})}$ events. The contour lines represent constant density values for each jet type in steps of 5%.

fined as shown in Fig. 1: five b-tagging categories (B0–B4), five c-tagging categories (C0–C4), and one untagged category (L0) enriched in light jets. Compared to the previously used DEEPJET algorithm [84], PARTICLENET improves background jet rejection by up to a factor of two at the same signal jet efficiency, demonstrating superior performance in distinguishing jet flavors.

To correct for potential mismodeling of tagging efficiencies in simulation, flavor-dependent scale factors are derived using data samples targeting the production of W+jets, dileptonic $\mathrm{t\bar{t}}$, and Z+jets, which are enriched in c, b, and light jets, respectively. These scale factors, defined as data-to-simulation efficiency ratios for each jet type in the 11 tagging categories as functions of jet $p_{\mathrm{T}}$, are extracted via a simultaneous profile likelihood fit to all three data samples. Further details about the tagger performance and calibration are provided in Supplemental Material (Section B.2). The scale factors typically range from 0.75 to 1.5, with uncertainties of up to ≈15% for b jets and up to ≈50% for c and light jets.

A further challenge involves distinguishing the $\mathrm{t\bar{t}H}$ signal from the $\mathrm{t\bar{t}}$+jets background. Both processes produce numerous jets, including multiple b and c jets, which may originate from top quark or Higgs boson decays, or from additional quark or gluon radiation. This complexity hinders precise jet origin identification and full decay chain reconstruction. To overcome this, a multiclass event classifier based on PART [43] is developed to classify events directly from final-state objects—jets, leptons, and missing transverse momentum—without requiring explicit reconstruction of the top quarks or the Higgs boson. For every object, the classifier receives kinematic inputs in terms of $\ln(p_{\mathrm{T}}/\mathrm{GeV})$, $\ln(E/\mathrm{GeV})$, and $\eta$. Jet flavor is encoded via 10 boolean values corresponding to the tagging categories B0–B4 and C0–C4. For each lepton, a flag is included to distinguish between electrons and muons. To better capture event kinematic

values and object correlations, PARTICLE TRANSFORMER constructs pairwise features (e.g., angular separation and invariant mass) for all object pairs using their four-momenta. The classifier is trained to assign likelihood scores across 10 (9) classes in the 0L (1L, 2L) channel:

- Two $t\bar{t}H$ classes: $t\bar{t}H(H\to c\bar{c})$, $t\bar{t}H(H\to b\bar{b})$.
- Two $t\bar{t}Z$ classes: $t\bar{t}Z(Z\to c\bar{c})$, $t\bar{t}Z(Z\to b\bar{b})$.
- Five $t\bar{t}$+jets classes: $t\bar{t}$+b, $t\bar{t}+\geq$2b, $t\bar{t}$+c, $t\bar{t}+\geq$2c, $t\bar{t}$+light.
- (Only in the 0L channel) one class for QCD multijet.

The PARTICLE TRANSFORMER classifier is used to refine event selection and categorization. In the 0L channel, a stringent requirement on the QCD multijet discriminant suppresses this background by nearly four orders of magnitude, allowing it to be neglected relative to $t\bar{t}$+jets and enabling a uniform event categorization strategy across all three channels, as depicted in Fig. 5 in the End Matter. Only events with a high $t\bar{t}H$ or $t\bar{t}Z$ likelihood—defined as $\mathcal{D}_{t\bar{t}X} > 0.6$, where $\mathcal{D}_{t\bar{t}X}$ is the sum of all four $t\bar{t}H$ and $t\bar{t}Z$ discriminants—are retained for signal extraction and background estimation. A requirement on the $t\bar{t}$+light discriminant, $\mathcal{D}_{t\bar{t}+\text{light}} < 0.05$ (0.02) in the 0L and 2L (1L) channels, further reduces $t\bar{t}$+light contamination. Events passing these criteria are categorized into four signal regions (SRs) with $\mathcal{D}_{t\bar{t}X} > 0.85$, each enriched in $t\bar{t}H(H\to c\bar{c})$, $t\bar{t}H(H\to b\bar{b})$, $t\bar{t}Z(Z\to c\bar{c})$, and $t\bar{t}Z(Z\to b\bar{b})$, along with five control regions (CRs) with $0.6 < \mathcal{D}_{t\bar{t}X} < 0.85$, which are used to estimate the normalizations of various $t\bar{t}$+jets background components in a phase space similar to that of the SRs. Additional requirements on heavy-flavor jet multiplicity enhance purity: at least three b jets are required in the b-enriched regions ($t\bar{t}H(H\to b\bar{b})$, $t\bar{t}Z(Z\to b\bar{b})$, $t\bar{t}+\geq$2b, and $t\bar{t}$+b), at least two c jets in the c-enriched $t\bar{t}H(H\to c\bar{c})$, $t\bar{t}Z(Z\to c\bar{c})$, and $t\bar{t}+\geq$2c regions, and at least one c jet in the $t\bar{t}$+c region. A signal-depleted sideband region, defined by $0.4 < \mathcal{D}_{t\bar{t}X} < 0.6$ with an analogous SR and CR structure, is used to validate the background estimation strategy.

Production rates of the signal processes are determined via a binned profile likelihood fit to data. The fitted variable is the PARTICLE TRANSFORMER classifier discriminant for each category. For each of the $t\bar{t}H(H\to c\bar{c})$, $t\bar{t}H(H\to b\bar{b})$, $t\bar{t}Z(Z\to c\bar{c})$, and $t\bar{t}Z(Z\to b\bar{b})$ processes, the expected yield is scaled by an independent signal strength modifier $\mu$, defined as $(\sigma\mathcal{B})_{\text{obs}}/(\sigma\mathcal{B})_{\text{SM}}$. Here $\sigma$ is the production cross section and $\mathcal{B}$ is the branching fraction, which is allowed to freely float in the fit, following the procedure in Ref. [17]. The dominant background, $t\bar{t}$+jets, is estimated by including CRs in the fit, with the normalizations of the $t\bar{t}$+c, $t\bar{t}+\geq$2c, $t\bar{t}$+b, $t\bar{t}+\geq$2b, and $t\bar{t}$+light components allowed to float independently. The normalization factors for each $t\bar{t}$+jets component are shared between the 1L and 2L channels but not with the 0L channel, to account for potential phase space differences due to the requirement of more energetic jets in the 0L case. Minor backgrounds, such as single top quark production, $t\bar{t}W$, and tWZ, are estimated directly from simulations assuming SM production rates. Results are obtained using COMBINE [85], the CMS statistical analysis tool based on the ROOFIT [86] and ROOSTATS [87] frameworks.

Systematic uncertainties affecting normalizations and shapes of fitted variables are incorporated via nuisance parameters that encode the appropriate correlations across channels. The contributions of each uncertainty source to the total uncertainty in the fitted $\mu_{t\bar{t}H(H\to c\bar{c})}$ and $\mu_{t\bar{t}H(H\to b\bar{b})}$ are summarized in Table 2 in the End Matter. For $\mu_{t\bar{t}H(H\to c\bar{c})}$, the leading uncertainty is statistical because of the limited number of events in the SRs as well as in the CRs used to extract background normalizations. The main systematic uncertainty arises from the theoretical modeling of the $t\bar{t}$+c and $t\bar{t}$+light processes, contributing ≈32% and ≈29% of the total uncertainty, respectively. For $\mu_{t\bar{t}H(H\to b\bar{b})}$, the largest uncertainties are theoretical, in-

cluding those associated with the renormalization and factorization scales, flavor scheme, and parton shower modeling in the $t\bar{t}b\bar{b}$ simulation, representing ≈60% of the total uncertainty. Theoretical uncertainties in the $t\bar{t}H$ signal simulation contribute an additional ≈47%. For both measurements, the primary experimental uncertainty is associated with jet flavor identification efficiencies, representing ≈39% (≈28%) of the total uncertainty in $\mu_{t\bar{t}H(H\to c\bar{c})}$ ($\mu_{t\bar{t}H(H\to b\bar{b})}$).

The analysis is validated by measuring the $t\bar{t}Z$ signal strengths:

$$\begin{aligned} \mu_{t\bar{t}Z(Z\to c\bar{c})} &= 1.02^{+0.79}_{-0.84}, \\ \mu_{t\bar{t}Z(Z\to b\bar{b})} &= 1.47^{+0.45}_{-0.41}, \end{aligned} \tag{1}$$

which are consistent with the SM prediction within uncertainties and with measurements in the leptonic decay channel [88–90]. The significance of the excess over the background-only hypothesis is computed using the asymptotic distribution of a test statistic based on the profile likelihood ratio [91, 92]. The observed (expected) significance is 1.2 (1.3) standard deviations for $t\bar{t}Z(Z\to c\bar{c})$ and 3.5 (2.4) standard deviations for $t\bar{t}Z(Z\to b\bar{b})$.

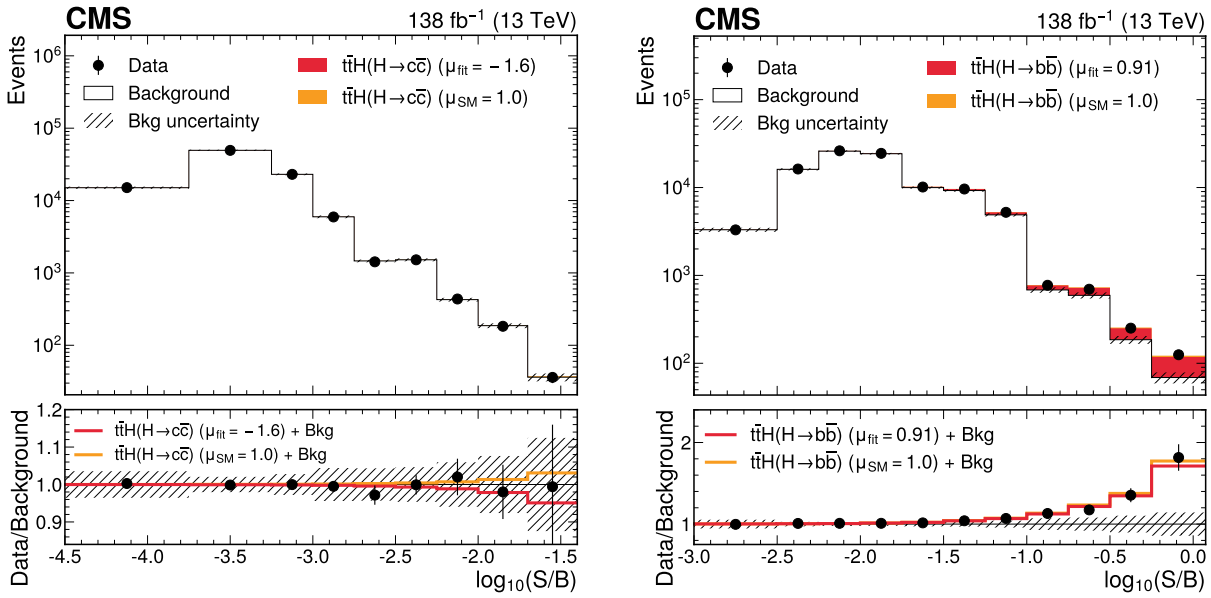


Figure 2: Observed and expected event yields from all SRs and CRs as a function of $\log_{10}(S/B)$, where $S$ are the expected $t\bar{t}H(H\to c\bar{c})$ (left) and $t\bar{t}H(H\to b\bar{b})$ (right) yields, and $B$ are the post-fit total background yields. Signal contributions are shown for the best fit signal strength (red) and for the SM prediction, $\mu = 1$ (orange). The lower panel shows the ratio of the data to the post-fit background predictions, compared to the signal-plus-background predictions.

Figure 2 shows the observed and expected event yields from all CRs and SRs as a function of $\log_{10}(S/B)$, the logarithm of the ratio of $t\bar{t}H(H\to c\bar{c})$ (or $t\bar{t}H(H\to b\bar{b})$) and background yields. The best fit signal strengths for $t\bar{t}H$ production are

$$\begin{aligned} \mu_{t\bar{t}H(H\to c\bar{c})} &= -1.6 \pm 4.5, \\ \mu_{t\bar{t}H(H\to b\bar{b})} &= 0.91^{+0.26}_{-0.22}, \end{aligned} \tag{2}$$

with an observed (expected) significance of 4.4 (4.5) standard deviations for the $t\bar{t}H(H\to b\bar{b})$ process. The best fit $\mu_{t\bar{t}H(H\to b\bar{b})}$ value is closer to the SM prediction than was the previous measurement [93], with a compatibility $p$-value of 10% (3%) between the two measurements,

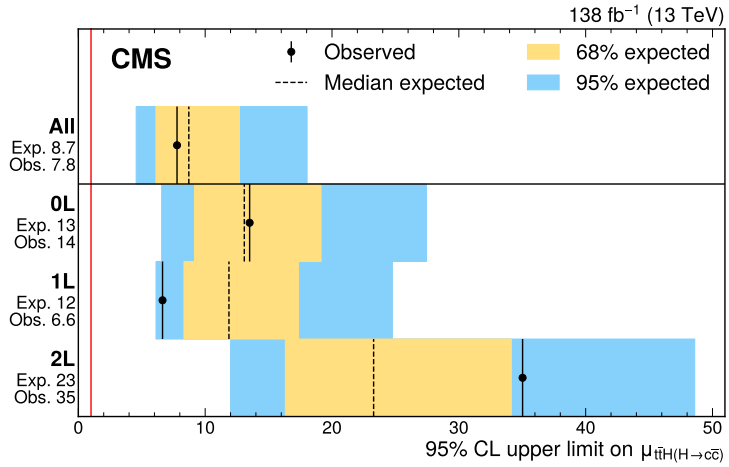


Figure 3: The 95% CL upper limits on $\mu_{t\bar{t}H(H\to c\bar{c})}$. The yellow and blue bands indicate the expected 68% and 95% CL regions, respectively, under the background-only hypothesis. The vertical red line indicates the SM value $\mu_{t\bar{t}H(H\to c\bar{c})} = 1$.

assuming uncorrelated (50% correlated) systematic uncertainties. Because of a very different background model, a more inclusive event selection, and a low correlation of the neural network scores, the total systematic uncertainty can be considered mostly uncorrelated. No excess over the background-only hypothesis is observed in the search for $t\bar{t}H(H\to c\bar{c})$. An upper limit on $\mu_{t\bar{t}H(H\to c\bar{c})}$ is extracted using the $CL_s$ criterion [94, 95]. The test statistic is the profile likelihood ratio modified for upper limits [91], with the asymptotic approximation [92] used in the limit setting procedure. The observed (expected) 95% CL upper limit on $\mu_{t\bar{t}H(H\to c\bar{c})}$ is 7.8 (8.7), corresponding to an observed (expected) upper limit on $\sigma(t\bar{t}H)\mathcal{B}(H\to c\bar{c})$ of 0.11 (0.13) pb. The contributions from the individual channels are summarized in Fig. 3. Tabulated results are provided in the HEPData record for this analysis [96].

The result is interpreted in the $\kappa$-framework [97, 98] by reparameterizing $\mathcal{B}(H\to c\bar{c})$ and $\mathcal{B}(H\to b\bar{b})$ in terms of the charm and bottom quark Yukawa coupling modifiers $\kappa_c$ and $\kappa_b$, assuming that only the Higgs boson decay widths are altered:

$$\begin{aligned}\mathcal{B}(H\to c\bar{c}) &= \frac{\kappa_c^2\,\mathcal{B}_{SM}^{H\to c\bar{c}}}{1+(\kappa_c^2-1)\,\mathcal{B}_{SM}^{H\to c\bar{c}}+(\kappa_b^2-1)\,\mathcal{B}_{SM}^{H\to b\bar{b}}},\\ \mathcal{B}(H\to b\bar{b}) &= \frac{\kappa_b^2\,\mathcal{B}_{SM}^{H\to b\bar{b}}}{1+(\kappa_c^2-1)\,\mathcal{B}_{SM}^{H\to c\bar{c}}+(\kappa_b^2-1)\,\mathcal{B}_{SM}^{H\to b\bar{b}}}.\end{aligned} \tag{3}$$

Figure 4 shows the two-dimensional profile likelihood scan of $\kappa_c$ and $\kappa_b$. When fixing $\kappa_b$ to the SM expectation, the observed (expected) 95% CL interval is $|\kappa_c| < 3.0$ (3.3).

A combined analysis with the previous search in the VH channel [36] is performed. Common experimental uncertainties are correlated, except for jet flavor tagging, which differs in algorithms and calibration methods. Background modeling uncertainties are uncorrelated because of differing dominant backgrounds, while theoretical uncertainties in Higgs boson production and decay for the same processes are correlated. The expected 95% CL upper limit on $\mu_{H\to c\bar{c}}$, assuming SM production rates for $t\bar{t}H$ and VH, is 5.6, representing a 36% (26%) improvement over the $t\bar{t}H$ (VH) channel alone. The observed limit is 9.3, driven by a small upward statistical fluctuation in the VH channel. For $\kappa_c$, the combination improves the expected 95% CL interval to $|\kappa_c| < 2.7$, while the observed is $|\kappa_c| < 3.5$.

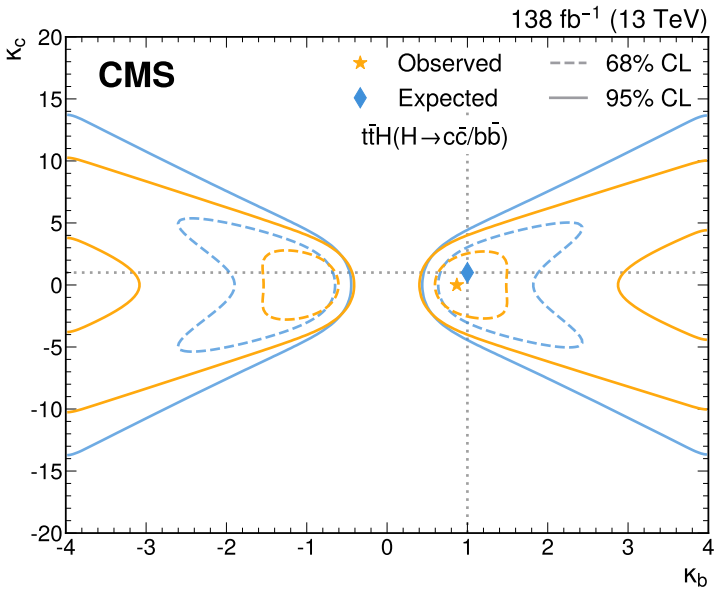


Figure 4: Constraints on the Higgs boson coupling modifiers $\kappa_c$ and $\kappa_b$. The 68% (95%) CL intervals are indicated by the dashed (solid) lines. The observed (expected) best fit values are shown by the orange (blue) markers.

In summary, a search for the SM Higgs boson decaying to a charm quark-antiquark pair via $t\bar{t}H$ production is presented, alongside a simultaneous measurement of the Higgs boson decay to a bottom quark-antiquark pair. Novel jet flavor identification tools and event classification techniques using advanced machine learning algorithms are developed for this analysis. The observed $t\bar{t}H$ signals relative to the SM predictions are $\mu_{t\bar{t}H(H\to c\bar{c})} = -1.6 \pm 4.5$ and $\mu_{t\bar{t}H(H\to b\bar{b})} = 0.91^{+0.26}_{-0.22}$, with an observed (expected) significance of 4.4 (4.5) standard deviations for the $t\bar{t}H(H\to b\bar{b})$ process. The observed (expected) upper limit on $\sigma(t\bar{t}H)\mathcal{B}(H\to c\bar{c})$ is 0.11 (0.13) pb, corresponding to 7.8 (8.7) times the theoretical prediction for an SM Higgs boson mass of 125.38 GeV. When combined with the previous search for $H\to c\bar{c}$ via associated production with a W or Z boson, the observed (expected) 95% CL interval on the charm quark Yukawa coupling modifier, $\kappa_c$, is $|\kappa_c| < 3.5$ (2.7). This represents the most stringent constraint on $\kappa_c$ to date.

## Acknowledgments

We congratulate our colleagues in the CERN accelerator departments for the excellent performance of the LHC and thank the technical and administrative staffs at CERN and at other CMS institutes for their contributions to the success of the CMS effort. In addition, we gratefully acknowledge the computing centers and personnel of the Worldwide LHC Computing Grid and other centers for delivering so effectively the computing infrastructure essential to our analyses. Finally, we acknowledge the enduring support for the construction and operation of the LHC, the CMS detector, and the supporting computing infrastructure provided by the following funding agencies: SC (Armenia), BMBWF and FWF (Austria); FNRS and FWO (Belgium); CNPq, CAPES, FAPERJ, FAPERGS, and FAPESP (Brazil); MES and BNSF (Bulgaria); CERN; CAS, MoST, and NSFC (China); MINCIENCIAS (Colombia); MSES and CSF (Croatia); RIF (Cyprus); SENESCYT (Ecuador); ERC PRG, TARISTU24-TK10 and MoER TK202 (Estonia); Academy of Finland, MEC, and HIP (Finland); CEA and CNRS/IN2P3 (France); SRNSF (Georgia); BMFTR, DFG, and HGF (Germany); GSRI (Greece); NKFIH (Hungary); DAE and

DST (India); IPM (Iran); SFI (Ireland); INFN (Italy); MSIT and NRF (Republic of Korea); MES (Latvia); LMTLT (Lithuania); MOE and UM (Malaysia); BUAP, CINVESTAV, CONACYT, LNS, SEP, and UASLP-FAI (Mexico); MOS (Montenegro); MBIE (New Zealand); PAEC (Pakistan); MES, NSC, and NAWA (Poland); FCT (Portugal); MESTD (Serbia); MICIU/AEI and PCTI (Spain); MOSTR (Sri Lanka); Swiss Funding Agencies (Switzerland); MST (Taipei); MHESI (Thailand); TUBITAK and TENMAK (Türkiye); NASU (Ukraine); STFC (United Kingdom); DOE and NSF (USA).

## References

[1] ATLAS Collaboration, "Observation of a new particle in the search for the standard model Higgs boson with the ATLAS detector at the LHC", *Phys. Lett. B* **716** (2012) 1, doi:10.1016/j.physletb.2012.08.020.

[2] CMS Collaboration, "Observation of a new boson at a mass of 125 GeV with the CMS experiment at the LHC", *Phys. Lett. B* **716** (2012) 30, doi:10.1016/j.physletb.2012.08.021.

[3] CMS Collaboration, "Observation of a new boson with mass near 125 GeV in pp collisions at $\sqrt{s} = 7$ and 8 TeV", *J. High Energy Phys.* **2013** (2013), no. 06, 081, doi:10.1007/JHEP06(2013)081.

[4] CMS Collaboration, "A measurement of the Higgs boson mass in the diphoton decay channel", *Phys. Lett. B* **805** (2020) 135425, doi:10.1016/j.physletb.2020.135425.

[5] ATLAS Collaboration, "Measurement of Higgs boson production in the diphoton decay channel in pp collisions at center-of-mass energies of 7 and 8 TeV with the ATLAS detector", *Phys. Rev. D* **90** (2014) 112015, doi:10.1103/PhysRevD.90.112015.

[6] CMS Collaboration, "Observation of the diphoton decay of the Higgs boson and measurement of its properties", *Eur. Phys. J. C* **74** (2014) 3076, doi:10.1140/epjc/s10052-014-3076-z.

[7] ATLAS Collaboration, "Measurements of Higgs boson production and couplings in the four-lepton channel in pp collisions at center-of-mass energies of 7 and 8 TeV with the ATLAS detector", *Phys. Rev. D* **91** (2015) 012006, doi:10.1103/PhysRevD.91.012006.

[8] CMS Collaboration, "Measurement of the properties of a Higgs boson in the four-lepton final state", *Phys. Rev. D* **89** (2014) 092007, doi:10.1103/PhysRevD.89.092007.

[9] ATLAS Collaboration, "Observation and measurement of Higgs boson decays to $WW^*$ with the ATLAS detector", *Phys. Rev. D* **92** (2015) 012006, doi:10.1103/PhysRevD.92.012006.

[10] ATLAS Collaboration, "Study of (W/Z)H production and Higgs boson couplings using $H \to WW^*$ decays with the ATLAS detector", *J. High Energy Phys.* **2015** (2015), no. 08, 137, doi:10.1007/JHEP08(2015)137.

[11] CMS Collaboration, "Measurement of Higgs boson production and properties in the WW decay channel with leptonic final states", *J. High Energy Phys.* **2014** (2014), no. 01, 096, doi:10.1007/JHEP01(2014)096.

[12] ATLAS Collaboration, "Evidence for the Higgs-boson Yukawa coupling to tau leptons with the ATLAS detector", *J. High Energy Phys.* **2015** (2015), no. 04, 117, doi:10.1007/JHEP04(2015)117.

[13] CMS Collaboration, "Evidence for the 125 GeV Higgs boson decaying to a pair of $\tau$ leptons", *J. High Energy Phys.* **2014** (2014), no. 05, 104, doi:10.1007/JHEP05(2014)104.

[14] CMS Collaboration, "Observation of the Higgs boson decay to a pair of $\tau$ leptons", *Phys. Lett. B* **779** (2018) 283, doi:10.1016/j.physletb.2018.02.004.

[15] CMS Collaboration, "Measurements of properties of the Higgs boson decaying to a W boson pair in pp collisions at $\sqrt{s} = 13$ TeV", *Phys. Lett. B* **791** (2019) 96, doi:10.1016/j.physletb.2018.12.073.

[16] ATLAS Collaboration, "Measurements of the Higgs boson production and decay rates and coupling strengths using pp collision data at $\sqrt{s} = 7$ and 8 TeV in the ATLAS experiment", *Eur. Phys. J. C* **76** (2016) 6, doi:10.1140/epjc/s10052-015-3769-y.

[17] CMS Collaboration, "Precise determination of the mass of the Higgs boson and tests of compatibility of its couplings with the standard model predictions using proton collisions at 7 and 8 TeV", *Eur. Phys. J. C* **75** (2015) 212, doi:10.1140/epjc/s10052-015-3351-7.

[18] CMS Collaboration, "Study of the mass and spin-parity of the Higgs boson candidate via its decays to Z boson pairs", *Phys. Rev. Lett.* **110** (2013) 081803, doi:10.1103/PhysRevLett.110.081803.

[19] ATLAS Collaboration, "Evidence for the spin-0 nature of the Higgs boson using ATLAS data", *Phys. Lett. B* **726** (2013) 120, doi:10.1016/j.physletb.2013.08.026.

[20] ATLAS and CMS Collaborations, "Measurements of the Higgs boson production and decay rates and constraints on its couplings from a combined ATLAS and CMS analysis of the LHC pp collision data at $\sqrt{s} = 7$ and 8 TeV", *J. High Energy Phys.* **2016** (2016), no. 08, 045, doi:10.1007/JHEP08(2016)045.

[21] ATLAS and CMS Collaborations, "Combined measurement of the Higgs boson mass in pp collisions at $\sqrt{s} = 7$ and 8 TeV with the ATLAS and CMS experiments", *Phys. Rev. Lett.* **114** (2015) 191803, doi:10.1103/PhysRevLett.114.191803.

[22] CMS Collaboration, "Measurements of properties of the Higgs boson decaying into the four-lepton final state in pp collisions at $\sqrt{s} = 13$ TeV", *J. High Energy Phys.* **2017** (2017), no. 11, 047, doi:10.1007/JHEP11(2017)047.

[23] ATLAS Collaboration, "Combined measurement of differential and total cross sections in the $H \to \gamma\gamma$ and the $H \to ZZ^* \to 4\ell$ decay channels at $\sqrt{s} = 13$ TeV with the ATLAS detector", *Phys. Lett. B* **786** (2018) 114, doi:10.1016/j.physletb.2018.09.019.

[24] ATLAS Collaboration, "Measurement of the Higgs boson mass in the $H \to ZZ^* \to 4\ell$ and $H \to \gamma\gamma$ channels with $\sqrt{s} = 13$ TeV pp collisions using the ATLAS detector", *Phys. Lett. B* **784** (2018) 345, doi:10.1016/j.physletb.2018.07.050.

[25] CMS Collaboration, "Search for the Higgs boson decaying to two muons in proton-proton collisions at $\sqrt{s} = 13$ TeV", *Phys. Rev. Lett.* **122** (2019) 021801, doi:10.1103/PhysRevLett.122.021801.

[26] C. Delaunay, T. Golling, G. Perez, and Y. Soreq, "Enhanced Higgs boson coupling to charm pairs", *Phys. Rev. D* **89** (2014) 033014, doi:10.1103/PhysRevD.89.033014.

[27] G. Perez, Y. Soreq, E. Stamou, and K. Tobioka, "Constraining the charm Yukawa and Higgs-quark coupling universality", *Phys. Rev. D* **92** (2015) 033016, doi:10.1103/PhysRevD.92.033016.

[28] G. Perez, Y. Soreq, E. Stamou, and K. Tobioka, "Prospects for measuring the Higgs boson coupling to light quarks", *Phys. Rev. D* **93** (2016) 013001, doi:10.1103/PhysRevD.93.013001.

[29] D. Ghosh, R. S. Gupta, and G. Perez, "Is the Higgs mechanism of fermion mass generation a fact? A Yukawa-less first-two-generation model", *Phys. Lett. B* **755** (2016) 504, doi:10.1016/j.physletb.2016.02.059.

[30] F. J. Botella, G. C. Branco, M. N. Rebelo, and J. I. Silva-Marcos, "What if the masses of the first two quark families are not generated by the standard model Higgs boson?", *Phys. Rev. D* **94** (2016) 115031, doi:10.1103/PhysRevD.94.115031.

[31] R. Harnik, J. Kopp, and J. Zupan, "Flavor violating Higgs decays", *J. High Energy Phys.* **2013** (2013), no. 03, 026, doi:10.1007/JHEP03(2013)026.

[32] W. Altmannshofer et al., "Collider signatures of flavorful Higgs bosons", *Phys. Rev. D* **94** (2016) 115032, doi:10.1103/PhysRevD.94.115032.

[33] B. A. Erdelyi, R. Gröber, and N. Selimovic, "How large can the light quark Yukawa couplings be?", *J. High Energy Phys.* **2025** (2025), no. 05, 189, doi:10.1007/JHEP05(2025)189.

[34] A. S. Giannakopoulou, P. Meade, and M. Valli, "How charming can the Higgs be?", *J. High Energy Phys.* **2025** (2025), no. 02, 067, doi:10.1007/JHEP02(2025)067.

[35] ATLAS Collaboration, "Measurements of WH and ZH production with Higgs boson decays into bottom quarks and direct constraints on the charm Yukawa coupling in 13 TeV pp collisions with the ATLAS detector", *J. High Energy Phys.* **2025** (2025), no. 04, 075, doi:10.1007/JHEP04(2025)075.

[36] CMS Collaboration, "Search for Higgs boson decay to a charm quark-antiquark pair in proton-proton collisions at $\sqrt{s} = 13\,\text{TeV}$", *Phys. Rev. Lett.* **131** (2023) 061801, doi:10.1103/PhysRevLett.131.061801.

[37] CMS Collaboration, "Search for boosted Higgs boson decay to a charm quark-antiquark pair in proton-proton collisions at $\sqrt{s} = 13\,\text{TeV}$", *Phys. Rev. Lett.* **131** (2023) 041801, doi:10.1103/PhysRevLett.131.041801.

[38] ATLAS and CMS Collaborations, "Snowmass white paper contribution: Physics with the Phase-2 ATLAS and CMS detectors", CMS Physics Analysis Summary CMS-PAS-FTR-22-001, ATL-PHYS-PUB-2022-018, 2022.

[39] CMS Collaboration, "Precision luminosity measurement in proton-proton collisions at $\sqrt{s} = 13\,\text{TeV}$ in 2015 and 2016 at CMS", *Eur. Phys. J. C* **81** (2021) 800, doi:10.1140/epjc/s10052-021-09538-2.

[40] CMS Collaboration, "CMS luminosity measurement for the 2017 data-taking period at $\sqrt{s} = 13\,\text{TeV}$", CMS Physics Analysis Summary CMS-PAS-LUM-17-004, 2018.

[41] CMS Collaboration, "CMS luminosity measurement for the 2018 data-taking period at $\sqrt{s} = 13\,\text{TeV}$", CMS Physics Analysis Summary CMS-PAS-LUM-18-002, 2019.

[42] H. Qu and L. Gouskos, "Jet tagging via particle clouds", *Phys. Rev. D* **101** (2020) 056019, doi:10.1103/PhysRevD.101.056019.

[43] H. Qu, C. Li, and S. Qian, "Particle transformer for jet tagging", in *Proc. 39th International Conference on Machine Learning (ICML 2022): Baltimore MD, USA, July 17–23, 2022*. 2022. arXiv:2202.03772. [PMLR 162 (2022) 18281].

[44] CMS Collaboration, "The CMS experiment at the CERN LHC", *J. Instrum.* **3** (2008) S08004, doi:10.1088/1748-0221/3/08/S08004.

[45] CMS Collaboration, "Development of the CMS detector for the CERN LHC Run 3", *J. Instrum.* **19** (2024) P05064, doi:10.1088/1748-0221/19/05/P05064.

[46] CMS Collaboration, "Performance of the CMS Level-1 trigger in proton-proton collisions at $\sqrt{s} = 13\,\text{TeV}$", *J. Instrum.* **15** (2020) P10017, doi:10.1088/1748-0221/15/10/P10017.

[47] CMS Collaboration, "The CMS trigger system", *J. Instrum.* **12** (2017) P01020, doi:10.1088/1748-0221/12/01/P01020.

[48] CMS Collaboration, "Performance of the CMS high-level trigger during LHC Run 2", *J. Instrum.* **19** (2024) P11021, doi:10.1088/1748-0221/19/11/P11021.

[49] CMS Collaboration, "Electron and photon reconstruction and identification with the CMS experiment at the CERN LHC", *J. Instrum.* **16** (2021) P05014, doi:10.1088/1748-0221/16/05/P05014.

[50] CMS Collaboration, "Performance of the CMS muon detector and muon reconstruction with proton-proton collisions at $\sqrt{s} = 13\,\text{TeV}$", *J. Instrum.* **13** (2018) P06015, doi:10.1088/1748-0221/13/06/P06015.

[51] CMS Collaboration, "Description and performance of track and primary-vertex reconstruction with the CMS tracker", *J. Instrum.* **9** (2014) P10009, doi:10.1088/1748-0221/9/10/P10009.

[52] CMS Collaboration, "Particle-flow reconstruction and global event description with the CMS detector", *J. Instrum.* **12** (2017) P10003, doi:10.1088/1748-0221/12/10/P10003.

[53] M. Cacciari, G. P. Salam, and G. Soyez, "The anti-$k_\text{T}$ jet clustering algorithm", *J. High Energy Phys.* **2008** (2008), no. 04, 063, doi:10.1088/1126-6708/2008/04/063.

[54] M. Cacciari, G. P. Salam, and G. Soyez, "FastJet user manual", *Eur. Phys. J. C* **72** (2012) 1896, doi:10.1140/epjc/s10052-012-1896-2.

[55] CMS Collaboration, "Jet energy scale and resolution in the CMS experiment in pp collisions at 8 TeV", *J. Instrum.* **12** (2017) P02014, doi:10.1088/1748-0221/12/02/P02014.

[56] CMS Collaboration, "Performance of missing transverse momentum reconstruction in proton-proton collisions at $\sqrt{s} = 13\,\text{TeV}$ using the CMS detector", *J. Instrum.* **14** (2019) P07004, doi:10.1088/1748-0221/14/07/P07004.

[57] P. Nason, "A new method for combining NLO QCD with shower Monte Carlo algorithms", *J. High Energy Phys.* **2004** (2004), no. 11, 040, doi:10.1088/1126-6708/2004/11/040.

[58] S. Frixione, P. Nason, and C. Oleari, "Matching NLO QCD computations with parton shower simulations: the POWHEG method", *J. High Energy Phys.* **2007** (2007), no. 11, 070, doi:10.1088/1126-6708/2007/11/070.

[59] S. Alioli, P. Nason, C. Oleari, and E. Re, "A general framework for implementing NLO calculations in shower Monte Carlo programs: the POWHEG BOX", *J. High Energy Phys.* **2010** (2010), no. 06, 043, doi:10.1007/JHEP06(2010)043.

[60] CMS Collaboration, "Identification of heavy-flavour jets with the CMS detector in pp collisions at 13 TeV", *J. Instrum.* **13** (2018) P05011, doi:10.1088/1748-0221/13/05/P05011.

[61] T. Ježo and P. Nason, "On the treatment of resonances in next-to-leading order calculations matched to a parton shower", *J. High Energy Phys.* **2015** (2015), no. 12, 065, doi:10.1007/JHEP12(2015)065.

[62] T. Ježo, J. M. Lindert, N. Moretti, and S. Pozzorini, "New NLOPS predictions for $t\bar{t}$+b-jet production at the LHC", *Eur. Phys. J. C* **78** (2018) 502, doi:10.1140/epjc/s10052-018-5956-0.

[63] F. Buccioni et al., "OPENLOOPS 2", *Eur. Phys. J. C* **79** (2019) 866, doi:10.1140/epjc/s10052-019-7306-2.

[64] S. Frixione, G. Ridolfi, and P. Nason, "A positive-weight next-to-leading-order Monte Carlo for heavy flavour hadroproduction", *J. High Energy Phys.* **2007** (2007), no. 09, 126, doi:10.1088/1126-6708/2007/09/126.

[65] CMS Collaboration, "Inclusive and differential cross section measurements of $t\bar{t}b\bar{b}$ production in the lepton+jets channel at $\sqrt{s} = 13$ TeV", *J. High Energy Phys.* **2024** (2024), no. 05, 042, doi:10.1007/JHEP05(2024)042.

[66] ATLAS Collaboration, "Measurement of $t\bar{t}$ production in association with additional b-jets in the e$\mu$ final state in proton-proton collisions at $\sqrt{s} = 13$ TeV with the ATLAS detector", *J. High Energy Phys.* **2025** (2025), no. 01, 068, doi:10.1007/JHEP01(2025)068.

[67] CMS Collaboration, "First measurement of the cross section for top quark pair production with additional charm jets using dileptonic final states in pp collisions at $\sqrt{s} = 13$ TeV", *Phys. Lett. B* **820** (2021) 136565, doi:10.1016/j.physletb.2021.136565.

[68] ATLAS Collaboration, "Measurement of top-quark pair production in association with charm quarks in proton-proton collisions at $\sqrt{s} = 13$ TeV with the ATLAS detector", *Phys. Lett. B* **860** (2024) 139177, doi:10.1016/j.physletb.2024.139177.

[69] E. Re, "Single-top Wt-channel production matched with parton showers using the POWHEG method", *Eur. Phys. J. C* **71** (2011) 1547, doi:10.1140/epjc/s10052-011-1547-z.

[70] R. Frederix, E. Re, and P. Torrielli, "Single-top $t$-channel hadroproduction in the four-flavors scheme with POWHEG and aMC@NLO", *J. High Energy Phys.* **2012** (2012), no. 09, 130, doi:10.1007/JHEP09(2012)130.

[71] S. Alioli, P. Nason, C. Oleari, and E. Re, "NLO single-top production matched with shower in POWHEG: $s$- and $t$-channel contributions", *J. High Energy Phys.* **2009** (2009), no. 09, 111, doi:10.1088/1126-6708/2009/09/111. [Erratum: doi:10.1007/JHEP02(2010)011].

[72] J. Alwall et al., "The automated computation of tree-level and next-to-leading order differential cross sections, and their matching to parton shower simulations", *J. High Energy Phys.* **2014** (2014), no. 07, 079, doi:10.1007/JHEP07(2014)079.

[73] M. Czakon and A. Mitov, "TOP++: a program for the calculation of the top-pair cross-section at hadron colliders", *Comput. Phys. Commun.* **185** (2014) 2930, doi:10.1016/j.cpc.2014.06.021.

[74] N. Kidonakis, "Top quark production", in *Proc. Helmholtz International Summer School on Physics of Heavy Quarks and Hadrons (HQ 2013): Dubna, Russia, July 15–28, 2013*. 2013. [DESY-PROC-2013-03]. doi:10.3204/DESY-PROC-2013-03/Kidonakis.

[75] M. Czakon et al., "Top-pair production at the LHC through NNLO QCD and NLO EW", *J. High Energy Phys.* **2017** (2017), no. 10, 186, doi:10.1007/JHEP10(2017)186.

[76] R. Frederix and S. Frixione, "Merging meets matching in MC@NLO", *J. High Energy Phys.* **2012** (2012), no. 12, 061, doi:10.1007/JHEP12(2012)061.

[77] J. Alwall et al., "Comparative study of various algorithms for the merging of parton showers and matrix elements in hadronic collisions", *Eur. Phys. J. C* **53** (2008) 473, doi:10.1140/epjc/s10052-007-0490-5.

[78] NNPDF Collaboration, "Parton distributions for the LHC run II", *J. High Energy Phys.* **2015** (2015), no. 04, 040, doi:10.1007/JHEP04(2015)040.

[79] T. Sjöstrand et al., "An introduction to PYTHIA 8.2", *Comput. Phys. Commun.* **191** (2015) 159, doi:10.1016/j.cpc.2015.01.024.

[80] CMS Collaboration, "Extraction and validation of a new set of CMS PYTHIA 8 tunes from underlying-event measurements", *Eur. Phys. J. C* **80** (2020) 4, doi:10.1140/epjc/s10052-019-7499-4.

[81] GEANT4 Collaboration, "GEANT4—a simulation toolkit", *Nucl. Instrum. Meth. A* **506** (2003) 250, doi:10.1016/S0168-9002(03)01368-8.

[82] "Supplemental Material: More details on simulated samples, jet flavor identification, baseline event selection, neural network event classifier, systematic uncertainties, validation of the background model, and additional results". [URL will be inserted by publisher].

[83] Y. Wang et al., "Dynamic graph CNN for learning on point clouds", *ACM Trans. Graph.* **38** (2018) 146, doi:10.1145/3326362.

[84] E. Bols et al., "Jet flavour classification using DeepJet", *J. Instrum.* **15** (2020) P12012, doi:10.1088/1748-0221/15/12/P12012.

[85] CMS Collaboration, "The CMS statistical analysis and combination tool: COMBINE", *Comput. Softw. Big Sci.* **8** (2024) 19, doi:10.1007/s41781-024-00121-4.

[86] W. Verkerke and D. Kirkby, "The ROOFIT toolkit for data modeling", in *Proc. 13th International Conference on Computing in High Energy and Nuclear Physics (CHEP 2003): La Jolla CA, United States, March 24–28, 2003*. 2003. arXiv:physics/0306116. [eConf C0303241 (2003) MOLT007].

[87] L. Moneta et al., "The ROOSTATS project", in *Proc. 13th International Workshop on Advanced Computing and Analysis Techniques in Physics Research (ACAT 2010): Jaipur, India, February 22–27, 2010*. 2010. [PoS (ACAT2010) 057]. doi:10.22323/1.093.0057.

[88] CMS Collaboration, "Measurement of top quark pair production in association with a Z boson in proton-proton collisions at $\sqrt{s} = 13$ TeV", *J. High Energy Phys.* **2020** (2020), no. 03, 056, doi:10.1007/JHEP03(2020)056.

[89] CMS Collaboration, "Measurements of inclusive and differential cross sections for top quark production in association with a Z boson in proton-proton collisions at $\sqrt{s} = 13$ TeV", *J. High Energy Phys.* **2025** (2025), no. 02, 177, doi:10.1007/JHEP02(2025)177.

[90] ATLAS Collaboration, "Inclusive and differential cross-section measurements of $t\bar{t}Z$ production in pp collisions at $\sqrt{s} = 13$ TeV with the ATLAS detector, including EFT and spin-correlation interpretations", *J. High Energy Phys.* **2024** (2024), no. 07, 163, doi:10.1007/JHEP07(2024)163.

[91] ATLAS and CMS Collaborations, and LHC Higgs Combination Group, "Procedure for the LHC Higgs boson search combination in Summer 2011", Technical Report CMS-NOTE-2011-005, ATL-PHYS-PUB-2011-11, 2011.

[92] G. Cowan, K. Cranmer, E. Gross, and O. Vitells, "Asymptotic formulae for likelihood-based tests of new physics", *Eur. Phys. J. C* **71** (2011) 1554, doi:10.1140/epjc/s10052-011-1554-0. [Erratum: doi:10.1140/epjc/s10052-013-2501-z].

[93] CMS Collaboration, "Measurement of the $t\bar{t}H$ and tH production rates in the $H \to b\bar{b}$ decay channel using proton-proton collision data at $\sqrt{s} = 13$ TeV", *J. High Energy Phys.* **2025** (2025), no. 02, 097, doi:10.1007/JHEP02(2025)097.

[94] T. Junk, "Confidence level computation for combining searches with small statistics", *Nucl. Instrum. Meth. A* **434** (1999) 435, doi:10.1016/S0168-9002(99)00498-2.

[95] A. L. Read, "Presentation of search results: The $CL_s$ technique", *J. Phys. G* **28** (2002) 2693, doi:10.1088/0954-3899/28/10/313.

[96] "HEPData record for this analysis", 2025. doi:10.17182/hepdata.159997.

[97] LHC Higgs Cross Section Working Group, S. Heinemeyer et al., "Handbook of LHC Higgs cross sections: 3. Higgs properties", CERN Report CERN-2013-004, 2013. doi:10.5170/CERN-2013-004.

[98] LHC Higgs Cross Section Working Group, D. de Florian et al., "Handbook of LHC Higgs cross sections: 4. Deciphering the nature of the Higgs sector", CERN Report CERN-2017-002-M, 2016. doi:10.23731/CYRM-2017-002.

[99] ATLAS Collaboration, "Study of the hard double-parton scattering contribution to inclusive four-lepton production in pp collisions at $\sqrt{s} = 8$ TeV with the ATLAS detector", *Phys. Lett. B* **790** (2019) 595, doi:10.1016/j.physletb.2019.01.062.

[100] P. Artoisenet, R. Frederix, O. Mattelaer, and R. Rietkerk, "Automatic spin-entangled decays of heavy resonances in Monte Carlo simulations", *J. High Energy Phys.* **2013** (2013), no. 03, 015, doi:10.1007/JHEP03(2013)015.

[101] CMS Collaboration, "Pileup mitigation at CMS in 13 TeV data", *J. Instrum.* **15** (2020) P09018, doi:10.1088/1748-0221/15/09/P09018.

[102] A. Kulesza et al., "Associated top quark pair production with a heavy boson: differential cross sections at NLO+NNLL accuracy", *Eur. Phys. J. C* **80** (2020) 428, doi:10.1140/epjc/s10052-020-7987-6.

[103] S. Mrenna and P. Skands, "Automated parton-shower variations in PYTHIA 8", *Phys. Rev. D* **94** (2016) 074005, doi:10.1103/PhysRevD.94.074005.

[104] CMS Collaboration, "Reweighting simulated events using machine-learning techniques in the CMS experiment", *Eur. Phys. J. C* **85** (2025) 495, doi:10.1140/epjc/s10052-025-14097-x.

[105] CMS Collaboration, "Evidence for tWZ production in proton-proton collisions at $\sqrt{s} = 13$ TeV in multilepton final states", *Phys. Lett. B* **855** (2024) 138815, doi:10.1016/j.physletb.2024.138815.

[106] L. Buonocore et al., "Precise predictions for the associated production of a W boson with a top-antitop quark pair at the LHC", *Phys. Rev. Lett.* **131** (2023) 231901, doi:10.1103/PhysRevLett.131.231901.

[107] ATLAS Collaboration, "Measurement of the associated production of a top-antitop-quark pair and a Higgs boson decaying into a $b\bar{b}$ pair in pp collisions at $\sqrt{s} = 13$ TeV using the ATLAS detector at the LHC", *Eur. Phys. J. C* **85** (2025) 210, doi:10.1140/epjc/s10052-025-13740-x.

# A End Matter

## A.1 Analysis strategy and event selection

The PART event classifier is used to select and categorize events, as illustrated in Fig. 5. The classifier outputs 10 (9) likelihood scores that sum to unity for the 0L (1L and 2L) channel. These include four scores for the signal processes, $\mathcal{D}_{t\bar{t}H(H\to c\bar{c})}$, $\mathcal{D}_{t\bar{t}H(H\to b\bar{b})}$, $\mathcal{D}_{t\bar{t}Z(Z\to c\bar{c})}$, and $\mathcal{D}_{t\bar{t}Z(Z\to b\bar{b})}$, and six (five) for the background processes, $\mathcal{D}_{t\bar{t}+light}$, $\mathcal{D}_{t\bar{t}+c}$, $\mathcal{D}_{t\bar{t}+\geq 2c}$, $\mathcal{D}_{t\bar{t}+b}$, $\mathcal{D}_{t\bar{t}+\geq 2b}$, and $\mathcal{D}_{QCD}$ (the last applies only to the 0L channel). The sum of the four signal scores is defined as $\mathcal{D}_{t\bar{t}X}$, while the sum of the five $t\bar{t}$+jets background scores is defined as $\mathcal{D}_{t\bar{t}+jets}$.

In the 0L channel, an initial requirement of $\mathcal{D}_{QCD} < 0.0001$ suppresses the QCD multijet background to below 1% of the $t\bar{t}$+jets background, allowing the QCD multijet contribution to be neglected. To reduce the $t\bar{t}$+light background, a requirement of $\mathcal{D}_{t\bar{t}+light} < 0.05$ (0.02) is applied in the 0L and 2L (1L) channels. Events with $\mathcal{D}_{t\bar{t}X} > 0.85$ are assigned to one of four SRs based on two pairs of signal discriminants, $\mathcal{D}_{t\bar{t}H}$ *vs.* $\mathcal{D}_{t\bar{t}Z}$ and $\mathcal{D}_{X\to c\bar{c}}$ *vs.* $\mathcal{D}_{X\to b\bar{b}}$, where $\mathcal{D}_{t\bar{t}H} = \mathcal{D}_{t\bar{t}H(H\to c\bar{c})} + \mathcal{D}_{t\bar{t}H(H\to b\bar{b})}$, $\mathcal{D}_{t\bar{t}Z} = \mathcal{D}_{t\bar{t}Z(Z\to c\bar{c})} + \mathcal{D}_{t\bar{t}Z(Z\to b\bar{b})}$, $\mathcal{D}_{X\to c\bar{c}} = \mathcal{D}_{t\bar{t}H(H\to c\bar{c})} + \mathcal{D}_{t\bar{t}Z(Z\to c\bar{c})}$, and $\mathcal{D}_{X\to b\bar{b}} = \mathcal{D}_{t\bar{t}H(H\to b\bar{b})} + \mathcal{D}_{t\bar{t}Z(Z\to b\bar{b})}$. Events with $0.6 < \mathcal{D}_{t\bar{t}X} < 0.85$ are

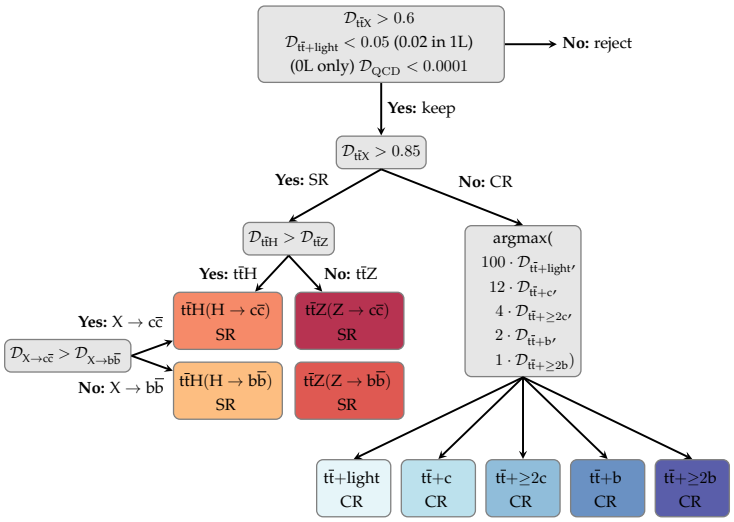


Figure 5: Event categorization flowchart.

categorized into one of the five CRs, determined by the background class with the highest weighted score. The weights—100, 12, 4, 2 and 1 for $\mathcal{D}_{t\bar{t}+light}$, $\mathcal{D}_{t\bar{t}+c}$, $\mathcal{D}_{t\bar{t}+\geq 2c}$, $\mathcal{D}_{t\bar{t}+b}$, $\mathcal{D}_{t\bar{t}+\geq 2b}$, respectively—are optimized to enhance the purity of each CR.

Figure 6 shows the fitted event yields in each bin for the CRs and SRs.

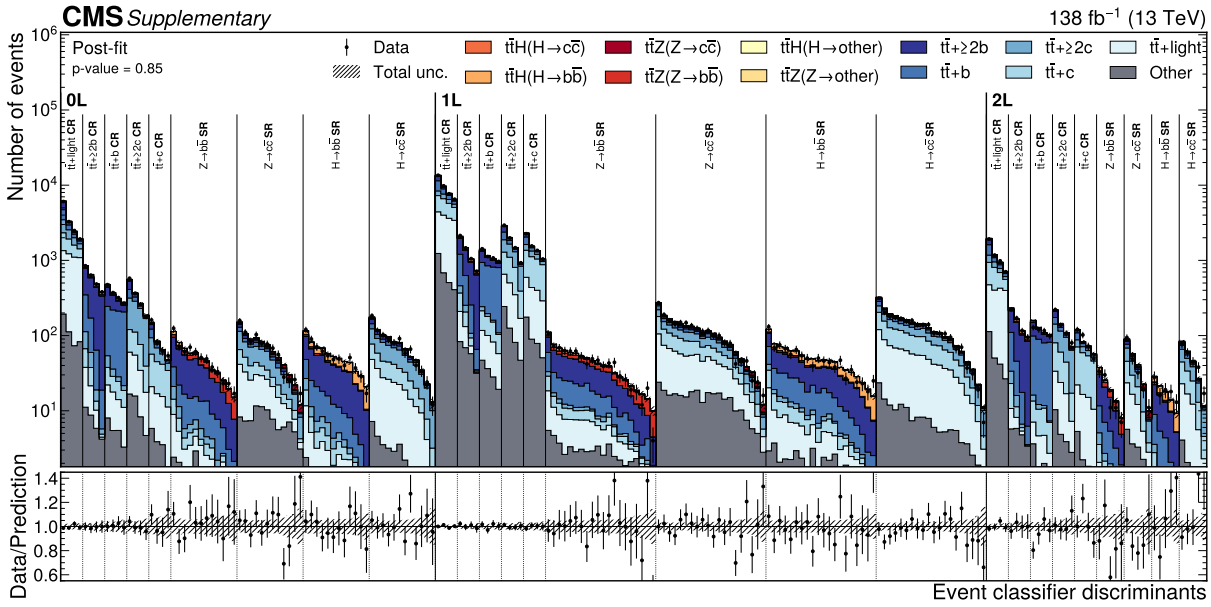


Figure 6: Distributions of the PART discriminants in data (points) and predicted signal and backgrounds (colored histograms) after the fit to data. The vertical bars on the points represent the statistical uncertainties in data. The hatched band represents the total uncertainty in the sum of the signal and background predictions. The lower panel shows the ratio of the data to the sum of the signal and background predictions.

## A.2 The $t\bar{t}$+jets background model

Simulated $t\bar{t}$+jets events are divided into five mutually exclusive components: $t\bar{t}+\geq$2b, $t\bar{t}$+b, $t\bar{t}+\geq$2c, $t\bar{t}$+c, and $t\bar{t}$+light. The $t\bar{t}+\geq$2b and $t\bar{t}$+b events are taken from a dedicated $t\bar{t}b\bar{b}$ sample, where the $t\bar{t}b\bar{b}$ matrix elements are calculated at NLO in QCD using the four-flavor

scheme (4FS). The b quark mass is set to 4.75 GeV, and the 4FS NNLO NNPDF3.1 PDF set is used to describe the proton structure. The $t\bar{t}b\bar{b}$ production cross section is computed at NLO in 4FS. The $t\bar{t}+\geq$2c, $t\bar{t}+$c, and $t\bar{t}+$light components are extracted from the inclusive $t\bar{t}$ simulation after removing the $t\bar{t}+\geq$2b and $t\bar{t}+$b contributions, thereby avoiding double counting. This inclusive $t\bar{t}$ sample is generated at NLO in QCD with up to one additional parton included at the matrix-element level, while additional emissions are modeled via parton showering with PYTHIA. The matrix element calculation is performed in the five-flavor scheme (5FS) using the 5FS NNLO NNPDF3.1 PDF set, where the b quarks are treated as massless. A subcomponent of $t\bar{t}+$b ($t\bar{t}+$c), referred to as $t\bar{t}+j_{bb}$ ($t\bar{t}+j_{cc}$), consists of events where the additional b (c) jet contains two or more b (c) hadrons. These events predominantly arise from collinear $g\to b\bar{b}$ ($g\to c\bar{c}$) splittings, which are not well modeled in simulation. To account for this modeling limitation, an additional 50% uncertainty is assigned to the $t\bar{t}+j_{bb}$ and $t\bar{t}+j_{cc}$ contributions in the background estimation.

Production of $t\bar{t}b\bar{b}$ via double parton scattering (DPS) also contributes to the $t\bar{t}+\geq$2b and $t\bar{t}+$b categories. This contribution is included in the inclusive $t\bar{t}$ sample but not in the dedicated $t\bar{t}b\bar{b}$ sample. It is therefore modeled separately by generating $t\bar{t}$ production at NLO in QCD using POWHEG, with additional $b\bar{b}$ production simulated by PYTHIA at LO in QCD using the `SecondHard` option. The cross section for this process is estimated to be 8 pb, assuming an effective DPS cross section of 30 mb [99] and an inclusive $b\bar{b}$ cross section of 0.3 mb, the latter estimated from simulation. In the background estimation, the DPS contributions are included in the corresponding $t\bar{t}+\geq$2b and $t\bar{t}+$b categories, with a 50% uncertainty assigned to the normalization of the DPS components.

Table 1 summarizes the best fit values of the $t\bar{t}+$jets background normalization factors obtained from a simultaneous fit to all CRs and SRs.

Table 1: Best fit values of the $t\bar{t}+$jets background normalization factors for each analysis category (Cat.).

| Cat. | $t\bar{t}+\geq$2b | $t\bar{t}+$b | $t\bar{t}+\geq$2c | $t\bar{t}+$c | $t\bar{t}+$light |
|---|---|---|---|---|---|
| 2L/1L | $0.88 \pm 0.07$ | $0.92 \pm 0.16$ | $1.39 \pm 0.23$ | $1.41 \pm 0.36$ | $0.89 \pm 0.11$ |
| 0L | $1.12 \pm 0.11$ | $0.89 \pm 0.18$ | $2.03 \pm 0.41$ | $0.95 \pm 0.34$ | $0.89 \pm 0.17$ |

## A.3 Uncertainty breakdown

The contributions of individual uncertainty sources to the total uncertainties in the fitted $\mu_{t\bar{t}H(H\to c\bar{c})}$ and $\mu_{t\bar{t}H(H\to b\bar{b})}$ are summarized in Table 2. The values are determined by repeating the fit with the nuisance parameters associated with each category fixed to their best fit values, and then subtracting the resulting uncertainty in quadrature from the total uncertainty. The total uncertainty differs from the quadrature sum of the individual components because of correlations among nuisance parameters in the fit.

Table 2: The absolute (relative) contributions to the total uncertainties, $\Delta\mu$ ($\Delta\mu/\Delta\mu_{\text{tot}}$).

| Uncertainty source | $\Delta\mu$ ($\Delta\mu/\Delta\mu_{\text{tot}}$) | | | |
|---|---|---|---|---|
| | $\mu_{t\bar{t}H(H\to c\bar{c})}$ | | $\mu_{t\bar{t}H(H\to b\bar{b})}$ | |
| Statistical | 3.3 | (74%) | 0.14 | (57%) |
| $t\bar{t}$+jets normalizations | 1.4 | (32%) | 0.06 | (26%) |
| $t\bar{t}Z$ normalizations | 0.4 | (8.4%) | 0.06 | (30%) |
| Theory | 2.1 | (47%) | 0.18 | (75%) |
| Signal | 0.7 | (15%) | 0.11 | (47%) |
| $t\bar{t}+\geq$1b | 0.7 | (15%) | 0.14 | (60%) |
| $t\bar{t}+\geq$1c | 1.4 | (32%) | 0.01 | (5.8%) |
| $t\bar{t}$+light | 1.3 | (29%) | 0.01 | (5.2%) |
| Minor backgrounds | 0.2 | (4.6%) | 0.01 | (4.6%) |
| Experimental | 2.0 | (47%) | 0.07 | (31%) |
| Jet flavor tagging | 1.7 | (39%) | 0.07 | (28%) |
| Size of the simulated samples | 1.1 | (24%) | 0.05 | (21%) |
| Jet energy scale and resolution | 0.8 | (18%) | 0.02 | (8.6%) |
| Lepton identification | 0.3 | (6.0%) | 0.02 | (6.3%) |
| Integrated luminosity | 0.1 | (2.0%) | 0.02 | (6.2%) |
| Total | 4.5 | (100%) | 0.24 | (100%) |

# B Supplemental Material

## B.1 Simulated samples

Signal and background processes are modeled using Monte Carlo (MC) simulations. The generators used for the $t\bar{t}H$, $t\bar{t}Z$, and $t\bar{t}$ processes are listed in Table B.1, while those for the other background processes are summarized in Table B.2. The decays of heavy particles in $t\bar{t}W$, $t\bar{t}Z$, and $t$-channel single top quark production are modeled using MADSPIN [100]. Details about the modeling parameters of the $t\bar{t}b\bar{b}$ sample in the four-flavor scheme (4FS) and of the inclusive $t\bar{t}$ sample in the five-flavor scheme (5FS) are provided in Table B.3.

The QCD multijet events are generated with MADGRAPH5_aMC@NLO at leading-order (LO) accuracy, employing the MLM scheme [77] for matrix element (ME) and parton shower (PS) matching, and are used only for training the neural network event classifier and are not included in the background estimation for the profile likelihood fits.

Table B.1: Generator settings for signal and major background samples. The "Groups" column refers to the grouping of processes in the maximum likelihood fits. Here, $t\bar{t}H(H\to\text{Other})$ and $t\bar{t}Z(Z\to\text{Other})$ refer to all Higgs boson and Z boson decay channels other than those to b and c quark pairs.

| Process | Groups | ME order | Generator | Notes |
|---|---|---|---|---|
| $t\bar{t}H$ | $t\bar{t}H(H\to c\bar{c})$, $t\bar{t}H(H\to b\bar{b})$, $t\bar{t}H(H\to\text{Other})$ | NLO | POWHEG v2 | |
| $t\bar{t}Z$ | $t\bar{t}Z(Z\to c\bar{c})$, $t\bar{t}Z(Z\to b\bar{b})$, $t\bar{t}Z(Z\to\text{Other})$ | NLO | MADGRAPH5_aMC@NLO v2.6.1 | MADSPIN for heavy particle decays |
| $t\bar{t}$ | $t\bar{t}$+light, $t\bar{t}+\geq$2c, $t\bar{t}$+c | NLO | POWHEG v2 | |
| $t\bar{t}b\bar{b}$ | $t\bar{t}+\geq$2b, $t\bar{t}$+b | NLO | POWHEG-BOX-RES | |
| $t\bar{t}b\bar{b}$ DPS | $t\bar{t}+\geq$2b, $t\bar{t}$+b | NLO / LO | POWHEG v2 / PYTHIA v8.240 | $t\bar{t}$ NLO ME with POWHEG / LO $b\bar{b}$ DPS with PYTHIA |

Table B.2: Generator settings for minor background samples. The "Group" column refers to the grouping of processes in the maximum likelihood fits.

| Process | Group | ME order | Generator | Notes |
|---|---|---|---|---|
| tW | single t | NLO | POWHEG v2 | MADSPIN for heavy particle decays |
| $t$ channel | | | POWHEG v2 | |
| $s$ channel | | | MADGRAPH5_aMC@NLO v2.6.1 | |
| $t\bar{t}W$ | $t\bar{t}W$ | NLO | MADGRAPH5_aMC@NLO v2.6.1 | FxFx merging up to 1 additional jet<br>MADSPIN for heavy particle decays |
| tWZ | tWZ | LO | MADGRAPH5_aMC@NLO v2.6.5 | MADSPIN for heavy particle decays |
| QCD | QCD | LO | MADGRAPH5_aMC@NLO v2.5.1 | MLM merging for ME-PS matching |

## B.2 Jet flavor identification

Jets containing b or c hadrons are identified using the PARTICLENET algorithm [42]. The PARTICLENET algorithm outputs eight probabilities, trained to discriminate jets containing one ($p_{\mathrm{b}}$) or two ($p_{\mathrm{bb}}$) b hadrons, one ($p_{\mathrm{c}}$) or two ($p_{\mathrm{cc}}$) c hadrons, jets originating from u, d, or s quarks ($p_{\mathrm{uds}}$), gluons ($p_{\mathrm{g}}$), pileup, or other sources. For this measurement, it is essential to distinguish jets originating from b quarks, c quarks, and those of other origins. Therefore, two discrimi-

Table B.3: Summary of generator settings used for the $t\bar{t}b\bar{b}$ and inclusive $t\bar{t}$ samples. The transverse mass is defined as $m_T = \sqrt{m^2 + p_T^2}$.

| | $t\bar{t}$ NLO (5FS) | $t\bar{t}b\bar{b}$ NLO (4FS) |
|---|---|---|
| ME generator | POWHEG v2 | POWHEG-BOX-RES |
| Parton shower | PYTHIA v8.230 | PYTHIA v8.230 |
| Flavor scheme | 5FS | 4FS |
| PDF set | NNPDF31_nnlo_hessian_pdfas | NNPDF31_nnlo_as_0118_nf_4 |
| $m_t$ | 172.5 GeV | 172.5 GeV |
| $m_b$ | 0 | 4.75 GeV |
| $\mu_R$ | $\sqrt{\frac{1}{2}\left(m^2_{rmT,t} + m^2_{T,\bar{t}}\right)}$ | $\frac{1}{2}\sqrt[4]{m_{t,t}\, m_{t,\bar{t}}\, m_{t,b}\, m_{t,\bar{b}}}$ |
| $\mu_F$ | $\mu_R$ | $\frac{1}{4}\left[m_{t,t} + m_{t,\bar{t}} + m_{t,b} + m_{t,\bar{b}} + m_{t,g}\right]$ |
| $h_{damp}$ | $1.379 m_t$ | $1.379 m_t$ |
| Tune | CP5 | CP5 |

nants are constructed, based on the individual output probabilities of the PARTICLENET tagger:

$$p_{B+C} = \frac{p_b + p_{bb} + p_c + p_{cc}}{p_b + p_{bb} + p_c + p_{cc} + p_{uds} + p_g}\,,$$
$$p_{BvsC} = \frac{p_b + p_{bb}}{p_b + p_{bb} + p_c + p_{cc}}\,. \tag{4}$$

The first discriminant, $p_{B+C}$, differentiates between heavy-flavor (HF) jets (i.e., of b or c origin) and light jets (i.e., of u, d, s, and g origin). The second discriminant, $p_{BvsC}$, further separates HF jets into b and c jets. Based on these two discriminants, 11 mutually exclusive tagging categories are defined: 5 categories for b tagging (B0–B4), 5 categories for c tagging (C0–C4), and one untagged category (L0).

In Fig. B.1, the rejection factors, i.e., the inverse of the efficiency, for the subdominant jet flavors in each of the categories are compared to the DEEPJET tagger [84] used in previous $H\to c\bar{c}$ searches. For this purpose, similar working points were derived for the DEEPJET tagger, mimicking the tagging efficiencies of the dominant jet flavor in each of the tagging bins, i.e., requiring the same light-jet efficiency in L0, the same c jet efficiency in C0–C4, and the same b jet efficiency in B1–B4. The bin B0 is not shown as no comparable b tagging efficiency for DEEPJET can be achieved for all bins at the same time due to its lower overall tagging efficiency. In summary, the tagging layout of the PARTICLENET algorithm improves the rejection factors of the subdominant jet flavors by factors of 1–2 in all tagging bins, compared to DEEPJET.

Differences in the flavor tagging efficiencies between simulation and data are measured using three data samples, enriched each in dileptonic $t\bar{t}$, W+jets, and Z+jets events, focusing on b, c, and light jets, respectively.

- The $t\bar{t}$ region is defined by selecting events that contain an $e^{\pm}\mu^{\mp}$ pair. In addition, the transverse mass $m_T(e, \mu, p_T^{miss})$ is required to be larger than 100 GeV to reduce contributions of Z+jets events.
- For the W+jets region, events with one isolated lepton are selected. Events further need to have exactly one jet that contains a nonisolated muon with a $p_T$ larger than 5 GeV inside the jet cone and with a charge opposite to that of the selected isolated lepton. The requirement of a non-isolated muon inside the jet cone enriches the selection in events with semileptonic c hadron decays in the jets, and thereby W+c

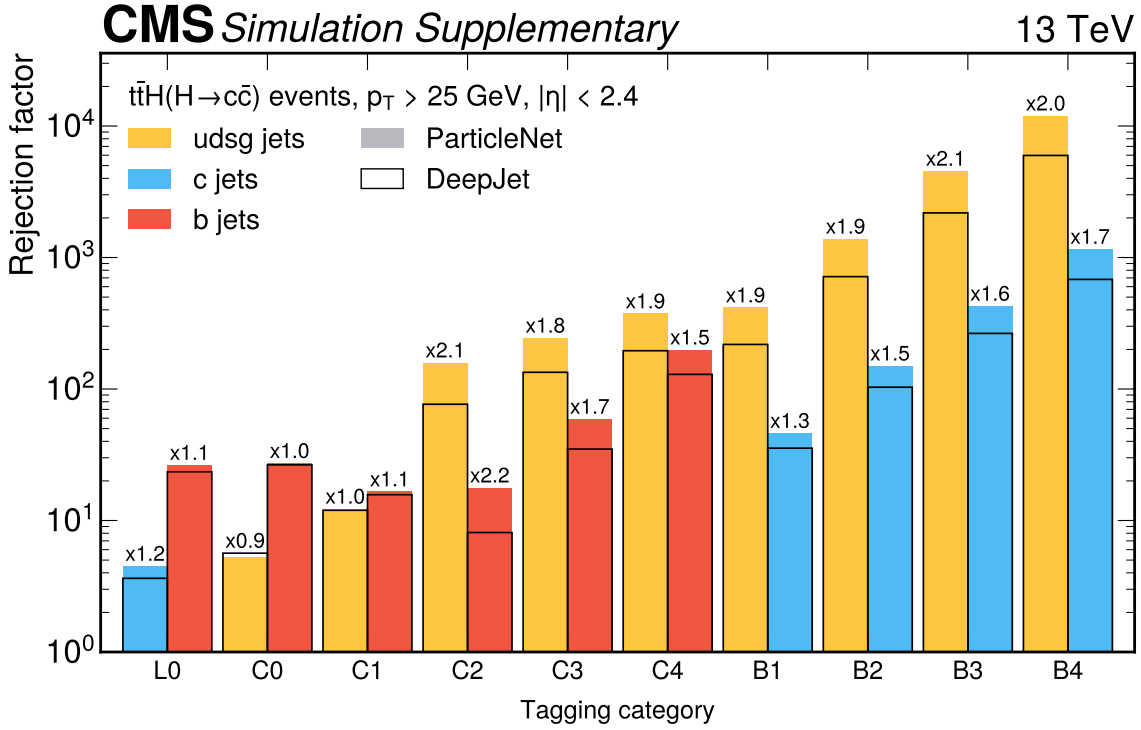


Figure B.1: Rejection factors for the subdominant jet flavors in each of the tagging bins. The filled bars represent the rejection factors achieved with the PARTICLENET tagger and the corresponding working point definitions. The black bars represent the rejection factors achieved with the DEEPJET tagger with working points mimicking the dominant flavor tagging efficiencies. Each bin is labeled with the relative improvement of the PARTICLENET tagger compared to the DEEPJET tagger. All rejection factors and tagging efficiencies are evaluated using simulated $\mathrm{t\bar{t}H(H{\to}c\bar{c})}$ events with 2018 detector conditions.

signatures. A set of additional kinematic requirements are imposed to reduce contributions from other background processes and enrich the selection with W+jets events.

- Finally, for the Z+jets region, events with two opposite-charge same-flavor ($e^+e^-$, $\mu^+\mu^-$) lepton candidates are selected. The leading lepton is required to have $p_T >$ 25 GeV, and $m_{\ell\ell}$ has to be within the range of 81–101 GeV. Exactly one additional jet in the event that balances the reconstructed Z boson $p_T$ is required.

For all regions, the jets are selected using the same criteria as used in the present $\mathrm{t\bar{t}H(H{\to}c\bar{c})}$ analysis.

Simulation-to-data scale factors (SFs) are then derived as a function of jet $p_T$ with the following procedure. Tagging SFs are derived by simultaneously fitting all three flavor-enriched regions (Z+jets, W+jets, $\mathrm{t\bar{t}}$) in a profile likelihood fit. The tagging SFs are discretized into the eleven aforementioned tagging bins `L0`, `C0`–`C4`, and `B0`–`B4`. For each of the ten exclusive `C0`–`C4` and `B0`–`B4` bins, one parameter of interest (POI) is defined per jet flavor (i.e., in total 30 independent POIs per jet $p_T$ bin), which corresponds to the jet tagging scale factor for the exclusive tagging bin and jet flavor. In order to preserve unitarity, the SFs for the tagger bin `L0` are not associated with an independent POI but are constructed such that the sum of tagging probabilities per jet

flavor is retained, i.e., requiring

$$\sum_{\mathrm{WP}\in[\texttt{L0},\texttt{C0}-\texttt{C4},\texttt{B0}-\texttt{B4}]} \epsilon_{\mathrm{MC}}\big(\mathrm{WP}\big|\mathrm{flav}\big) = \sum_{\mathrm{WP}} \epsilon_{\mathrm{data}}\big(\mathrm{WP}\big|\mathrm{flav}\big) \equiv 1. \tag{5}$$

This constraint guarantees that the overall normalization of each type (b, c, and light) component is retained in the fits, and the resulting SFs correct for only the efficiencies but do not alter the normalizations. This helps preserve the normalization of each flavor component when the SFs are applied to a different phase space region. To be insensitive to the overall normalization of the total background prediction as obtained by the simulation and to fit only the relative tagging efficiencies, the overall expected yields are scaled to match the observed data in the scale factor derivation regions, inclusive in jet flavor. The fits are performed in six independent jet $p_{\mathrm{T}}$ ranges, to introduce a $p_{\mathrm{T}}$ dependence on the tagging SFs:

$$p_{\mathrm{T}}(\mathrm{jet}) \in [25, 35, 50, 70, 90, 120, \infty]\,\mathrm{GeV}. \tag{6}$$

The normalization and derivation of SFs is completely independent for each of the $p_{\mathrm{T}}$ ranges.

In some cases, where the contribution of a certain jet flavor to a certain tagging bin is very small, the SFs cannot be determined well. For example, in the high b tagging bins `B3` or `B4`, the contamination of c and LF jets is almost negligible. In cases where the fits for these parameters do not lead to a well-converged result, i.e., where the expected uncertainty in the SF exceeds 50%, the SF value is set to unity in the fit to data, and the corresponding SF is assigned an uncertainty covering the range $[0.3, 3]$. Changes in these SFs have negligible impact on the analysis results, as the contamination of jets of the affected flavors in the corresponding tagging bins is negligible.

In the fit to data, a range of experimental and modeling uncertainties are considered. The same set of experimental uncertainties as described in Section B.6 is considered for the calibration measurement. Modeling uncertainties due to renormalization scale $\mu_{\mathrm{R}}$ and factorization scale $\mu_{\mathrm{F}}$ choices, and uncertainties due to initial-state and final-state radiation scales (ISR and FSR) are applied, following the same procedures as described in Section B.7. These uncertainties are treated as uncorrelated between major processes in the SF derivation regions ($\mathrm{t\bar{t}}$, W+jets, Z+jets, etc.). Normalization uncertainties are included to account for the limited knowledge of the cross sections of the relevant processes. A 5% normalization uncertainty is applied to the minor $\mathrm{t\bar{t}}$ background in the W+jets and Z+jets regions. In the $\mathrm{t\bar{t}}$ channel, the $\mathrm{t\bar{t}}$ normalization is fitted to data. A 10% normalization uncertainty is applied for tW production, and 15% for single top $t$-channel production. Diboson production is associated with a 15% normalization uncertainty. For the production of a W or Z boson with HF jets, dedicated normalization uncertainties are applied, as the modeling of these processes is known to be insufficient. An 8% normalization uncertainty is applied to W+c production. The W+b, Z+b, and Z+c processes are each associated with a free parameter in the fit to determine the normalization in-situ.

The impacts of systematic uncertainties in the final tagging SFs are derived from the impacts of the corresponding nuisance parameters. Variations of a systematic source are considered fully correlated between all SFs, $p_{\mathrm{T}}$ ranges, and years when applied in the $\mathrm{t\bar{t}H(H\to c\bar{c})}$ analysis. The statistical uncertainties are derived by freezing all nuisance parameters to their best fit values and refitting the tagging SFs. The resulting uncertainty in the SFs is considered the statistical uncertainty. In cases where the SFs could not be determined, i.e., cases where the SFs are fixed to a value of 1 and the uncertainties are inflated to the range $[0.3, 3]$, the full uncertainty is treated as a statistical uncertainty. Statistical uncertainties of different jet flavors, tagging bins, and years are all treated as uncorrelated parameters when applied in the $\mathrm{t\bar{t}H(H\to c\bar{c})}$ analysis.

The large majority of SFs for b, c, and light jets are within the range $[0.75, 1.5]$, with only few SFs outside this range. Uncertainties in the b jet SFs in the b jet enriched regions are generally small (of order 1–5%), and show continuous trends (i.e., SF values appear smooth for neighboring bins). Similarly, b jet SFs are well described in the c jet enriched bins `C0`–`C4`, but have somewhat larger uncertainties (of order 50%) in the `L0` bin. SFs for c jets converge mostly well in c jet and light jet enriched bins. In higher b jet tagging bins (`B1`–`B4`), c jet SFs often cannot be constrained in the fit and are assigned a default value of one with large uncertainties. Similarly, light jet SFs cannot be well constrained in most c and b jet enriched bins, because of the low light-jet mistagging efficiencies.

## B.3 Baseline event selection

The baseline event selection of this analysis is summarized in Table B.4. Corrections are applied to the simulated samples to account for differences in the jet energy scale and resolution, lepton selection efficiencies, and trigger efficiencies. Corrections for the variations in jet flavor identification efficiencies, discussed above, are also applied. Different selection criteria for different data-taking periods are motivated by changes in the trigger selection.

Table B.4: Baseline selection criteria in the 0L, 1L, and 2L channels. Where the selection criteria differ per year, they are quoted as 2016/2017/2018.

| Selection criteria | 0L channel | 1L channel | 2L channel |
|---|---|---|---|
| Number of leptons | 0 | 1 | 2 |
| Sign and flavor of leptons | — | $e^{\pm}$, $\mu^{\pm}$ | $e^{+}e^{-}$, $\mu^{\pm}e^{\mp}$, $\mu^{+}\mu^{-}$ |
| Min. $p_T$ of $p_T$-leading electron [GeV] | — | 29/30/30 | 25 |
| Electron identification | — | Tight (80% efficiency) | Loose (90% efficiency) |
| Electron isolation | — | Tight (80% efficiency) | Loose (90% efficiency) |
| Min. $p_T$ of $p_T$-leading muon [GeV] | — | 26/29/26 | 25 |
| Max. muon relative isolation | — | 0.15 | 0.25 |
| Min. $m_{ee/\mu\mu}$ [GeV] | — | — | 20 |
| Range of $m_{ee/\mu\mu}$ [GeV] | — | — | $<76$, $>106$ |
| Min. $p_T$ of jets [GeV] | 25 | 25 | 25 |
| Min. $p_T$ of 6$^{th}$ jet [GeV] | 40 | — | — |
| Max. $\lvert\eta\rvert$ of jets | 2.4 | 2.4 | 2.4 |
| Min. number of jets | 7 | 5 | 4 |
| Min. number of b-tagged jets | 1 | 1 | 1 |
| Min. number of HF (b- or c-tagged) jets | 3 | 3 | 3 |
| Min. $H_T$ [GeV] | 500 | — | — |
| Min. $p_T^{miss}$ [GeV] | — | 20 | 20 |

## B.4 Neural network event classifier

The performance of the PARTICLE NET event classifier is summarized via the confusion matrices shown in Fig. B.2.

The fitted variable is the PARTICLE NET event classifier discriminant for the corresponding category as summarized in Table B.5. Several selections on the classifier discriminants define the analysis and validation regions (AR and VR), summarized in Fig. 5. In the 0L channel the classifier discriminant for the QCD multijet is used to remove the multijet background. The discriminant and the corresponding cut are shown in Fig. B.3. In all three channels, a cut on $\mathcal{D}_{t\bar{t}+\text{light}}$ is applied to reduce the overwhelming background from $t\bar{t}$+light production, shown in Fig. B.4.

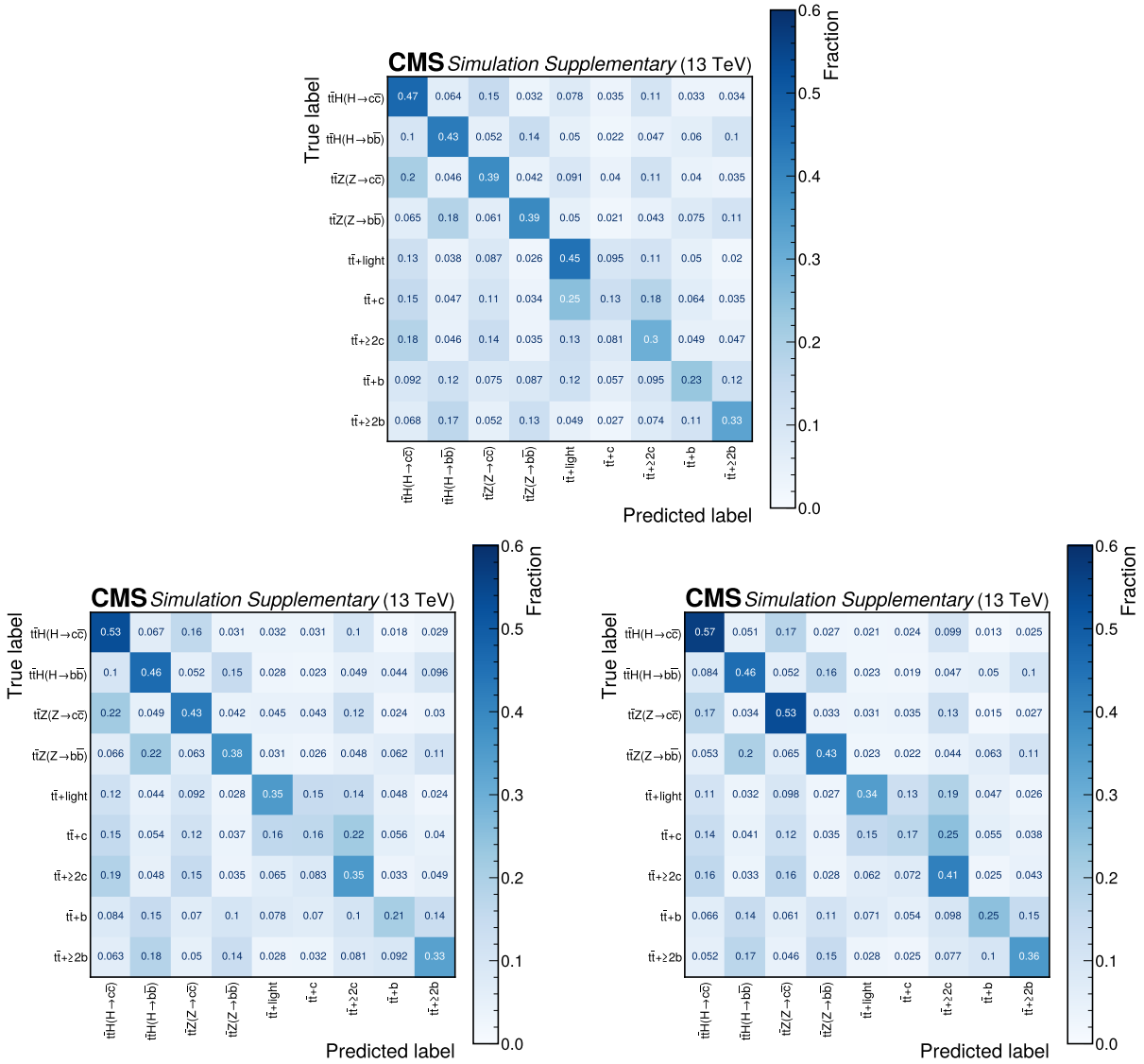


Figure B.2: Confusion matrices of the PART event classifier in the 0L (upper), 1L (lower left), and 2L (lower right) channels after the baseline selection. For each event, the predicted label is the process with the highest output discriminant. The event yield fractions are normalized per true label such that each row sums up to unity.

Table B.5: Definition of the PART event classifier discriminant for each category in the maximum likelihood fit.

| Category | Discriminant |
|---|---|
| H→c$\bar{c}$ SR | $\mathcal{D}_{t\bar{t}H(H\to c\bar{c})}$ |
| H→b$\bar{b}$ SR | $\mathcal{D}_{t\bar{t}H(H\to b\bar{b})}$ |
| Z→c$\bar{c}$ SR | $\mathcal{D}_{t\bar{t}Z(Z\to c\bar{c})}$ |
| Z→b$\bar{b}$ SR | $\mathcal{D}_{t\bar{t}Z(Z\to b\bar{b})}$ |
| t$\bar{t}$+light CR | $\mathcal{D}_{t\bar{t}+\text{light}}/\mathcal{D}_{t\bar{t}+\text{jets}}$ |
| t$\bar{t}$+c CR | $\mathcal{D}_{t\bar{t}+c}/\mathcal{D}_{t\bar{t}+\text{jets}}$ |
| t$\bar{t}$+≥2c CR | $\mathcal{D}_{t\bar{t}+\geq 2c}/\mathcal{D}_{t\bar{t}+\text{jets}}$ |
| t$\bar{t}$+b CR | $\mathcal{D}_{t\bar{t}+b}/\mathcal{D}_{t\bar{t}+\text{jets}}$ |
| t$\bar{t}$+≥2b CR | $\mathcal{D}_{t\bar{t}+\geq 2b}/\mathcal{D}_{t\bar{t}+\text{jets}}$ |

After these selections, the AR and VR, and the SRs and CRs are defined via requirements on $\mathcal{D}_{t\bar{t}X}$, summarized in Fig. B.5.

The event yields in the AR after the fit to data are summarized in Tables B.6–B.8 for the three individual channels, and in Tables B.9–B.10 for the full analysis.

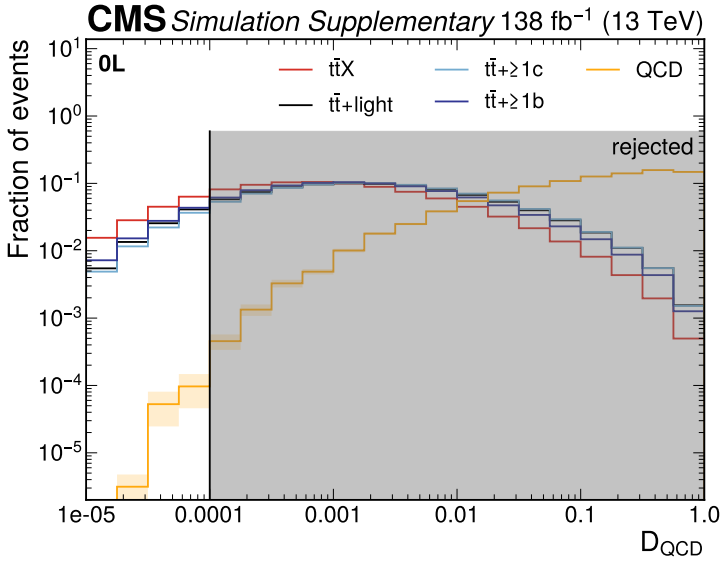


Figure B.3: Distribution of the PART $\mathcal{D}_{QCD}$ discriminant used in the 0L channel to remove the QCD background. The gray area indicates the region that is rejected in the analysis. The shaded band indicates the uncertainty in the QCD prediction due to limited size of simulated QCD multijet samples. All contributions are normalized to unity.

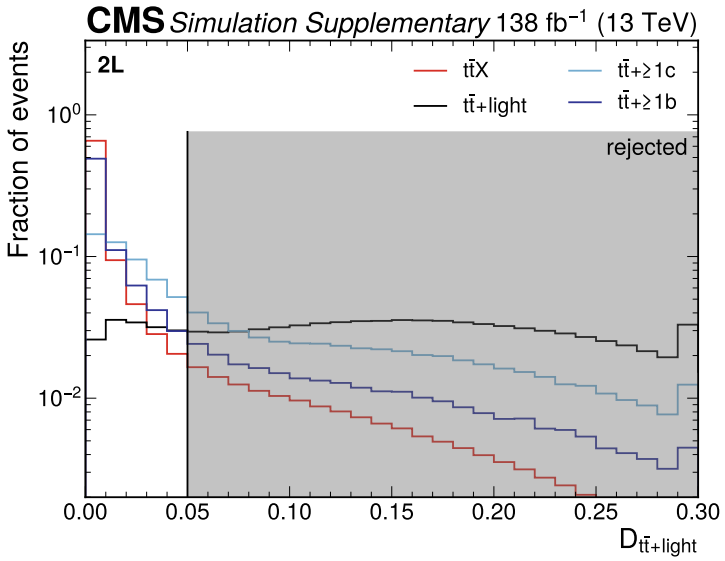


Figure B.4: Distribution of the PART $\mathcal{D}_{t\bar{t}+light}$ discriminant used to reduce the $t\bar{t}$+light background in the 2L channel. The gray area indicates the region that is rejected in the analysis. All contributions are normalized to unity. The last bin includes the overflow.

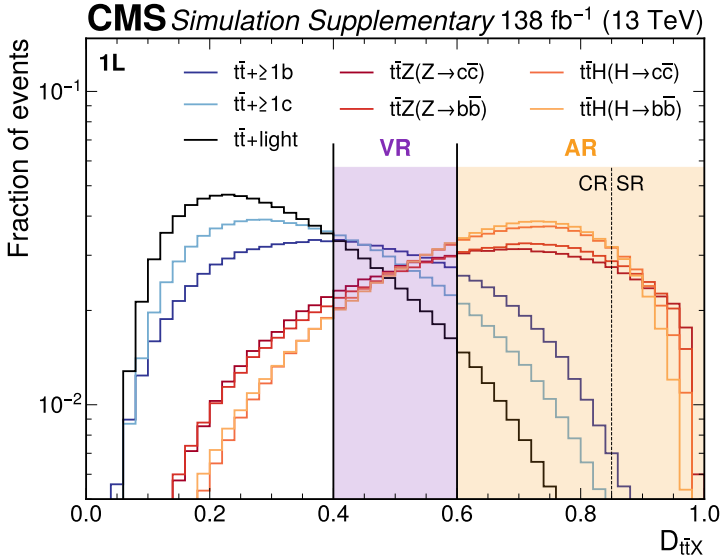


Figure B.5: Distribution of the PART $\mathcal{D}_{t\bar{t}X}$ discriminant used to define the different regions in the 1L channel. The purple (yellow) area indicates the region that is used for the validation (analysis). The dashed line indicates the separation of SRs and CRs in the analysis. All contributions are normalized to unity.

Table B.6: Event yields in the 2L channel. Values in brackets correspond to the pre-fit expectations.

| Process | SR $t\bar{t}H(H\to c\bar{c})$ | SR $t\bar{t}H(H\to b\bar{b})$ | SR $t\bar{t}Z(Z\to c\bar{c})$ | SR $t\bar{t}Z(Z\to b\bar{b})$ | CR $t\bar{t}$+≥2b | CR $t\bar{t}$+b | CR $t\bar{t}$+≥2c | CR $t\bar{t}$+c | CR $t\bar{t}$+light |
|---|---|---|---|---|---|---|---|---|---|
| $t\bar{t}H(H\to c\bar{c})$ | $-2.5\pm4.4$ ($1.5\pm2.8$) | $-0.06\pm0.62$ ($0.03\pm0.37$) | $-0.5\pm1.8$ ($0.3\pm1.1$) | $-0.02\pm0.35$ ($0.01\pm0.21$) | $-0.13\pm0.83$ ($0.08\pm0.50$) | $-0.04\pm0.51$ ($0.02\pm0.31$) | $-1.2\pm2.8$ ($0.7\pm1.7$) | $-0.4\pm1.5$ ($0.24\pm0.97$) | $-4.4\pm5.2$ ($2.7\pm3.2$) |
| $t\bar{t}H(H\to b\bar{b})$ | $2.4\pm3.1$ ($2.7\pm3.4$) | $20.2\pm9.6$ ($22\pm11$) | $1.3\pm2.1$ ($1.4\pm2.2$) | $6.4\pm4.7$ ($7.1\pm5.2$) | $37\pm12$ ($40\pm13$) | $18.6\pm8.1$ ($20.8\pm9.0$) | $4.1\pm3.4$ ($4.4\pm3.6$) | $1.8\pm2.4$ ($2.1\pm2.6$) | $45\pm11$ ($50\pm13$) |
| $t\bar{t}Z(Z\to c\bar{c})$ | $1.9\pm2.7$ | $0.11\pm0.64$ | $9.9\pm7.1$ | $0.21\pm0.90$ | $0.4\pm1.1$ | $0.12\pm0.71$ | $4.3\pm4.2$ | $1.2\pm2.2$ | $14.2\pm7.4$ |
| $t\bar{t}Z(Z\to b\bar{b})$ | $0.7\pm2.1$ | $3.8\pm4.7$ | $1.1\pm2.7$ | $16\pm11$ | $19\pm11$ | $9.1\pm7.2$ | $2.1\pm3.1$ | $0.9\pm2.2$ | $23\pm10$ |
| $t\bar{t}$+≥2b | $12.7\pm7.9$ | $45\pm16$ | $11.8\pm7.4$ | $52\pm17$ | $370\pm42$ | $121\pm24$ | $52\pm15$ | $14.3\pm8.0$ | $385\pm40$ |
| $t\bar{t}$+b | $19\pm14$ | $14\pm13$ | $16\pm12$ | $17\pm14$ | $120\pm32$ | $303\pm56$ | $54\pm22$ | $37\pm19$ | $727\pm81$ |
| $t\bar{t}$+≥2c | $67\pm21$ | $1.9\pm3.7$ | $63\pm20$ | $2.4\pm3.3$ | $16.0\pm7.7$ | $5.5\pm5.6$ | $214\pm35$ | $44\pm15$ | $524\pm52$ |
| $t\bar{t}$+c | $61\pm28$ | $1.7\pm4.0$ | $49\pm24$ | $3.4\pm6.8$ | $16\pm11$ | $23\pm16$ | $121\pm37$ | $166\pm43$ | $1290\pm120$ |
| $t\bar{t}$+light | $50\pm14$ | $1.7\pm2.7$ | $44\pm12$ | $1.8\pm2.7$ | $8.1\pm4.7$ | $11.2\pm6.1$ | $60\pm14$ | $54\pm13$ | $1470\pm74$ |
| Other | $15\pm18$ | $2.8\pm7.3$ | $24\pm24$ | $5.4\pm9.7$ | $22\pm17$ | $8.5\pm8.1$ | $32\pm25$ | $13\pm14$ | $313\pm75$ |
| Total | $228\pm14$ | $90.7\pm7.9$ | $220\pm14$ | $103.6\pm9.1$ | $608\pm22$ | $499\pm19$ | $541\pm27$ | $332\pm18$ | $4790\pm110$ |
| Data | 236 | 93 | 204 | 92 | 605 | 463 | 546 | 343 | 4784 |

Table B.7: Event yields in the 1L channel. Values in brackets correspond to the pre-fit expectations.

| Process | SR $t\bar{t}H(H\to c\bar{c})$ | SR $t\bar{t}H(H\to b\bar{b})$ | SR $t\bar{t}Z(Z\to c\bar{c})$ | SR $t\bar{t}Z(Z\to b\bar{b})$ | CR $t\bar{t}$+≥2b | CR $t\bar{t}$+b | CR $t\bar{t}$+≥2c | CR $t\bar{t}$+c | CR $t\bar{t}$+light |
|---|---|---|---|---|---|---|---|---|---|
| $t\bar{t}H(H\to c\bar{c})$ | $-16\pm22$ ($10\pm14$) | $-0.5\pm3.6$ ($0.3\pm2.1$) | $-3.1\pm8.9$ ($1.9\pm5.4$) | $-0.2\pm1.9$ ($0.1\pm1.1$) | $-1.2\pm2.6$ ($0.7\pm1.5$) | $-0.5\pm1.8$ ($0.3\pm1.0$) | $-11.7\pm8.8$ ($7.0\pm5.3$) | $-5.4\pm5.9$ ($3.3\pm3.6$) | $-24\pm13$ ($14.8\pm7.7$) |
| $t\bar{t}H(H\to b\bar{b})$ | $21\pm18$ ($23\pm19$) | $166\pm55$ ($181\pm60$) | $9\pm11$ ($10\pm12$) | $43\pm25$ ($47\pm27$) | $264\pm31$ ($284\pm34$) | $139\pm22$ ($153\pm25$) | $52\pm12$ ($55\pm13$) | $35\pm10$ ($38\pm11$) | $327\pm32$ ($356\pm35$) |
| $t\bar{t}Z(Z\to c\bar{c})$ | $16\pm16$ | $1.1\pm4.1$ | $59\pm35$ | $1.5\pm4.9$ | $3.5\pm3.6$ | $1.6\pm2.5$ | $37\pm12$ | $18.1\pm8.6$ | $78\pm18$ |
| $t\bar{t}Z(Z\to b\bar{b})$ | $6\pm12$ | $32\pm28$ | $8\pm14$ | $114\pm58$ | $136\pm28$ | $70\pm20$ | $25\pm11$ | $19.2\pm9.7$ | $166\pm29$ |
| $t\bar{t}$+≥2b | $109\pm48$ | $387\pm91$ | $85\pm41$ | $360\pm88$ | $2760\pm120$ | $957\pm67$ | $633\pm51$ | $293\pm34$ | $2830\pm110$ |
| $t\bar{t}$+b | $198\pm96$ | $205\pm97$ | $168\pm88$ | $165\pm87$ | $1300\pm110$ | $2700\pm170$ | $841\pm88$ | $719\pm81$ | $5760\pm240$ |
| $t\bar{t}$+≥2c | $470\pm110$ | $26\pm24$ | $389\pm99$ | $19\pm21$ | $153\pm26$ | $60\pm18$ | $2080\pm110$ | $718\pm63$ | $3400\pm140$ |
| $t\bar{t}$+c | $700\pm190$ | $61\pm54$ | $470\pm150$ | $45\pm46$ | $256\pm48$ | $291\pm59$ | $1910\pm150$ | $2680\pm180$ | $9220\pm330$ |
| $t\bar{t}$+light | $780\pm110$ | $73\pm33$ | $605\pm94$ | $69\pm33$ | $205\pm24$ | $226\pm29$ | $1180\pm65$ | $1326\pm70$ | $12620\pm220$ |
| Other | $190\pm120$ | $43\pm48$ | $320\pm160$ | $58\pm55$ | $249\pm50$ | $136\pm33$ | $550\pm86$ | $423\pm70$ | $3080\pm190$ |
| Total | $2470\pm92$ | $993\pm52$ | $2115\pm80$ | $875\pm48$ | $5330\pm110$ | $4580\pm110$ | $7300\pm200$ | $6230\pm190$ | $37450\pm530$ |
| Data | 2411 | 983 | 2108 | 879 | 5372 | 4594 | 7317 | 6209 | 37497 |

Table B.8: Event yields in the 0L channel. Values in brackets correspond to the pre-fit expectations.

| Process | SR $t\bar{t}H(H\to c\bar{c})$ | SR $t\bar{t}H(H\to b\bar{b})$ | SR $t\bar{t}Z(Z\to c\bar{c})$ | SR $t\bar{t}Z(Z\to b\bar{b})$ | CR $t\bar{t}$+≥2b | CR $t\bar{t}$+b | CR $t\bar{t}$+≥2c | CR $t\bar{t}$+c | CR $t\bar{t}$+light |
|---|---|---|---|---|---|---|---|---|---|
| $t\bar{t}H(H\to c\bar{c})$ | $-9\pm13$ ($5.5\pm8.1$) | $-0.4\pm2.5$ ($0.2\pm1.4$) | $-1.6\pm5.0$ ($1.0\pm3.0$) | $-0.1\pm1.4$ ($0.08\pm0.79$) | $-0.7\pm1.9$ ($0.4\pm1.1$) | $-0.3\pm1.4$ ($0.17\pm0.79$) | $-3.4\pm4.7$ ($2.0\pm2.8$) | $-0.5\pm1.9$ ($0.3\pm1.1$) | $-17\pm10$ ($10.2\pm6.2$) |
| $t\bar{t}H(H\to b\bar{b})$ | $12\pm10$ ($13\pm11$) | $128\pm38$ ($137\pm41$) | $5.4\pm6.5$ ($5.9\pm7.1$) | $31\pm16$ ($34\pm17$) | $140\pm23$ ($151\pm24$) | $62\pm15$ ($68\pm16$) | $14.9\pm6.5$ ($15.8\pm6.9$) | $2.9\pm2.8$ ($3.1\pm3.0$) | $185\pm23$ ($201\pm25$) |
| $t\bar{t}Z(Z\to c\bar{c})$ | $8.0\pm9.0$ | $0.8\pm2.9$ | $36\pm21$ | $1.3\pm3.6$ | $1.9\pm2.6$ | $1.0\pm2.0$ | $10.4\pm6.7$ | $2.0\pm2.9$ | $51\pm14$ |
| $t\bar{t}Z(Z\to b\bar{b})$ | $3.1\pm6.5$ | $22\pm18$ | $4.7\pm8.3$ | $87\pm40$ | $62\pm19$ | $28\pm13$ | $6.2\pm5.4$ | $1.5\pm2.7$ | $75\pm19$ |
| $t\bar{t}$+≥2b | $73\pm32$ | $336\pm73$ | $55\pm28$ | $320\pm70$ | $1548\pm97$ | $452\pm50$ | $178\pm30$ | $28\pm11$ | $1677\pm89$ |
| $t\bar{t}$+b | $86\pm47$ | $96\pm49$ | $70\pm43$ | $88\pm50$ | $405\pm60$ | $742\pm86$ | $159\pm37$ | $45\pm20$ | $2040\pm130$ |
| $t\bar{t}$+≥2c | $296\pm81$ | $22\pm21$ | $260\pm75$ | $20\pm19$ | $74\pm22$ | $30\pm15$ | $653\pm72$ | $85\pm25$ | $2410\pm130$ |
| $t\bar{t}$+c | $163\pm59$ | $21\pm20$ | $113\pm48$ | $16\pm17$ | $49\pm18$ | $44\pm19$ | $180\pm39$ | $113\pm30$ | $2520\pm140$ |
| $t\bar{t}$+light | $213\pm42$ | $27\pm15$ | $165\pm36$ | $21\pm13$ | $44\pm11$ | $43\pm12$ | $122\pm20$ | $50\pm13$ | $4310\pm120$ |
| Other | $39\pm40$ | $13\pm20$ | $106\pm67$ | $18\pm23$ | $32\pm19$ | $24\pm15$ | $52\pm29$ | $17\pm16$ | $565\pm88$ |
| Total | $883\pm50$ | $665\pm42$ | $814\pm47$ | $602\pm40$ | $2357\pm74$ | $1426\pm63$ | $1372\pm64$ | $343\pm26$ | $13800\pm310$ |
| Data | 898 | 668 | 831 | 622 | 2345 | 1435 | 1382 | 357 | 13733 |

Table B.9: Event yields in the full analysis, separated in the SRs and CRs. Values in brackets correspond to the pre-fit expectations.

| Process | SR $t\bar{t}H(H\to c\bar{c})$ | SR $t\bar{t}H(H\to b\bar{b})$ | SR $t\bar{t}Z(Z\to c\bar{c})$ | SR $t\bar{t}Z(Z\to b\bar{b})$ | CR $t\bar{t}+\geq$2b | CR $t\bar{t}$+b | CR $t\bar{t}+\geq$2c | CR $t\bar{t}$+c | CR $t\bar{t}$+light |
|---|---|---|---|---|---|---|---|---|---|
| $t\bar{t}H(H\to c\bar{c})$ | $-27\pm40$ ($17\pm25$) | $-0.9\pm6.7$ ($0.5\pm3.8$) | $-5\pm16$ ($3.2\pm9.5$) | $-0.3\pm3.7$ ($0.2\pm2.1$) | $-2.0\pm5.4$ ($1.2\pm3.1$) | $-0.8\pm3.6$ ($0.5\pm2.1$) | $-16\pm16$ ($9.8\pm9.8$) | $-6.3\pm9.3$ ($3.9\pm5.7$) | $-46\pm28$ ($28\pm17$) |
| $t\bar{t}H(H\to b\bar{b})$ | $35\pm31$ ($38\pm34$) | $310\pm100$ ($340\pm110$) | $16\pm20$ ($17\pm21$) | $81\pm45$ ($88\pm49$) | $441\pm65$ ($475\pm71$) | $220\pm45$ ($242\pm50$) | $71\pm22$ ($75\pm24$) | $40\pm15$ ($43\pm17$) | $557\pm67$ ($607\pm73$) |
| $t\bar{t}Z(Z\to c\bar{c})$ | $25\pm28$ | $2.0\pm7.6$ | $105\pm63$ | $2.9\pm9.4$ | $5.8\pm7.3$ | $2.7\pm5.3$ | $51\pm23$ | $21\pm14$ | $143\pm40$ |
| $t\bar{t}Z(Z\to b\bar{b})$ | $10\pm21$ | $57\pm51$ | $14\pm25$ | $220\pm110$ | $218\pm58$ | $108\pm40$ | $34\pm20$ | $22\pm15$ | $263\pm58$ |
| $t\bar{t}+\geq$2b | $194\pm88$ | $770\pm180$ | $152\pm76$ | $730\pm170$ | $4680\pm260$ | $1530\pm140$ | $862\pm95$ | $335\pm53$ | $4890\pm240$ |
| $t\bar{t}$+b | $300\pm160$ | $320\pm160$ | $250\pm140$ | $270\pm150$ | $1830\pm200$ | $3740\pm310$ | $1050\pm150$ | $800\pm120$ | $8520\pm450$ |
| $t\bar{t}+\geq$2c | $830\pm210$ | $50\pm49$ | $710\pm190$ | $41\pm43$ | $244\pm56$ | $96\pm39$ | $2950\pm220$ | $850\pm100$ | $6330\pm320$ |
| $t\bar{t}$+c | $920\pm270$ | $84\pm78$ | $640\pm230$ | $64\pm70$ | $321\pm77$ | $358\pm94$ | $2210\pm230$ | $2960\pm250$ | $13030\pm590$ |
| $t\bar{t}$+light | $1050\pm160$ | $102\pm51$ | $810\pm140$ | $92\pm49$ | $257\pm39$ | $280\pm47$ | $1362\pm99$ | $1430\pm96$ | $18390\pm410$ |
| Other | $240\pm180$ | $58\pm76$ | $450\pm250$ | $82\pm88$ | $303\pm87$ | $169\pm56$ | $630\pm140$ | $453\pm100$ | $3950\pm350$ |
| Total | $3580\pm160$ | $1750\pm100$ | $3150\pm140$ | $1580\pm97$ | $8300\pm210$ | $6500\pm200$ | $9210\pm290$ | $6910\pm240$ | $56040\pm950$ |
| Data | 3545 | 1744 | 3143 | 1593 | 8322 | 6492 | 9245 | 6909 | 56014 |

Table B.10: Event yields in the full analysis, separated per lepton channel. Values in brackets correspond to the pre-fit expectations.

| Process | 2L | 1L | 0L | Total |
|---|---|---|---|---|
| $t\bar{t}H(H\to c\bar{c})$ | $-9\pm18$ ($6\pm11$) | $-62\pm69$ ($38\pm42$) | $-33\pm42$ ($20\pm25$) | $-100\pm130$ ($64\pm78$) |
| $t\bar{t}H(H\to b\bar{b})$ | $137\pm56$ ($151\pm62$) | $1060\pm220$ ($1150\pm240$) | $580\pm140$ ($630\pm150$) | $1770\pm410$ ($1930\pm450$) |
| $t\bar{t}Z(Z\to c\bar{c})$ | $32\pm27$ | $210\pm110$ | $112\pm65$ | $360\pm200$ |
| $t\bar{t}Z(Z\to b\bar{b})$ | $75\pm53$ | $580\pm210$ | $290\pm130$ | $940\pm400$ |
| $t\bar{t}+\geq$2b | $1060\pm180$ | $8420\pm650$ | $4670\pm480$ | $14100\pm1300$ |
| $t\bar{t}$+b | $1310\pm260$ | $12100\pm1000$ | $3730\pm530$ | $17100\pm1800$ |
| $t\bar{t}+\geq$2c | $940\pm160$ | $7320\pm610$ | $3850\pm460$ | $12100\pm1200$ |
| $t\bar{t}$+c | $1730\pm290$ | $15600\pm1200$ | $3220\pm390$ | $20600\pm1900$ |
| $t\bar{t}$+light | $1700\pm140$ | $17080\pm670$ | $4990\pm280$ | $23800\pm1100$ |
| Other | $430\pm200$ | $5040\pm810$ | $870\pm320$ | $6300\pm1300$ |
| Total | $7410\pm240$ | $67300\pm1400$ | $22270\pm720$ | $97000\pm2400$ |
| Data | 7366 | 67370 | 22271 | 97007 |

## B.5 Systematic uncertainties

Systematic uncertainties are evaluated by appropriate variations of the signal and background simulations. The uncertainty sources affect either the rate or the discriminant shape of the signal or background processes, or both. They are taken into account via nuisance parameters in the final profile likelihood fit. The effects from the same source are treated as fully correlated among the different categories.

The considered sources of uncertainties are listed in Table B.11 and described in detail in the following sections, grouped by experimental uncertainties in Section B.6 and modeling uncertainties in Section B.7. Their impact on the final result is discussed in Section B.9.

As for the final statistical inference, the templates corresponding to individual years are merged to obtain only one template. We then consider the appropriate correlation scheme in the following way. For correlated systematic uncertainties the templates are varied simultaneously in all years, while for decorrelated systematics the template of the corresponding year(s) are varied, and for all other years the nominal template is considered. This way, partial effects are correctly taken into account as partial variations.

Table B.11: Summary of the systematic uncertainty sources in the measurement. The first column lists the source of the uncertainty. The second (third) column indicates the treatment of correlations of the uncertainties between different data-taking periods (processes), where ✓ means fully correlated, $\sim$ means partially correlated (i.e., contains sub-sources that are either fully correlated or uncorrelated), and $\times$ means uncorrelated. The last column indicates whether the uncertainties are applied to all processes or only a subset.

| | Source | Corr. (period) | Corr. (process) | Processes |
|---|---|---|---|---|
| Experimental | Integrated luminosity | $\sim$ | ✓ | all |
| | Electron reconstruction and identification | ✓ | ✓ | all |
| | Muon reconstruction and identification | ✓ | ✓ | all |
| | Trigger efficiencies | $\times$ | ✓ | all |
| | Pileup reweighting | ✓ | ✓ | all |
| | Jet energy scale (11 sources) | $\sim$ | ✓ | all |
| | Jet energy resolution | $\times$ | ✓ | all |
| | Unclustered $p_{\mathrm{T}}^{\mathrm{miss}}$ | $\times$ | ✓ | all |
| | Jet flavor tagging | $\sim$ | ✓ | all |
| Modeling | Incl. cross sections & normalization | ✓ | $\sim$ | all |
| | $\mu_{\mathrm{R}}$ scale | ✓ | $\times$ | $\mathrm{t\bar{t}}$+jets, $\mathrm{t\bar{t}X}$, single t |
| | $\mu_{\mathrm{F}}$ scale | ✓ | $\times$ | $\mathrm{t\bar{t}}$+jets, $\mathrm{t\bar{t}X}$, single t |
| | PDF shape | ✓ | $\times$ | $\mathrm{t\bar{t}}$+jets, $\mathrm{t\bar{t}X}$ |
| | PS scales: ISR | ✓ | $\times$ | $\mathrm{t\bar{t}}$+jets, $\mathrm{t\bar{t}X}$, single t |
| | PS scales: FSR | ✓ | $\times$ | $\mathrm{t\bar{t}}$+jets, $\mathrm{t\bar{t}X}$, single t |
| | ME-PS matching ($h_{\mathrm{damp}}$) | ✓ | $\times$ | $\mathrm{t\bar{t}}$+jets |
| | ME (4 *vs.* 5 flavor scheme) | ✓ | $\times$ | $\mathrm{t\bar{t}}+\geq$1b |

## B.6 Experimental uncertainties

- **Luminosity:** The integrated luminosities of the data-taking periods are individually measured with uncertainties of 1.2, 2.3, and 2.5% for 2016, 2017, and 2018 data-taking periods, respectively [39–41]. The uncertainty in the integrated luminosity of the combined data set is 1.6%, when taking into account the correlations between the periods.

- **Lepton scale factors:** Separate $p_T$ and $\eta$ dependent uncertainties are assigned to the reconstruction and identification efficiencies for electrons in the simulation. Similarly, the muon tracking, identification, and isolation efficiencies are estimated. The associated uncertainties are propagated to the final discriminant distributions as a total shape uncertainty estimated from the sum of all sources and of the statistical and systematic components, separately for electrons and muons. The impact of the lepton calibration uncertainties in the final result is negligible.
- **Trigger scale factors:** The trigger efficiency scale factors are varied within their uncertainties, separately for each lepton number and flavor combination and the hadronic trigger selection.
- **Pileup reweighting:** The prediction of number of pileup interactions in simulation is performed with a total inelastic pp cross section of 69.2 mb. Changes in the assumed pileup multiplicity are estimated by varying the total inelastic cross section by $\pm 4.6\%$ [101]. This uncertainty is treated as fully correlated between data-taking periods.
- **L1 prefiring issue:** During the 2016–2017 data-taking periods, a gradual shift in the timing of the inputs of the ECAL L1 trigger in the forward endcap region ($|\eta| > 2.4$) led to a specific inefficiency, known as "prefiring". A similar effect is present for the muon system because of its limited time resolution, which was most pronounced in 2016 but also impacted data collected in 2017–2018. Corrections for this effect are applied to simulated events, and 20% of the corrections are assigned as the associated uncertainties.
- **Jet energy scale:** Uncertainties in the determination of the jet energy scale are taken into account by shifting the jet energy scale applied to the reconstructed jets in the simulation up and down by one standard deviation, separately for each of several sources of uncertainty, such as the overall energy scale, differences in flavor response, and residual differences between energy scale measurements [55]. Some of these sources are treated separately per data-taking period, while some are correlated for all periods.
- **Jet energy resolution:** Uncertainties in the jet energy resolution are evaluated by increasing or decreasing the difference between jet energies at reconstructed and particle level, or by smearing the measured jet energy in case no matching particle-level jet could be found [55]. This uncertainty is uncorrelated between data-taking periods.
- **Unclustered $p_T^{miss}$:** An additional uncertainty in $p_T^{miss}$ is derived by varying the energies of reconstructed particles not clustered into jets.
- **Jet flavor tagging:** Uncertainties in the flavor tagging calibration described in Section B.2 are taken into account. The flavor tagging uncertainties include statistical uncertainties in the derived SFs, effects due to the choice of the $\mu_F$ and $\mu_R$ scales, variations in PS ISR and FSR in PYTHIA, uncertainties in the fraction of b and c jets in the simulated W+jets and Z+jets events, jet energy scale and resolution uncertainties, and pileup uncertainties. The statistical uncertainties in the scale factors are treated as uncorrelated, while all the other uncertainties in the scale factors are treated as fully correlated.

## B.7 Modeling uncertainties

This measurement is strongly affected by uncertainties in the modeling of the $t\bar{t}$+jets background processes, especially the $t\bar{t}+\geq 1b$ processes. Variations applied to the $t\bar{t}$+jets background processes are defined such that the predicted yields in the inclusive phase space region before acceptance effects or any event selection remain constant for the individual processes. This procedure ensures that the modeling uncertainties for the $t\bar{t}$+jets processes only have an effect on the selection efficiency, and not on the cross section of the processes. The normalization of the individual processes are degrees of freedom in the binned profile likelihood fit. Furthermore, the uncertainty in the overall normalization of the $t\bar{t}$ process is covered with separate systematic uncertainties, as detailed below.

All modeling uncertainties are correlated between the data-taking years. Some uncertainties are correlated between processes.

- **Inclusive cross sections:** The expectation for the inclusive signal and background cross sections are derived from theoretical predictions of at least NLO accuracy. Uncertainties affecting these normalizations are split into a component due to the $\mu_R$ and $\mu_F$ scale uncertainties in the ME calculation and a component due to the PDF set and choice of the strong coupling constant $\alpha_S$ (PDF+$\alpha_S$) for the $t\bar{t}H$ signal and the $t\bar{t}Z$ process. These uncertainties are taken into account as rate-changing uncertainties in the final fit and are on the order of 9% for $t\bar{t}Z$ [102] and are split into three components for $t\bar{t}H$ production [98], taking into account the effects from variations of the scales ($^{+5.8\%}_{-9.2\%}$), $\alpha_S$ (2%), and the PDFs (3%).
- **Branching fractions:** For the $t\bar{t}H$ process, several rate-changing uncertainties are assigned to the signal and background contributions, depending on the final state. The uncertainties are taken from Ref. [98] and denote about 1.3% (10%) in total for $H\to b\bar{b}$ ($H\to c\bar{c}$) decays.
- **Renormalization and factorization scales:** Uncertainties due to the renormalization scale $\mu_R$ and the factorization scale $\mu_F$ in the ME generators are modeled by shifting the scales independently up and down by a factor of two. These uncertainties are treated separately for each process and for each of the seven $t\bar{t}$+jets background components.
- **PDF shape:** The NNPDF3.1 NNLO PDF set is used for the description of the substructure of the colliding protons in simulation. The shape variations of the fit distribution are evaluated by reweighting the simulated events with the replicas of the PDF set. We calculate the root-mean-square of all residuals for the 4FS PDF set, used for the $t\bar{t}+\geq 1b$ backgrounds. For the other processes, using the 5FS PDF set, the variations correspond to the eigenvectors of the PDF fit covariance matrix, and individual uncertainties are obtained from each eigenvector. Each eigenvector variation is treated as one separate uncertainty in the fit. An additional uncertainty from the value of $\alpha_S$, used in the PDFs, is included. These uncertainties are treated as correlated for all processes of common PDF flavor schemes.
- **PS scales ISR/FSR:** In order to estimate the impact of the choice of scale at which $\alpha_S$ is evaluated in the PS simulation, the scales in the shower simulation are varied up and down by a factor of two, independently for ISR and FSR. For both ISR and FSR, the uncertainties are split into 8 separate components. We individually vary the scales and nonsingular terms for the splitting kernels $g\to gg$, $g\to q\bar{q}$, $q\to qg$, $x\to xg$, where $x = t, b$, as implemented in PYTHIA v8 [103]. These uncertainties are considered as uncorrelated for all processes.

- **ME-PS matching ($h_{\mathrm{damp}}$):** In the POWHEG generator, the scale that separates the phase space of the first QCD emission into soft and hard parts is controlled via the $h_{\mathrm{damp}}$ parameter. For the CP5 tune, when POWHEG is matched to the PYTHIA v8 [103] PS, the central value of $h_{\mathrm{damp}}$ is set to $h_{\mathrm{damp}} = 1.379 m_{\mathrm{t}}$, and the uncertainties are estimated with varied values of $h_{\mathrm{damp}} = 2.305 m_{\mathrm{t}}$ and $0.874 m_{\mathrm{t}}$ for the $\mathrm{t\bar{t}}$ and $\mathrm{t\bar{t}}+{\geq}1\mathrm{b}$ simulations. The alternative predictions with varied $h_{\mathrm{damp}}$ values are obtained via an ML-reweighting approach [104]. This uncertainty is treated as uncorrelated between the different $\mathrm{t\bar{t}}$+jets processes.
- **Background normalization:** To account for the known issues in the modeling of different background processes, we assign the following normalization uncertainties: 25% for single top quark, 100% for tWZ due to the discrepancies between prediction and measurements [105], 6.8% for $\mathrm{t\bar{t}W}$ [106], and 50% for the relative $\mathrm{t\bar{t}}+\mathrm{j_{bb}}$ and $\mathrm{t\bar{t}}+\mathrm{j_{cc}}$ contributions with respect to $\mathrm{t\bar{t}}+\mathrm{j_b}$ and $\mathrm{t\bar{t}}+\mathrm{j_c}$, respectively, to account for the limited knowledge of the rate of collinear gluon splitting.
- **$\mathrm{t\bar{t}b\bar{b}}$ DPS normalization:** The $\mathrm{t\bar{t}b\bar{b}}$ DPS cross section is not precisely known and an estimate of the effective cross section for DPS is used, which is process dependent. Different measurements of this effective cross section range between 10–30 mb [99], while the PYTHIA reference value is 30 mb. Given the limited knowledge of the effective cross section value for $\mathrm{t\bar{t}b\bar{b}}$ DPS, a 50% normalization uncertainty is applied to the $\mathrm{t\bar{t}b\bar{b}}$ DPS contributions.
- **$\mathrm{t\bar{t}}+{\geq}$1b modeling differences:** The nominal model for the estimation of the $\mathrm{t\bar{t}}+{\geq}1\mathrm{b}$ background relies on the NLO ME description of $\mathrm{t\bar{t}}+{\geq}2\mathrm{b}$ using POWHEG-BOX-RES, interfaced with PYTHIA for parton showering and hadronization. Dedicated measurements of $\mathrm{t\bar{t}}+{\geq}1\mathrm{b}$ production show that this simulation approach is able to describe the most relevant observables in data [65], when taking into account the systematic modeling uncertainties described previously. Nevertheless, in order to provide additional freedom for the background model, the difference between the nominal model and the description of $\mathrm{t\bar{t}}+{\geq}1\mathrm{b}$ with the $\mathrm{t\bar{t}}$-inclusive NLO POWHEG model, interfaced with PYTHIA, is used as a systematic uncertainty. The variations are normalized to the nominal event yield after baseline selection. This alternative $\mathrm{t\bar{t}}+{\geq}1\mathrm{b}$ model does not describe relevant physics objects significantly differently than the nominal background model. This uncertainty is considered decorrelated for the $\mathrm{t\bar{t}}+\mathrm{j_b}$ processes and decorrelated among all four SRs.

## B.8 Validation of the background model

A signal-depleted sideband validation region (VR), with a partition into a control-like region for $0.40 < \mathcal{D}_{\mathrm{t\bar{t}X}} < 0.58$ and a signal-like region for $0.58 < \mathcal{D}_{\mathrm{t\bar{t}X}} < 0.60$, analogous to the AR partition into a CR and a SR, is used to validate the background estimation strategy, and good agreement is observed between data and estimated backgrounds, as shown in Fig. B.6. Each region in the VR is defined such that the purity of the background components is as close as possible to those in the CRs and SRs.

## B.9 Additional results

The production rates of the signal processes and the normalization factors of the $\mathrm{t\bar{t}}$ background components are determined via a binned profile likelihood fit to data in all the SRs and CRs. The fitted observables are described in Section B.4. Figure B.7 shows the observed yields in each bin of the event classifier discriminant for all CRs and SRs, along with the fitted signal and background yields. Figures B.8–B.9 summarize the results of the measurements of the

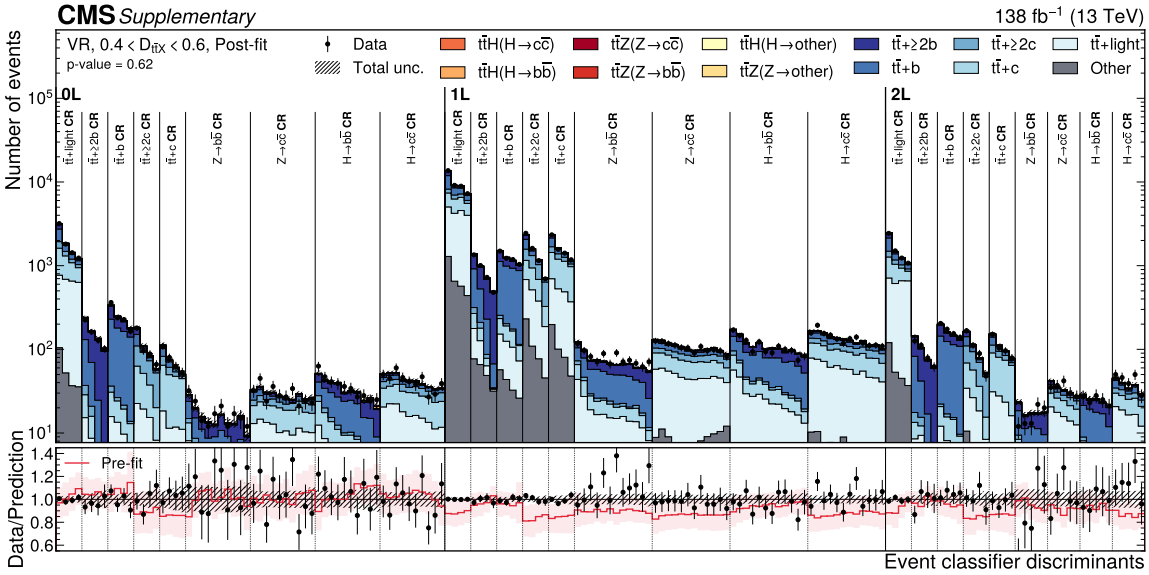


Figure B.6: Distributions of the PART discriminants in data (points) and predicted signal and backgrounds (colored histograms) after the maximum likelihood fit to data in the VR, defined by $0.4 < \mathcal{D}_{t\bar{t}X} < 0.6$. The vertical bars on the points represent the statistical uncertainties in data. The hatched band represents the total uncertainty in the sum of the signal and background predictions. The lower panel shows the ratio of the data to the sum of the signal and background predictions. The ratio of the pre-fit expectation to the sum of the signal and background predictions after the fit is shown as a red line in the lower panel, including the pre-fit uncertainties as a shaded band.

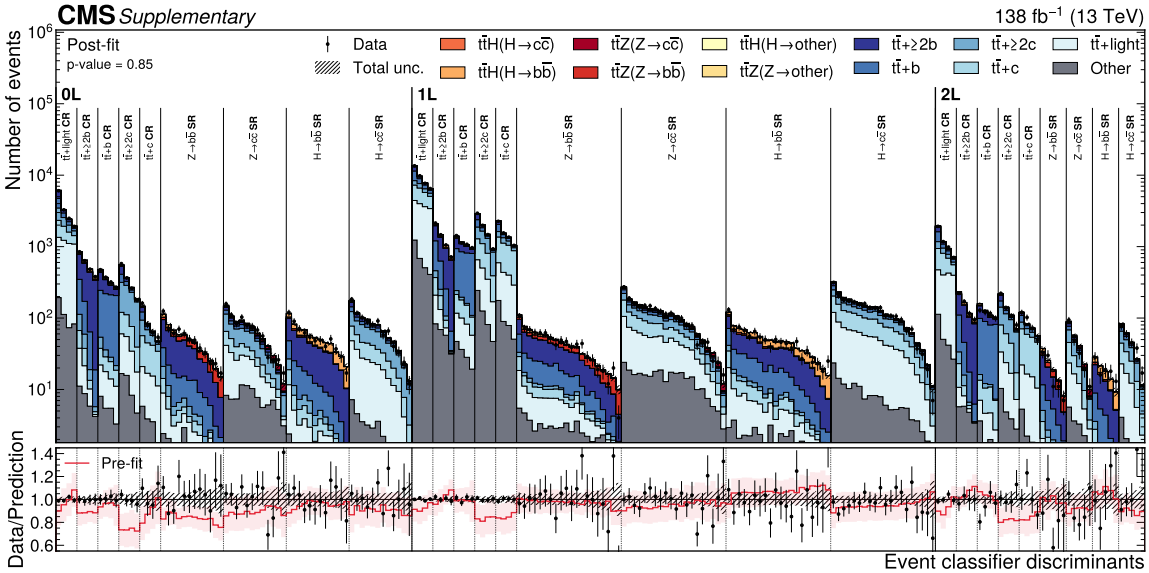


Figure B.7: Distributions of the PART discriminants in data (points) and predicted signal and backgrounds (colored histograms) after the maximum likelihood fit to data. The vertical bars on the points represent the statistical uncertainties in data. The hatched band represents the total uncertainty in the sum of the signal and background predictions. The lower panel shows the ratio of the data to the sum of the signal and background predictions. The ratio of the pre-fit expectation to the sum of the signal and background predictions after the fit is shown as a red line in the lower panel, including the pre-fit uncertainties as a shaded band.

$t\bar{t}Z(Z\to c\bar{c})$ and $t\bar{t}Z(Z\to b\bar{b})$ signal strengths, respectively, obtained from the simultaneous fit of all four signal strength parameters and all SRs and CRs. Figure B.10 shows the contributions from the individual channels for the best fit values of $\mu_{t\bar{t}H(H\to b\bar{b})}$.

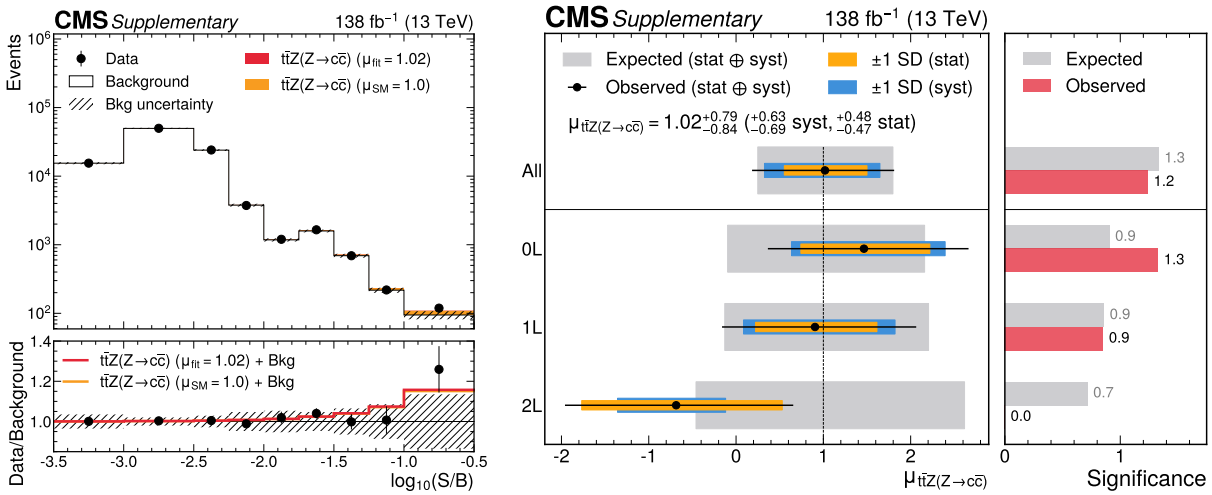


Figure B.8: On the left, observed and expected event yields from all SRs and CRs as a function of $\log_{10}(S/B)$, where $S$ are the observed $t\bar{t}Z(Z\to c\bar{c})$ yields, and $B$ are the total background yields in the combined fit to data. The signals are shown for the best fit signal strength (red), and the SM prediction, $\mu = 1$ (orange). The lower panel shows the ratio of the data to the post-fit background prediction, compared to the signal-plus-background predictions. On the right, fit results of $\mu_{t\bar{t}Z(Z\to c\bar{c})}$ in the combination of channels (first row) and the channels individually (lower rows). The left panel shows the observed signal strength, compared to the expected results. The right panel shows the expected and observed significance.

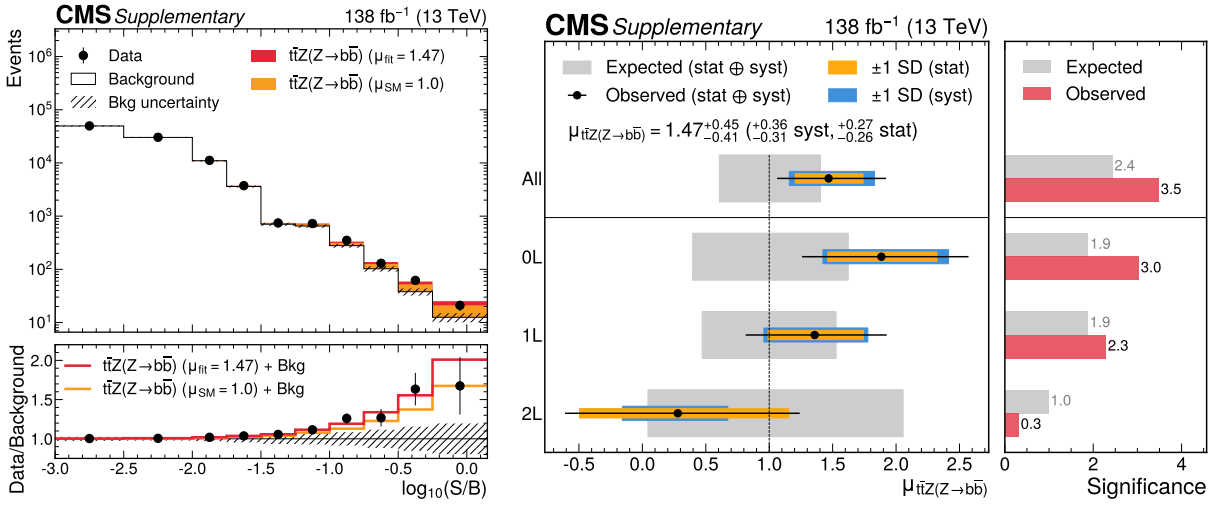


Figure B.9: On the left, observed and expected event yields from all SRs and CRs as a function of $\log_{10}(S/B)$, where $S$ are the observed $t\bar{t}Z(Z\to b\bar{b})$ yields, and $B$ are the total background yields in the combined fit to data. The signals are shown for the best fit signal strength (red), and the SM prediction, $\mu = 1$ (orange). The lower panel shows the ratio of the data to the post-fit background prediction, compared to the signal-plus-background predictions. On the right, fit results of $\mu_{t\bar{t}Z(Z\to b\bar{b})}$ in the combination of channels (first row) and the channels individually (lower rows). The left panel shows the observed signal strength, compared to the expected results. The right panel shows the expected and observed significance.

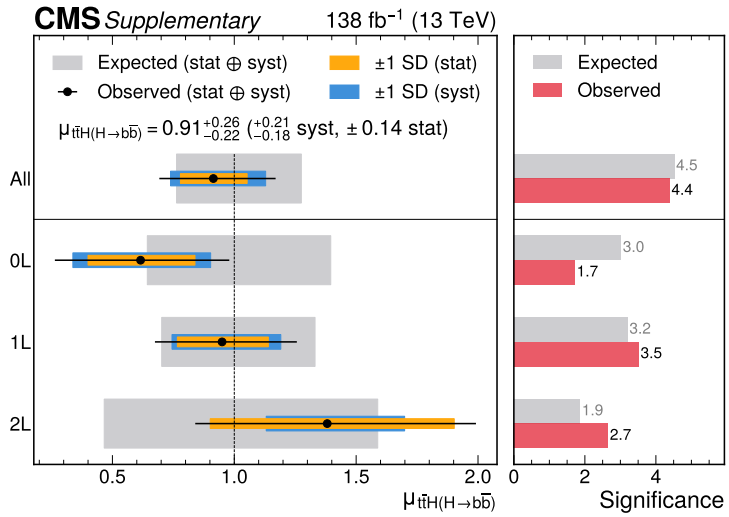


Figure B.10: Fit results of $\mu_{t\bar{t}H(H\to b\bar{b})}$. The left panel shows the observed signal strength, compared to the expected results. The right panel shows the expected and observed significance.

The result is interpreted in the $\kappa$-framework [97, 98]. The one-dimensional likelihood scan for $\kappa_c$ is shown in Fig. B.11, both for a fixed and a floating $\kappa_b$ value.

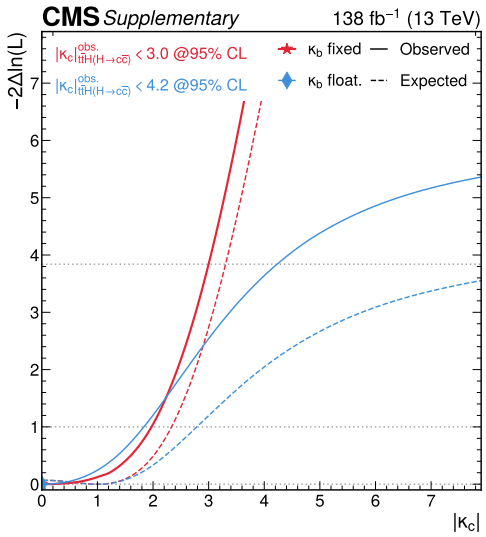


Figure B.11: Likelihood scans of $\kappa_c$ with fixed $\kappa_b = 1$ (red) and floating $\kappa_b$ (blue). The 68% and 95% CL intervals are indicated by the horizontal dotted lines.

The search is combined with a previous search in the VH channel [36]. All uncertainties in experimental effects, such as jet energy scale and resolution, lepton identification efficiencies, the modeling of detector effects, pileup and $p_T^{miss}$ modeling, and the integrated luminosity are correlated. The flavor (mis-)tagging scale factors of the merged and resolved VH analyses are treated as uncorrelated with this measurement because of the differences in jet tagging algorithms and jet cone sizes, as well as in calibration methods. All uncertainties in the background and signal modeling are considered uncorrelated as well, since the main background in the VH analysis, Z+jets and W+jets production in association with heavy-flavor jets, and the VH signal contribution are negligible for this analysis. The dominant systematic uncertainties in each measurement are the normalization and modeling of the background components, which are negligible in the respective other measurement. Theoretical uncertainties such as in the Higgs boson branching fraction and production cross section are correlated. Each input mea-

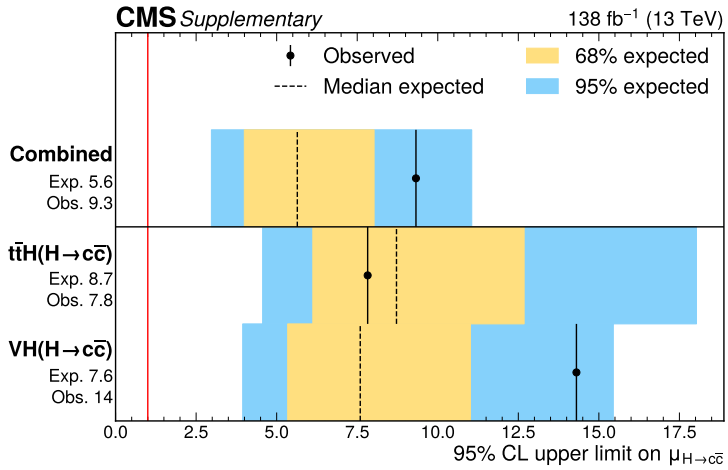


Figure B.12: The 95% CL upper limits on $\mu_{H\to c\bar{c}}$. The blue and yellow bands indicate the expected 68% and 95% CL regions, respectively, under the background-only hypothesis. The vertical red line indicates the SM value $\mu_{H\to c\bar{c}} = 1$.

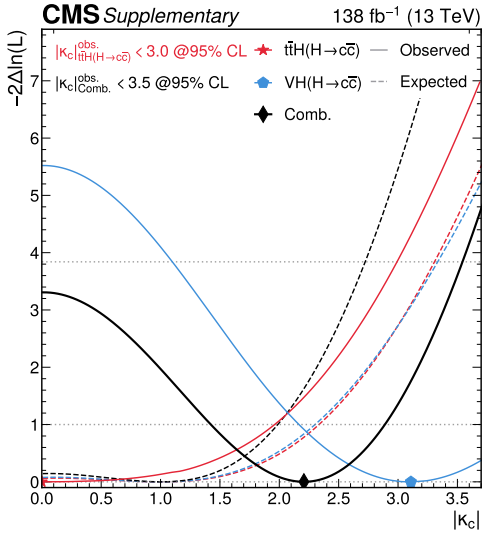


Figure B.13: Likelihood scans of $\kappa_c$ with fixed $\kappa_b = 1$ in the individual $t\bar{t}H$ (red) and VH (blue) channels and their combination (black). The 68% and 95% CL intervals are indicated by the horizontal dotted lines.

surement is limited by statistical uncertainties. The observed and expected 95% CL upper limit on $\mu_{H\to c\bar{c}}$, the signal strength for the $H\to c\bar{c}$ decay channel assuming SM production rates for $t\bar{t}H$ and VH, is displayed in Fig. B.12, along with the contributions from individual analyses. Figure B.13 shows the profile likelihood scan of $|\kappa_c|$ in the combined analysis.

Figures B.14–B.16 show likelihood scans for the simultaneous fit of two parameters each, e.g., for pairs of the four signal strength parameters $\mu_{t\bar{t}H(H\to c\bar{c})}$, $\mu_{t\bar{t}H(H\to b\bar{b})}$, $\mu_{t\bar{t}Z(Z\to b\bar{b})}$, and $\mu_{t\bar{t}Z(Z\to c\bar{c})}$, and for pairs of the normalization scale factors of the $t\bar{t}$+jets background components $t\bar{t}+\geq$2b, $t\bar{t}$+b, $t\bar{t}+\geq$2c, and $t\bar{t}$+c.

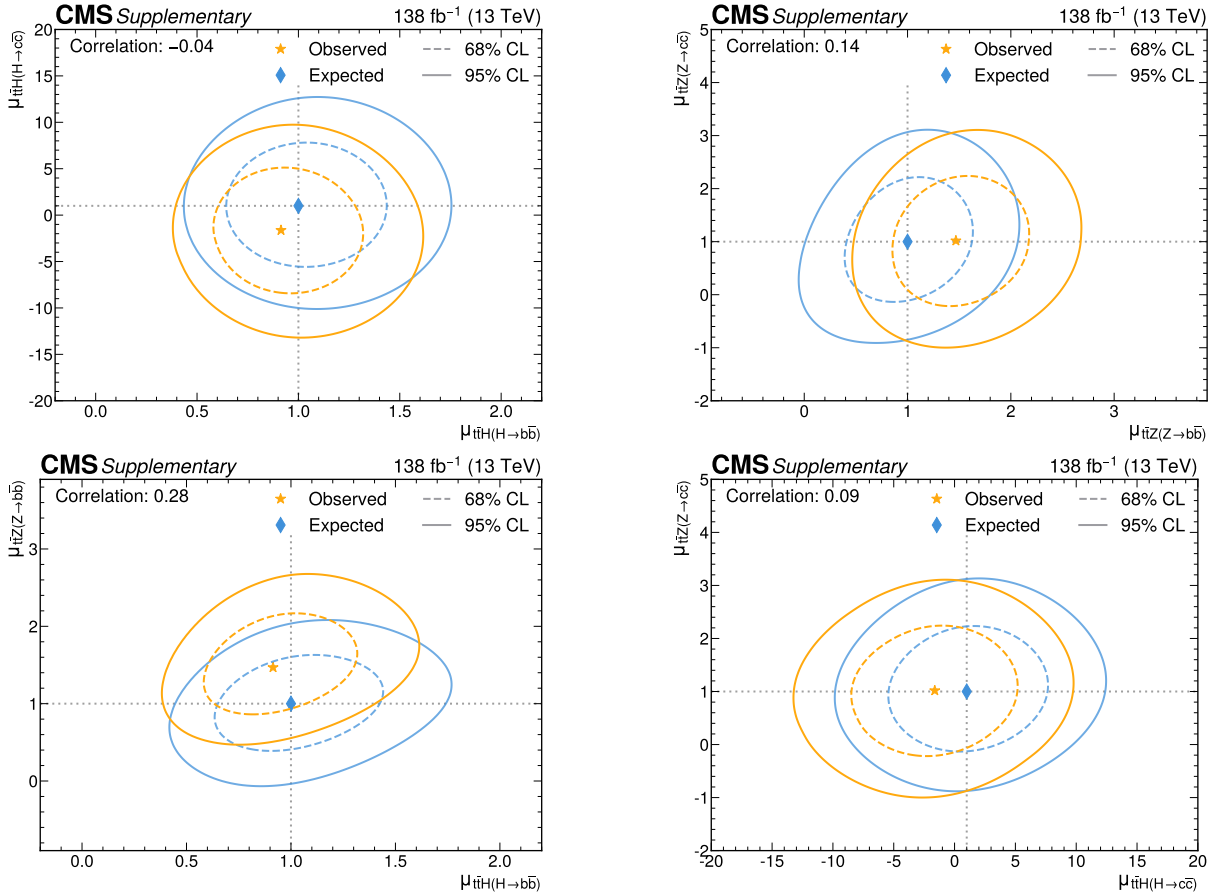


Figure B.14: Likelihood scans for the simultaneous fit of $\mu_{t\bar{t}H(H\to b\bar{b})}$ and $\mu_{t\bar{t}H(H\to c\bar{c})}$ (upper left), $\mu_{t\bar{t}Z(Z\to b\bar{b})}$ and $\mu_{t\bar{t}Z(Z\to c\bar{c})}$ (upper right), $\mu_{t\bar{t}H(H\to b\bar{b})}$ and $\mu_{t\bar{t}Z(Z\to b\bar{b})}$ (lower left), and $\mu_{t\bar{t}H(H\to c\bar{c})}$ and $\mu_{t\bar{t}Z(Z\to c\bar{c})}$ (lower right). The 68% (95%) CL intervals are indicated by the dotted (solid) lines. The observed (expected) best fit values are shown by the orange (blue) markers.

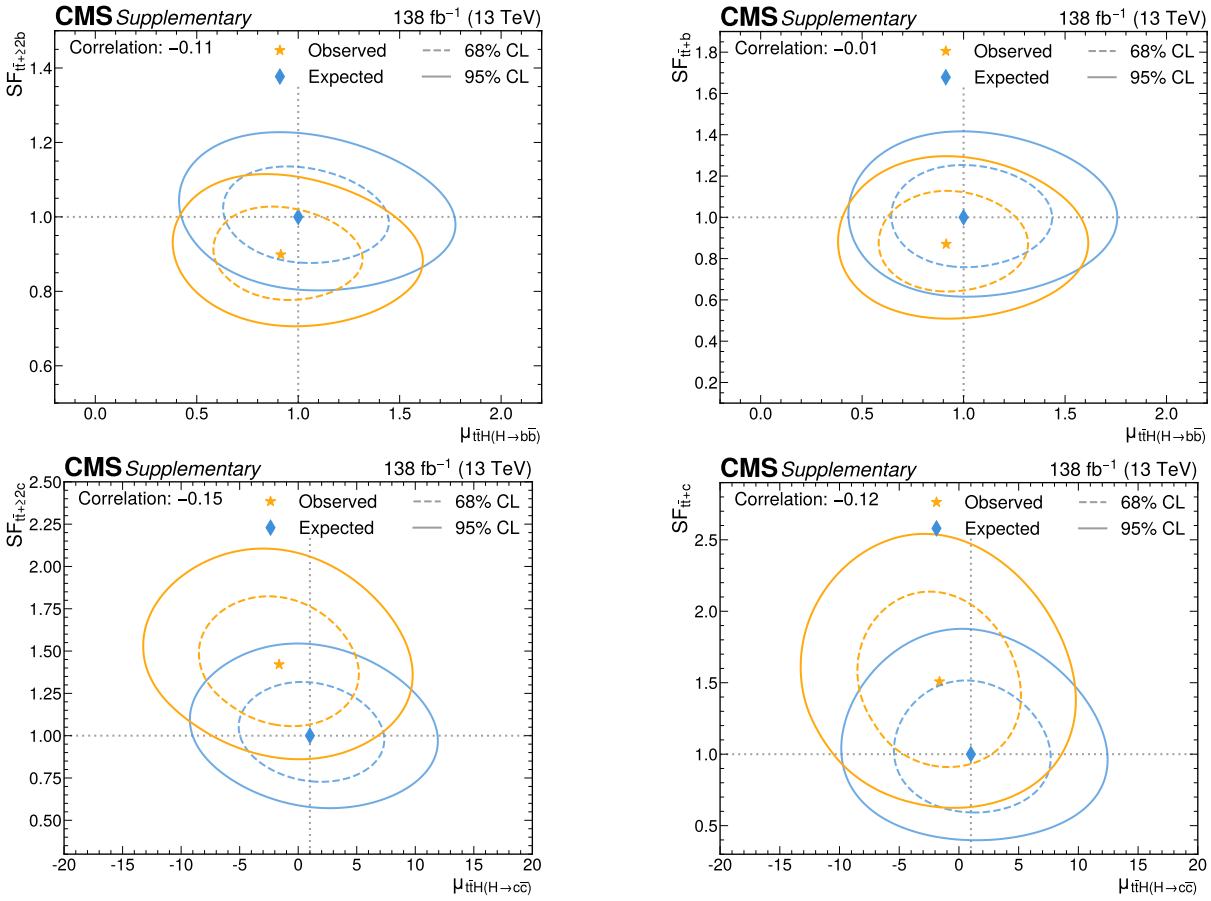


Figure B.15: Likelihood scans for the simultaneous fit of $\mu_{t\bar{t}H(H\to b\bar{b})}$ and the $t\bar{t}+\geq 2b$ scale factor (upper left), $\mu_{t\bar{t}H(H\to b\bar{b})}$ and the $t\bar{t}+b$ scale factor (upper right), $\mu_{t\bar{t}H(H\to c\bar{c})}$ and the $t\bar{t}+\geq 2c$ scale factor (lower left), and $\mu_{t\bar{t}H(H\to c\bar{c})}$ and the $t\bar{t}+c$ scale factor (lower right). The 68% (95%) CL intervals are indicated by the dotted (solid) lines. The observed (expected) best fit values are shown by the orange (blue) markers.

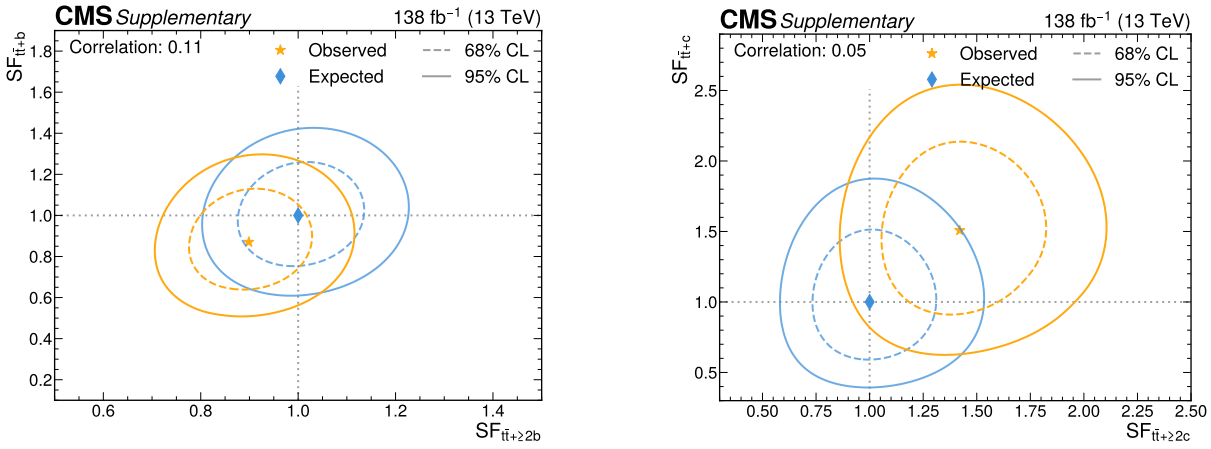


Figure B.16: Likelihood scans for the simultaneous fit of the $t\bar{t}+\geq 2b$ and $t\bar{t}+b$ scale factors (left), and of the $t\bar{t}+\geq 2c$ and $t\bar{t}+c$ scale factors (right). The 68% (95%) CL intervals are indicated by the dotted (solid) lines. The observed (expected) best fit values are shown by the orange (blue) markers.

## B.10 Cross checks with alternative $t\bar{t}+\geq 1b$ background models

The robustness of the results is assessed by performing the fit for the signal strength parameters using alternative background models, focusing on variations of the $t\bar{t}+\geq 1b$ background model:

(1) **Simple PS:** Using a simplified scheme of the PS uncertainties with only one ISR and FSR scale uncertainty instead of the 16 individual components.

(2) $\boldsymbol{\mu_F \times 2}$**:** Changing $\mu_F$ by a factor two in the $t\bar{t}+\geq 1b$ simulation and otherwise using the same $t\bar{t}+\geq 1b$ uncertainty model. This alternative $\mu_F$ and $\mu_R$ choice corresponds to the setup used in the recent measurement of $t\bar{t}H(H\to b\bar{b})$ production by the ATLAS Collaboration [107].

(3) $\boldsymbol{\mu_F \times 2}$ **& Simple PS:** As described in (2), but using the simplification of (1).

(4) **5FS** $\boldsymbol{t\bar{t}+\geq 1b}$**:** Using the 5FS $t\bar{t}+\geq 1b$ simulation as the nominal background model.

(5) **5FS** $\boldsymbol{t\bar{t}+\geq 1b}$ **& Simple PS:** As described in (4), but using the simplification of (1).

The results for the nominal fit setup as well as for variations are given in Table B.12 for the best fit signal strength parameters, the observed upper limits and the significance on the signal strengths, and in Table B.13 for the $t\bar{t}+\geq 1b$ background normalization parameters.

Table B.12: Observed signal strengths for $t\bar{t}H(H\to c\bar{c})$, $t\bar{t}H(H\to b\bar{b})$, $t\bar{t}Z(Z\to c\bar{c})$, and $t\bar{t}Z(Z\to b\bar{b})$ as obtained by the fits using alternative background models. In brackets are the observed upper limits for $t\bar{t}H(H\to c\bar{c})$ and the significance values for $t\bar{t}H(H\to b\bar{b})$, $t\bar{t}Z(Z\to c\bar{c})$, and $t\bar{t}Z(Z\to b\bar{b})$, respectively.

| $t\bar{t}+\geq 1b$ bkg. model | $\mu_{t\bar{t}H(H\to c\bar{c})}$ | (95% CL) | $\mu_{t\bar{t}H(H\to b\bar{b})}$ | (Sign. [s.d.]) | $\mu_{t\bar{t}Z(Z\to c\bar{c})}$ | (Sign. [s.d.]) | $\mu_{t\bar{t}Z(Z\to b\bar{b})}$ | (Sign. [s.d.]) |
|---|---|---|---|---|---|---|---|---|
| Default | $-1.6 \pm 4.5$ | (<7.8) | $0.91^{+0.26}_{-0.22}$ | (4.4) | $1.02^{+0.79}_{-0.84}$ | (1.2) | $1.47^{+0.45}_{-0.41}$ | (3.5) |
| Simple PS | $-0.4 \pm 4.4$ | (<8.8) | $0.91^{+0.27}_{-0.22}$ | (4.4) | $0.94^{+0.82}_{-0.73}$ | (1.3) | $1.47^{+0.44}_{-0.39}$ | (3.6) |
| $\mu_F \times 2$ | $-1.7^{+4.2}_{-4.3}$ | (<8.0) | $0.94^{+0.26}_{-0.23}$ | (4.4) | $1.06^{+0.77}_{-0.75}$ | (1.4) | $1.62^{+0.43}_{-0.38}$ | (4.1) |
| $\mu_F \times 2$ & Simple PS | $-1.0 \pm 4.4$ | (<8.5) | $0.97^{+0.28}_{-0.23}$ | (4.5) | $1.04^{+0.77}_{-0.78}$ | (1.3) | $1.67^{+0.42}_{-0.37}$ | (4.2) |
| 5FS | $-1.8 \pm 4.3$ | (<7.7) | $0.97^{+0.24}_{-0.20}$ | (5.7) | $1.17^{+0.77}_{-0.71}$ | (1.6) | $1.14^{+0.41}_{-0.38}$ | (3.0) |
| 5FS & Simple PS | $-0.9 \pm 4.5$ | (<7.6) | $1.02^{+0.26}_{-0.21}$ | (6.0) | $1.19^{+0.77}_{-0.71}$ | (1.6) | $1.10^{+0.40}_{-0.37}$ | (2.9) |

Table B.13: Observed normalization scale factors for the background components as obtained by the fits using alternative background models. The background normalization scale factors are given for the 2L & 1L (0L) channels.

| $t\bar{t}+\geq 1b$ background model | $t\bar{t}+\geq 2b$ | $t\bar{t}+b$ |
|---|---|---|
| Default | $0.90 \pm 0.08$ ($1.14 \pm 0.12$) | $0.87 \pm 0.15$ ($0.83 \pm 0.16$) |
| Simple PS | $0.88 \pm 0.07$ ($1.12 \pm 0.11$) | $0.92 \pm 0.16$ ($0.89 \pm 0.18$) |
| $\mu_F \times 2$ | $0.89 \pm 0.06$ ($1.37 \pm 0.10$) | $0.94 \pm 0.17$ ($1.05 \pm 0.21$) |
| $\mu_F \times 2$ & Simple PS | $0.90 \pm 0.05$ ($1.41 \pm 0.10$) | $0.95 \pm 0.16$ ($1.06 \pm 0.22$) |
| 5FS | $1.54 \pm 0.11$ ($2.06 \pm 0.19$) | $0.91 \pm 0.36$ ($0.62 \pm 0.64$) |
| 5FS & Simple PS | $1.57 \pm 0.09$ ($2.25 \pm 0.21$) | $0.83 \pm 0.34$ ($0.60 \pm 0.62$) |

# C The CMS Collaboration

**Yerevan Physics Institute, Yerevan, Armenia**
A. Hayrapetyan, V. Makarenko, A. Tumasyan[1]

**Institut für Hochenergiephysik, Vienna, Austria**
W. Adam, J.W. Andrejkovic, L. Benato, T. Bergauer, M. Dragicevic, C. Giordano, P.S. Hussain, M. Jeitler[2], N. Krammer, A. Li, D. Liko, M. Matthewman, I. Mikulec, J. Schieck[2], R. Schöfbeck[2], D. Schwarz, M. Shooshtari, M. Sonawane, W. Waltenberger, C.-E. Wulz[2]

**Universiteit Antwerpen, Antwerpen, Belgium**
T. Janssen, H. Kwon, D. Ocampo Henao, T. Van Laer, P. Van Mechelen

**Vrije Universiteit Brussel, Brussel, Belgium**
J. Bierkens, N. Breugelmans, J. D'Hondt, S. Dansana, A. De Moor, M. Delcourt, F. Heyen, Y. Hong, P. Kashko, S. Lowette, I. Makarenko, D. Müller, J. Song, S. Tavernier, M. Tytgat[3], G.P. Van Onsem, S. Van Putte, D. Vannerom

**Université Libre de Bruxelles, Bruxelles, Belgium**
B. Bilin, B. Clerbaux, A.K. Das, I. De Bruyn, G. De Lentdecker, H. Evard, L. Favart, P. Gianneios, A. Khalilzadeh, F.A. Khan, A. Malara, M.A. Shahzad, L. Thomas, M. Vanden Bemden, C. Vander Velde, P. Vanlaer, F. Zhang

**Ghent University, Ghent, Belgium**
M. De Coen, D. Dobur, G. Gokbulut, J. Knolle, D. Marckx, K. Skovpen, N. Van Den Bossche, J. van der Linden, J. Vandenbroeck, L. Wezenbeek

**Université Catholique de Louvain, Louvain-la-Neuve, Belgium**
S. Bein, A. Benecke, A. Bethani, G. Bruno, A. Cappati, J. De Favereau De Jeneret, C. Delaere, A. Giammanco, A.O. Guzel, V. Lemaitre, J. Lidrych, P. Malek, P. Mastrapasqua, S. Turkcapar

**Centro Brasileiro de Pesquisas Fisicas, Rio de Janeiro, Brazil**
G.A. Alves, M. Barroso Ferreira Filho, E. Coelho, C. Hensel, T. Menezes De Oliveira, C. Mora Herrera[4], P. Rebello Teles, M. Soeiro, E.J. Tonelli Manganote[5], A. Vilela Pereira[4]

**Universidade do Estado do Rio de Janeiro, Rio de Janeiro, Brazil**
W.L. Aldá Júnior, H. Brandao Malbouisson, W. Carvalho, J. Chinellato[6], M. Costa Reis, E.M. Da Costa, G.G. Da Silveira[7], D. De Jesus Damiao, S. Fonseca De Souza, R. Gomes De Souza, S. S. Jesus, T. Laux Kuhn[7], M. Macedo, K. Mota Amarilo, L. Mundim, H. Nogima, J.P. Pinheiro, A. Santoro, A. Sznajder, M. Thiel, F. Torres Da Silva De Araujo[8]

**Universidade Estadual Paulista, Universidade Federal do ABC, São Paulo, Brazil**
C.A. Bernardes[7], F. Damas, T.R. Fernandez Perez Tomei, E.M. Gregores, B. Lopes Da Costa, I. Maietto Silverio, P.G. Mercadante, S.F. Novaes, B. Orzari, Sandra S. Padula, V. Scheurer

**Institute for Nuclear Research and Nuclear Energy, Bulgarian Academy of Sciences, Sofia, Bulgaria**
A. Aleksandrov, G. Antchev, P. Danev, R. Hadjiiska, P. Iaydjiev, M. Shopova, G. Sultanov

**University of Sofia, Sofia, Bulgaria**
A. Dimitrov, L. Litov, B. Pavlov, P. Petkov, A. Petrov

**Instituto De Alta Investigación, Universidad de Tarapacá, Casilla 7 D, Arica, Chile**
S. Keshri, D. Laroze, S. Thakur

**Universidad Tecnica Federico Santa Maria, Valparaiso, Chile**
W. Brooks

**Beihang University, Beijing, China**
T. Cheng, T. Javaid, L. Wang, L. Yuan

**Department of Physics, Tsinghua University, Beijing, China**
Z. Hu, Z. Liang, J. Liu, X. Wang

**Institute of High Energy Physics, Beijing, China**
G.M. Chen[9], H.S. Chen[9], M. Chen[9], Y. Chen, Q. Hou, X. Hou, F. Iemmi, C.H. Jiang, A. Kapoor[10], H. Liao, G. Liu, Z.-A. Liu[11], J.N. Song[11], S. Song, J. Tao, C. Wang[9], J. Wang, H. Zhang, J. Zhao

**State Key Laboratory of Nuclear Physics and Technology, Peking University, Beijing, China**
A. Agapitos, Y. Ban, A. Carvalho Antunes De Oliveira, S. Deng, B. Guo, Q. Guo, C. Jiang, A. Levin, C. Li, Q. Li, Y. Mao, S. Qian, S.J. Qian, X. Qin, C. Quaranta, X. Sun, D. Wang, J. Wang, H. Yang, M. Zhang, Y. Zhao, C. Zhou

**State Key Laboratory of Nuclear Physics and Technology, Institute of Quantum Matter, South China Normal University, Guangzhou, China**
S. Yang

**Sun Yat-Sen University, Guangzhou, China**
Z. You

**University of Science and Technology of China, Hefei, China**
K. Jaffel, N. Lu

**Nanjing Normal University, Nanjing, China**
G. Bauer[12,13], B. Li[14], H. Wang, K. Yi[15], J. Zhang

**Institute of Modern Physics and Key Laboratory of Nuclear Physics and Ion-beam Application (MOE) - Fudan University, Shanghai, China**
Y. Li

**Zhejiang University, Hangzhou, Zhejiang, China**
Z. Lin, C. Lu, M. Xiao[16]

**Universidad de Los Andes, Bogota, Colombia**
C. Avila, D.A. Barbosa Trujillo, A. Cabrera, C. Florez, J. Fraga, J.A. Reyes Vega

**Universidad de Antioquia, Medellin, Colombia**
C. Rendón, M. Rodriguez, A.A. Ruales Barbosa, J.D. Ruiz Alvarez

**University of Split, Faculty of Electrical Engineering, Mechanical Engineering and Naval Architecture, Split, Croatia**
N. Godinovic, D. Lelas, A. Sculac

**University of Split, Faculty of Science, Split, Croatia**
M. Kovac, A. Petkovic, T. Sculac

**Institute Rudjer Boskovic, Zagreb, Croatia**
P. Bargassa, V. Brigljevic, B.K. Chitroda, D. Ferencek, K. Jakovcic, A. Starodumov, T. Susa

**University of Cyprus, Nicosia, Cyprus**
A. Attikis, K. Christoforou, A. Hadjiagapiou, C. Leonidou, C. Nicolaou, L. Paizanos, F. Ptochos, P.A. Razis, H. Rykaczewski, H. Saka, A. Stepennov

**Charles University, Prague, Czech Republic**
M. Finger[†], M. Finger Jr.

**Escuela Politecnica Nacional, Quito, Ecuador**
E. Ayala

**Universidad San Francisco de Quito, Quito, Ecuador**
E. Carrera Jarrin

**Academy of Scientific Research and Technology of the Arab Republic of Egypt, Egyptian Network of High Energy Physics, Cairo, Egypt**
A.A. Abdelalim[17,18], R. Aly[19,17]

**Center for High Energy Physics (CHEP-FU), Fayoum University, El-Fayoum, Egypt**
M. Abdullah Al-Mashad, A. Hussein, H. Mohammed

**National Institute of Chemical Physics and Biophysics, Tallinn, Estonia**
K. Ehataht, M. Kadastik, T. Lange, C. Nielsen, J. Pata, M. Raidal, N. Seeba, L. Tani

**Department of Physics, University of Helsinki, Helsinki, Finland**
A. Milieva, K. Osterberg, M. Voutilainen

**Helsinki Institute of Physics, Helsinki, Finland**
N. Bin Norjoharuddeen, E. Brücken, F. Garcia, P. Inkaew, K.T.S. Kallonen, R. Kumar Verma, T. Lampén, K. Lassila-Perini, B. Lehtela, S. Lehti, T. Lindén, N.R. Mancilla Xinto, M. Myllymäki, M.m. Rantanen, S. Saariokari, N.T. Toikka, J. Tuominiemi

**Lappeenranta-Lahti University of Technology, Lappeenranta, Finland**
H. Kirschenmann, P. Luukka, H. Petrow

**IRFU, CEA, Université Paris-Saclay, Gif-sur-Yvette, France**
M. Besancon, F. Couderc, M. Dejardin, D. Denegri, P. Devouge, J.L. Faure, F. Ferri, P. Gaigne, S. Ganjour, P. Gras, G. Hamel de Monchenault, M. Kumar, V. Lohezic, J. Malcles, F. Orlandi, L. Portales, S. Ronchi, M.Ö. Sahin, A. Savoy-Navarro[20], P. Simkina, M. Titov, M. Tornago

**Laboratoire Leprince-Ringuet, CNRS/IN2P3, Ecole Polytechnique, Institut Polytechnique de Paris, Palaiseau, France**
F. Beaudette, G. Boldrini, P. Busson, C. Charlot, M. Chiusi, T.D. Cuisset, O. Davignon, A. De Wit, T. Debnath, I.T. Ehle, B.A. Fontana Santos Alves, S. Ghosh, A. Gilbert, R. Granier de Cassagnac, L. Kalipoliti, M. Manoni, M. Nguyen, S. Obraztsov, C. Ochando, R. Salerno, J.B. Sauvan, Y. Sirois, G. Sokmen, L. Urda Gómez, A. Zabi, A. Zghiche

**Université de Strasbourg, CNRS, IPHC UMR 7178, Strasbourg, France**
J.-L. Agram[21], J. Andrea, D. Bloch, J.-M. Brom, E.C. Chabert, C. Collard,

G. Coulon, S. Falke, U. Goerlach, R. Haeberle, A.-C. Le Bihan, M. Meena, O. Poncet, G. Saha, P. Vaucelle

**Centre de Calcul de l'Institut National de Physique Nucleaire et de Physique des Particules, CNRS/IN2P3, Villeurbanne, France**
A. Di Florio

**Institut de Physique des 2 Infinis de Lyon (IP2I ), Villeurbanne, France**
D. Amram, S. Beauceron, B. Blancon, G. Boudoul, N. Chanon, D. Contardo, P. Depasse, H. El Mamouni, J. Fay, S. Gascon, M. Gouzevitch, C. Greenberg, G. Grenier, B. Ille, E. Jourd'huy, I.B. Laktineh, M. Lethuillier, B. Massoteau, L. Mirabito, A. Purohit, M. Vander Donckt, J. Xiao

**Georgian Technical University, Tbilisi, Georgia**
I. Lomidze, T. Toriashvili[22], Z. Tsamalaidze[23]

**RWTH Aachen University, I. Physikalisches Institut, Aachen, Germany**
V. Botta, S. Consuegra Rodríguez, L. Feld, K. Klein, M. Lipinski, D. Meuser, P. Nattland, V. Oppenländer, A. Pauls, D. Pérez Adán, N. Röwert, M. Teroerde

**RWTH Aachen University, III. Physikalisches Institut A, Aachen, Germany**
C. Daumann, S. Diekmann, A. Dodonova, N. Eich, D. Eliseev, F. Engelke, J. Erdmann, M. Erdmann, B. Fischer, T. Hebbeker, K. Hoepfner, F. Ivone, A. Jung, N. Kumar, M.y. Lee, F. Mausolf, M. Merschmeyer, A. Meyer, F. Nowotny, A. Pozdnyakov, W. Redjeb, H. Reithler, U. Sarkar, V. Sarkisovi, A. Schmidt, C. Seth, A. Sharma, J.L. Spah, V. Vaulin, S. Zaleski

**RWTH Aachen University, III. Physikalisches Institut B, Aachen, Germany**
M.R. Beckers, C. Dziwok, G. Flügge, N. Hoeflich, T. Kress, A. Nowack, O. Pooth, A. Stahl, A. Zotz

**Deutsches Elektronen-Synchrotron, Hamburg, Germany**
H. Aarup Petersen, A. Abel, M. Aldaya Martin, J. Alimena, S. Amoroso, Y. An, I. Andreev, J. Bach, S. Baxter, M. Bayatmakou, H. Becerril Gonzalez, O. Behnke, A. Belvedere, F. Blekman[24], K. Borras[25], A. Campbell, S. Chatterjee, L.X. Coll Saravia, G. Eckerlin, D. Eckstein, E. Gallo[24], A. Geiser, V. Guglielmi, M. Guthoff, A. Hinzmann, L. Jeppe, M. Kasemann, C. Kleinwort, R. Kogler, M. Komm, D. Krücker, W. Lange, D. Leyva Pernia, K.-Y. Lin, K. Lipka[26], W. Lohmann[27], J. Malvaso, R. Mankel, I.-A. Melzer-Pellmann, M. Mendizabal Morentin, A.B. Meyer, G. Milella, K. Moral Figueroa, A. Mussgiller, L.P. Nair, J. Niedziela, A. Nürnberg, J. Park, E. Ranken, A. Raspereza, D. Rastorguev, L. Rygaard, M. Scham[28,25], S. Schnake[25], P. Schütze, C. Schwanenberger[24], D. Selivanova, K. Sharko, M. Shchedrolosiev, D. Stafford, M. Torkian, F. Vazzoler, A. Ventura Barroso, R. Walsh, D. Wang, Q. Wang, K. Wichmann, L. Wiens[25], C. Wissing, Y. Yang, S. Zakharov, A. Zimermmane Castro Santos

**University of Hamburg, Hamburg, Germany**
A.R. Alves Andrade, M. Antonello, S. Bollweg, M. Bonanomi, K. El Morabit, Y. Fischer, M. Frahm, E. Garutti, A. Grohsjean, A.A. Guvenli, J. Haller, D. Hundhausen, G. Kasieczka, P. Keicher, R. Klanner, W. Korcari, T. Kramer, C.c. Kuo, F. Labe, J. Lange, A. Lobanov, L. Moureaux, A. Nigamova, K. Nikolopoulos, A. Paasch, K.J. Pena Rodriguez, N. Prouvost, T. Quadfasel, B. Raciti, M. Rieger, D. Savoiu, P. Schleper, M. Schröder, J. Schwandt,

M. Sommerhalder, H. Stadie, G. Steinbrück, R. Ward, B. Wiederspan, M. Wolf

**Karlsruher Institut fuer Technologie, Karlsruhe, Germany**
S. Brommer, E. Butz, Y.M. Chen, T. Chwalek, A. Dierlamm, G.G. Dincer, U. Elicabuk, N. Faltermann, M. Giffels, A. Gottmann, F. Hartmann[29], M. Horzela, F. Hummer, U. Husemann, J. Kieseler, M. Klute, R. Kunnilan Muhammed Rafeek, O. Lavoryk, J.M. Lawhorn, A. Lintuluoto, S. Maier, M. Mormile, Th. Müller, E. Pfeffer, M. Presilla, G. Quast, K. Rabbertz, B. Regnery, R. Schmieder, N. Shadskiy, I. Shvetsov, H.J. Simonis, L. Sowa, L. Stockmeier, K. Tauqeer, M. Toms, B. Topko, N. Trevisani, C. Verstege, T. Voigtländer, R.F. Von Cube, J. Von Den Driesch, M. Wassmer, R. Wolf, W.D. Zeuner, X. Zuo

**Institute of Nuclear and Particle Physics (INPP), NCSR Demokritos, Aghia Paraskevi, Greece**
G. Anagnostou, G. Daskalakis, A. Kyriakis

**National and Kapodistrian University of Athens, Athens, Greece**
P. Katris, G. Melachroinos, Z. Painesis, I. Paraskevas, N. Plastiras, N. Saoulidou, K. Theofilatos, E. Tziaferi, E. Tzovara, K. Vellidis, I. Zisopoulos

**National Technical University of Athens, Athens, Greece**
T. Chatzistavrou, G. Karapostoli, K. Kousouris, E. Siamarkou, G. Tsipolitis

**University of Ioánnina, Ioánnina, Greece**
I. Bestintzanos, I. Evangelou, C. Foudas, P. Katsoulis, P. Kokkas, P.G. Kosmoglou Kioseoglou, N. Manthos, I. Papadopoulos, J. Strologas

**HUN-REN Wigner Research Centre for Physics, Budapest, Hungary**
D. Druzhkin, C. Hajdu, D. Horvath[30,31], K. Márton, A.J. Rádl[32], F. Sikler, V. Veszpremi

**MTA-ELTE Lendület CMS Particle and Nuclear Physics Group, Eötvös Loránd University, Budapest, Hungary**
M. Csanád, K. Farkas, A. Fehérkuti[33], M.M.A. Gadallah[34], Á. Kadlecsik, M. León Coello, G. Pásztor, G.I. Veres

**Faculty of Informatics, University of Debrecen, Debrecen, Hungary**
B. Ujvari, G. Zilizi

**HUN-REN ATOMKI - Institute of Nuclear Research, Debrecen, Hungary**
G. Bencze, S. Czellar, J. Molnar, Z. Szillasi

**Karoly Robert Campus, MATE Institute of Technology, Gyongyos, Hungary**
T. Csorgo[33], F. Nemes[33], T. Novak, I. Szanyi[35]

**Panjab University, Chandigarh, India**
S. Bansal, S.B. Beri, V. Bhatnagar, G. Chaudhary, S. Chauhan, N. Dhingra[36], A. Kaur, A. Kaur, H. Kaur, M. Kaur, S. Kumar, T. Sheokand, J.B. Singh, A. Singla

**University of Delhi, Delhi, India**
A. Bhardwaj, A. Chhetri, B.C. Choudhary, A. Kumar, A. Kumar, M. Naimuddin, S. Phor, K. Ranjan, M.K. Saini

**University of Hyderabad, Hyderabad, India**
S. Acharya[37], B. Gomber[37], B. Sahu[37]

**Indian Institute of Technology Kanpur, Kanpur, India**
S. Mukherjee

**Saha Institute of Nuclear Physics, HBNI, Kolkata, India**
S. Baradia, S. Bhattacharya, S. Das Gupta, S. Dutta, S. Dutta, S. Sarkar

**Indian Institute of Technology Madras, Madras, India**
M.M. Ameen, P.K. Behera, S. Chatterjee, G. Dash, A. Dattamunsi, P. Jana, P. Kalbhor, S. Kamble, J.R. Komaragiri[38], T. Mishra, P.R. Pujahari, A.K. Sikdar, R.K. Singh, P. Verma, S. Verma, A. Vijay

**IISER Mohali, India, Mohali, India**
B.K. Sirasva

**Tata Institute of Fundamental Research-A, Mumbai, India**
L. Bhatt, S. Dugad, G.B. Mohanty, M. Shelake, P. Suryadevara

**Tata Institute of Fundamental Research-B, Mumbai, India**
A. Bala, S. Banerjee, S. Barman[39], R.M. Chatterjee, M. Guchait, Sh. Jain, A. Jaiswal, B.M. Joshi, S. Kumar, M. Maity[39], G. Majumder, K. Mazumdar, S. Parolia, R. Saxena, A. Thachayath

**National Institute of Science Education and Research, An OCC of Homi Bhabha National Institute, Bhubaneswar, Odisha, India**
S. Bahinipati[40], D. Maity[41], P. Mal, K. Naskar[41], A. Nayak[41], S. Nayak, K. Pal, R. Raturi, P. Sadangi, S.K. Swain, S. Varghese[41], D. Vats[41]

**Indian Institute of Science Education and Research (IISER), Pune, India**
A. Alpana, S. Dube, P. Hazarika, B. Kansal, A. Laha, R. Sharma, S. Sharma, K.Y. Vaish

**Indian Institute of Technology Hyderabad, Telangana, India**
S. Ghosh

**Isfahan University of Technology, Isfahan, Iran**
H. Bakhshiansohi[42], A. Jafari[43], V. Sedighzadeh Dalavi, M. Zeinali[44]

**Institute for Research in Fundamental Sciences (IPM), Tehran, Iran**
S. Bashiri, S. Chenarani[45], S.M. Etesami, Y. Hosseini, M. Khakzad, E. Khazaie, M. Mohammadi Najafabadi, S. Tizchang[46]

**University College Dublin, Dublin, Ireland**
M. Felcini, M. Grunewald

**INFN Sezione di Bari[a], Università di Bari[b], Politecnico di Bari[c], Bari, Italy**
M. Abbrescia[a,b], M. Barbieri[a,b], M. Buonsante[a,b], A. Colaleo[a,b], D. Creanza[a,c], N. De Filippis[a,c], M. De Palma[a,b], W. Elmetenawee[a,b,17], N. Ferrara[a,c], L. Fiore[a], L. Longo[a], M. Louka[a,b], G. Maggi[a,c], M. Maggi[a], I. Margjeka[a], V. Mastrapasqua[a,b], S. My[a,b], F. Nenna[a,b], S. Nuzzo[a,b], A. Pellecchia[a,b], A. Pompili[a,b], G. Pugliese[a,c], R. Radogna[a,b], D. Ramos[a], A. Ranieri[a], L. Silvestris[a], F.M. Simone[a,c], Ü. Sözbilir[a], A. Stamerra[a,b], D. Troiano[a,b], R. Venditti[a,b], P. Verwilligen[a], A. Zaza[a,b]

**INFN Sezione di Bologna[a], Università di Bologna[b], Bologna, Italy**
G. Abbiendi[a], C. Battilana[a,b], D. Bonacorsi[a,b], P. Capiluppi[a,b], F.R. Cavallo[a], M. Cuffiani[a,b], G.M. Dallavalle[a], T. Diotalevi[a,b], F. Fabbri[a], A. Fanfani[a,b],

D. Fasanella[a], P. Giacomelli[a], C. Grandi[a], L. Guiducci[a,b], S. Lo Meo[a,47], M. Lorusso[a,b], L. Lunerti[a], G. Masetti[a], F.L. Navarria[a,b], G. Paggi[a,b], A. Perrotta[a], F. Primavera[a,b], A.M. Rossi[a,b], S. Rossi Tisbeni[a,b], T. Rovelli[a,b], G.P. Siroli[a,b]

**INFN Sezione di Catania[a], Università di Catania[b], Catania, Italy**
S. Costa[a,b,48], A. Di Mattia[a], A. Lapertosa[a], R. Potenza[a,b], A. Tricomi[a,b,48]

**INFN Sezione di Firenze[a], Università di Firenze[b], Firenze, Italy**
J. Altork[a,b], P. Assiouras[a], G. Barbagli[a], G. Bardelli[a], M. Bartolini[a,b], A. Calandri[a,b], B. Camaiani[a,b], A. Cassese[a], R. Ceccarelli[a], V. Ciulli[a,b], C. Civinini[a], R. D'Alessandro[a,b], L. Damenti[a,b], E. Focardi[a,b], T. Kello[a], G. Latino[a,b], P. Lenzi[a,b], M. Lizzo[a], M. Meschini[a], S. Paoletti[a], A. Papanastassiou[a,b], G. Sguazzoni[a], L. Viliani[a]

**INFN Laboratori Nazionali di Frascati, Frascati, Italy**
L. Benussi, S. Bianco, S. Meola[49], D. Piccolo

**INFN Sezione di Genova[a], Università di Genova[b], Genova, Italy**
M. Alves Gallo Pereira[a], F. Ferro[a], E. Robutti[a], S. Tosi[a,b]

**INFN Sezione di Milano-Bicocca[a], Università di Milano-Bicocca[b], Milano, Italy**
A. Benaglia[a], F. Brivio[a], V. Camagni[a,b], F. Cetorelli[a,b], F. De Guio[a,b], M.E. Dinardo[a,b], P. Dini[a], S. Gennai[a], R. Gerosa[a,b], A. Ghezzi[a,b], P. Govoni[a,b], L. Guzzi[a], M.R. Kim[a], G. Lavizzari[a,b], M.T. Lucchini[a,b], M. Malberti[a], S. Malvezzi[a], A. Massironi[a], D. Menasce[a], L. Moroni[a], M. Paganoni[a,b], S. Palluotto[a,b], D. Pedrini[a], A. Perego[a,b], G. Pizzati[a,b], S. Ragazzi[a,b], T. Tabarelli de Fatis[a,b]

**INFN Sezione di Napoli[a], Università di Napoli 'Federico II'[b], Napoli, Italy; Università della Basilicata[c], Potenza, Italy; Scuola Superiore Meridionale (SSM)[d], Napoli, Italy**
S. Buontempo[a], C. Di Fraia[a,b], F. Fabozzi[a,c], L. Favilla[a,d], A.O.M. Iorio[a,b], L. Lista[a,b,50], P. Paolucci[a,29], B. Rossi[a]

**INFN Sezione di Padova[a], Università di Padova[b], Padova, Italy; Universita degli Studi di Cagliari[c], Cagliari, Italy**
P. Azzi[a], N. Bacchetta[a,51], D. Bisello[a,b], P. Bortignon[a,c], G. Bortolato[a,b], A.C.M. Bulla[a,c], R. Carlin[a,b], T. Dorigo[a,52], F. Gasparini[a,b], S. Giorgetti[a], E. Lusiani[a], M. Margoni[a,b], A.T. Meneguzzo[a,b], J. Pazzini[a,b], P. Ronchese[a,b], R. Rossin[a,b], M. Sgaravatto[a], F. Simonetto[a,b], M. Tosi[a,b], A. Triossi[a,b], S. Ventura[a], M. Zanetti[a,b], P. Zotto[a,b], A. Zucchetta[a,b], G. Zumerle[a,b]

**INFN Sezione di Pavia[a], Università di Pavia[b], Pavia, Italy**
A. Braghieri[a], S. Calzaferri[a], P. Montagna[a,b], M. Pelliccioni[a], V. Re[a], C. Riccardi[a,b], P. Salvini[a], I. Vai[a,b], P. Vitulo[a,b]

**INFN Sezione di Perugia[a], Università di Perugia[b], Perugia, Italy**
S. Ajmal[a,b], M.E. Ascioti[a,b], G.M. Bilei[a], C. Carrivale[a,b], D. Ciangottini[a,b], L. Della Penna[a,b], L. Fanò[a,b], V. Mariani[a,b], M. Menichelli[a], F. Moscatelli[a,53], A. Rossi[a,b], A. Santocchia[a,b], D. Spiga[a], T. Tedeschi[a,b]

**INFN Sezione di Pisa[a], Università di Pisa[b], Scuola Normale Superiore di Pisa[c], Pisa, Italy; Università di Siena[d], Siena, Italy**
C. Aimè[a,b], C.A. Alexe[a,c], P. Asenov[a,b], P. Azzurri[a], G. Bagliesi[a],

R. Bhattacharya[a], L. Bianchini[a,b], T. Boccali[a], E. Bossini[a], D. Bruschini[a,c], L. Calligaris[a,b], R. Castaldi[a], F. Cattafesta[a,c], M.A. Ciocci[a,d], M. Cipriani[a,b], R. Dell'Orso[a], S. Donato[a,b], R. Forti[a,b], A. Giassi[a], F. Ligabue[a,c], A.C. Marini[a,b], D. Matos Figueiredo[a], A. Messineo[a,b], S. Mishra[a], V.K. Muraleedharan Nair Bindhu[a,b], S. Nandan[a], F. Palla[a], M. Riggirello[a,c], A. Rizzi[a,b], G. Rolandi[a,c], S. Roy Chowdhury[a,54], T. Sarkar[a], A. Scribano[a], P. Solanki[a,b], P. Spagnolo[a], F. Tenchini[a,b], R. Tenchini[a], G. Tonelli[a,b], N. Turini[a,d], F. Vaselli[a,c], A. Venturi[a], P.G. Verdini[a]

**INFN Sezione di Roma[a], Sapienza Università di Roma[b], Roma, Italy**
P. Akrap[a,b], C. Basile[a,b], S.C. Behera[a], F. Cavallari[a], L. Cunqueiro Mendez[a,b], F. De Riggi[a,b], D. Del Re[a,b], E. Di Marco[a], M. Diemoz[a], F. Errico[a], L. Frosina[a,b], R. Gargiulo[a,b], B. Harikrishnan[a,b], F. Lombardi[a,b], E. Longo[a,b], L. Martikainen[a,b], J. Mijuskovic[a,b], G. Organtini[a,b], N. Palmeri[a,b], R. Paramatti[a,b], S. Rahatlou[a,b], C. Rovelli[a], F. Santanastasio[a,b], L. Soffi[a], V. Vladimirov[a,b]

**INFN Sezione di Torino[a], Università di Torino[b], Torino, Italy; Università del Piemonte Orientale[c], Novara, Italy**
N. Amapane[a,b], R. Arcidiacono[a,c], S. Argiro[a,b], M. Arneodo[a,c], N. Bartosik[a,c], R. Bellan[a,b], A. Bellora[a,b], C. Biino[a], C. Borca[a,b], N. Cartiglia[a], M. Costa[a,b], R. Covarelli[a,b], N. Demaria[a], L. Finco[a], M. Grippo[a,b], B. Kiani[a,b], L. Lanteri[a,b], F. Legger[a], F. Luongo[a,b], C. Mariotti[a], S. Maselli[a], A. Mecca[a,b], L. Menzio[a,b], P. Meridiani[a], E. Migliore[a,b], M. Monteno[a], M.M. Obertino[a,b], G. Ortona[a], L. Pacher[a,b], N. Pastrone[a], M. Ruspa[a,c], F. Siviero[a,b], V. Sola[a,b], A. Solano[a,b], A. Staiano[a], C. Tarricone[a,b], D. Trocino[a], G. Umoret[a,b], E. Vlasov[a,b], R. White[a,b]

**INFN Sezione di Trieste[a], Università di Trieste[b], Trieste, Italy**
J. Babbar[a,b], S. Belforte[a], V. Candelise[a,b], M. Casarsa[a], F. Cossutti[a], K. De Leo[a], G. Della Ricca[a,b], R. Delli Gatti[a,b]

**Kyungpook National University, Daegu, Korea**
S. Dogra, J. Hong, J. Kim, T. Kim, D. Lee, H. Lee, J. Lee, S.W. Lee, C.S. Moon, Y.D. Oh, S. Sekmen, B. Tae, Y.C. Yang

**Department of Mathematics and Physics - GWNU, Gangneung, Korea**
M.S. Kim

**Chonnam National University, Institute for Universe and Elementary Particles, Kwangju, Korea**
G. Bak, P. Gwak, H. Kim, D.H. Moon, J. Seo

**Hanyang University, Seoul, Korea**
E. Asilar, F. Carnevali, J. Choi[55], T.J. Kim, Y. Ryou

**Korea University, Seoul, Korea**
S. Ha, S. Han, B. Hong, J. Kim, K. Lee, K.S. Lee, S. Lee, J. Yoo

**Kyung Hee University, Department of Physics, Seoul, Korea**
J. Goh, J. Shin, S. Yang

**Sejong University, Seoul, Korea**
Y. Kang, H. S. Kim, Y. Kim, S. Lee

**Seoul National University, Seoul, Korea**
J. Almond, J.H. Bhyun, J. Choi, J. Choi, W. Jun, H. Kim, J. Kim, T. Kim, Y. Kim,

Y.W. Kim, S. Ko, H. Lee, J. Lee, J. Lee, B.H. Oh, S.B. Oh, J. Shin, U.K. Yang, I. Yoon

**University of Seoul, Seoul, Korea**
W. Jang, D.Y. Kang, D. Kim, S. Kim, B. Ko, J.S.H. Lee, Y. Lee, I.C. Park, Y. Roh, I.J. Watson

**Yonsei University, Department of Physics, Seoul, Korea**
G. Cho, K. Hwang, B. Kim, S. Kim, K. Lee, H.D. Yoo

**Sungkyunkwan University, Suwon, Korea**
M. Choi, Y. Lee, I. Yu

**College of Engineering and Technology, American University of the Middle East (AUM), Dasman, Kuwait**
T. Beyrouthy, Y. Gharbia

**Kuwait University - College of Science - Department of Physics, Safat, Kuwait**
F. Alazemi

**Riga Technical University, Riga, Latvia**
K. Dreimanis, O.M. Eberlins, A. Gaile, C. Munoz Diaz, D. Osite, G. Pikurs, R. Plese, A. Potrebko, M. Seidel, D. Sidiropoulos Kontos

**University of Latvia (LU), Riga, Latvia**
N.R. Strautnieks

**Vilnius University, Vilnius, Lithuania**
M. Ambrozas, A. Juodagalvis, S. Nargelas, A. Rinkevicius, G. Tamulaitis

**National Centre for Particle Physics, Universiti Malaya, Kuala Lumpur, Malaysia**
I. Yusuff[56], Z. Zolkapli

**Universidad de Sonora (UNISON), Hermosillo, Mexico**
J.F. Benitez, A. Castaneda Hernandez, A. Cota Rodriguez, L.E. Cuevas Picos, H.A. Encinas Acosta, L.G. Gallegos Maríñez, J.A. Murillo Quijada, L. Valencia Palomo

**Centro de Investigacion y de Estudios Avanzados del IPN, Mexico City, Mexico**
G. Ayala, H. Castilla-Valdez, H. Crotte Ledesma, R. Lopez-Fernandez, J. Mejia Guisao, R. Reyes-Almanza, A. Sánchez Hernández

**Universidad Iberoamericana, Mexico City, Mexico**
C. Oropeza Barrera, D.L. Ramirez Guadarrama, M. Ramírez García

**Benemerita Universidad Autonoma de Puebla, Puebla, Mexico**
I. Bautista, F.E. Neri Huerta, I. Pedraza, H.A. Salazar Ibarguen, C. Uribe Estrada

**University of Montenegro, Podgorica, Montenegro**
I. Bubanja, N. Raicevic

**University of Canterbury, Christchurch, New Zealand**
P.H. Butler

**National Centre for Physics, Quaid-I-Azam University, Islamabad, Pakistan**
A. Ahmad, M.I. Asghar, A. Awais, M.I.M. Awan, W.A. Khan

**AGH University of Krakow, Krakow, Poland**
V. Avati, L. Forthomme, L. Grzanka, M. Malawski, K. Piotrzkowski

**National Centre for Nuclear Research, Swierk, Poland**
M. Bluj, M. Górski, M. Kazana, M. Szleper, P. Zalewski

**Institute of Experimental Physics, Faculty of Physics, University of Warsaw, Warsaw, Poland**
K. Bunkowski, K. Doroba, A. Kalinowski, M. Konecki, J. Krolikowski, A. Muhammad

**Warsaw University of Technology, Warsaw, Poland**
P. Fokow, K. Pozniak, W. Zabolotny

**Laboratório de Instrumentação e Física Experimental de Partículas, Lisboa, Portugal**
M. Araujo, D. Bastos, C. Beirão Da Cruz E Silva, A. Boletti, M. Bozzo, T. Camporesi, G. Da Molin, M. Gallinaro, J. Hollar, N. Leonardo, G.B. Marozzo, A. Petrilli, M. Pisano, J. Seixas, J. Varela, J.W. Wulff

**Faculty of Physics, University of Belgrade, Belgrade, Serbia**
P. Adzic, L. Markovic, P. Milenovic, V. Milosevic

**VINCA Institute of Nuclear Sciences, University of Belgrade, Belgrade, Serbia**
D. Devetak, M. Dordevic, J. Milosevic, L. Nadderd, V. Rekovic, M. Stojanovic

**Centro de Investigaciones Energéticas Medioambientales y Tecnológicas (CIEMAT), Madrid, Spain**
M. Alcalde Martinez, J. Alcaraz Maestre, Cristina F. Bedoya, J.A. Brochero Cifuentes, Oliver M. Carretero, M. Cepeda, M. Cerrada, N. Colino, J. Cuchillo Ortega, B. De La Cruz, A. Delgado Peris, A. Escalante Del Valle, D. Fernández Del Val, J.P. Fernández Ramos, J. Flix, M.C. Fouz, M. Gonzalez Hernandez, O. Gonzalez Lopez, S. Goy Lopez, J.M. Hernandez, M.I. Josa, J. Llorente Merino, C. Martin Perez, E. Martin Viscasillas, D. Moran, C. M. Morcillo Perez, R. Paz Herrera, C. Perez Dengra, A. Pérez-Calero Yzquierdo, J. Puerta Pelayo, I. Redondo, J. Vazquez Escobar

**Universidad Autónoma de Madrid, Madrid, Spain**
J.F. de Trocóniz

**Universidad de Oviedo, Instituto Universitario de Ciencias y Tecnologías Espaciales de Asturias (ICTEA), Oviedo, Spain**
B. Alvarez Gonzalez, J. Ayllon Torresano, A. Cardini, J. Cuevas, J. Del Riego Badas, D. Estrada Acevedo, J. Fernandez Menendez, S. Folgueras, I. Gonzalez Caballero, P. Leguina, M. Obeso Menendez, E. Palencia Cortezon, J. Prado Pico, A. Soto Rodríguez, C. Vico Villalba, P. Vischia

**Instituto de Física de Cantabria (IFCA), CSIC-Universidad de Cantabria, Santander, Spain**
S. Blanco Fernández, I.J. Cabrillo, A. Calderon, J. Duarte Campderros, M. Fernandez, G. Gomez, C. Lasaosa García, R. Lopez Ruiz, C. Martinez Rivero, P. Martinez Ruiz del Arbol, F. Matorras, P. Matorras Cuevas, E. Navarrete Ramos, J. Piedra Gomez, C. Quintana San Emeterio, L. Scodellaro, I. Vila, R. Vilar Cortabitarte, J.M. Vizan Garcia

**University of Colombo, Colombo, Sri Lanka**
B. Kailasapathy[57], D.D.C. Wickramarathna

**University of Ruhuna, Department of Physics, Matara, Sri Lanka**
W.G.D. Dharmaratna[58], K. Liyanage, N. Perera

**CERN, European Organization for Nuclear Research, Geneva, Switzerland**
D. Abbaneo, C. Amendola, R. Ardino, E. Auffray, J. Baechler, D. Barney, J. Bendavid, M. Bianco, A. Bocci, L. Borgonovi, C. Botta, A. Bragagnolo, C.E. Brown, C. Caillol, G. Cerminara, P. Connor, D. d'Enterria, A. Dabrowski, A. David, A. De Roeck, M.M. Defranchis, M. Deile, M. Dobson, P.J. Fernández Manteca, W. Funk, A. Gaddi, S. Giani, D. Gigi, K. Gill, F. Glege, M. Glowacki, A. Gruber, J. Hegeman, J.K. Heikkilä, R. Hofsaess, B. Huber, V. Innocente, T. James, P. Janot, O. Kaluzinska, O. Karacheban[27], G. Karathanasis, S. Laurila, P. Lecoq, C. Lourenço, A.-M. Lyon, M. Magherini, L. Malgeri, M. Mannelli, A. Mehta, F. Meijers, J.A. Merlin, S. Mersi, E. Meschi, M. Migliorini, F. Monti, F. Moortgat, M. Mulders, M. Musich, I. Neutelings, S. Orfanelli, F. Pantaleo, M. Pari, G. Petrucciani, A. Pfeiffer, M. Pierini, M. Pitt, H. Qu, D. Rabady, A. Reimers, B. Ribeiro Lopes, F. Riti, P. Rosado, M. Rovere, H. Sakulin, R. Salvatico, S. Sanchez Cruz, S. Scarfi, M. Selvaggi, A. Sharma, K. Shchelina, P. Silva, P. Sphicas[59], A.G. Stahl Leiton, A. Steen, S. Summers, D. Treille, P. Tropea, E. Vernazza, J. Wanczyk[60], J. Wang, S. Wuchterl, M. Zarucki, P. Zehetner, P. Zejdl, G. Zevi Della Porta

**PSI Center for Neutron and Muon Sciences, Villigen, Switzerland**
T. Bevilacqua[61], L. Caminada[61], W. Erdmann, R. Horisberger, Q. Ingram, H.C. Kaestli, D. Kotlinski, C. Lange, U. Langenegger, L. Noehte[61], T. Rohe, A. Samalan

**ETH Zurich - Institute for Particle Physics and Astrophysics (IPA), Zurich, Switzerland**
T.K. Aarrestad, M. Backhaus, G. Bonomelli, C. Cazzaniga, K. Datta, P. De Bryas Dexmiers D'archiacchiac[60], A. De Cosa, G. Dissertori, M. Dittmar, M. Donegà, F. Eble, K. Gedia, F. Glessgen, C. Grab, N. Härringer, T.G. Harte, W. Lustermann, M. Malucchi, R.A. Manzoni, M. Marchegiani, L. Marchese, A. Mascellani[60], F. Nessi-Tedaldi, F. Pauss, V. Perovic, B. Ristic, R. Seidita, J. Steggemann[60], A. Tarabini, D. Valsecchi, R. Wallny

**Universität Zürich, Zurich, Switzerland**
C. Amsler[62], P. Bärtschi, F. Bilandzija, M.F. Canelli, G. Celotto, K. Cormier, M. Huwiler, W. Jin, A. Jofrehei, B. Kilminster, T.H. Kwok, S. Leontsinis, V. Lukashenko, A. Macchiolo, F. Meng, M. Missiroli, J. Motta, P. Robmann, M. Senger, E. Shokr, F. Stäger, R. Tramontano, P. Viscone

**National Central University, Chung-Li, Taiwan**
D. Bhowmik, C.M. Kuo, P.K. Rout, S. Taj, P.C. Tiwari[38]

**National Taiwan University (NTU), Taipei, Taiwan**
L. Ceard, K.F. Chen, Z.g. Chen, A. De Iorio, W.-S. Hou, T.h. Hsu, Y.w. Kao, S. Karmakar, G. Kole, Y.y. Li, R.-S. Lu, E. Paganis, X.f. Su, J. Thomas-Wilsker, L.s. Tsai, D. Tsionou, H.y. Wu, E. Yazgan

**High Energy Physics Research Unit, Department of Physics, Faculty of Science, Chulalongkorn University, Bangkok, Thailand**
C. Asawatangtrakuldee, N. Srimanobhas

**Tunis El Manar University, Tunis, Tunisia**
Y. Maghrbi

**Çukurova University, Physics Department, Science and Art Faculty, Adana, Turkey**

D. Agyel, F. Dolek, I. Dumanoglu[63], Y. Guler[64], E. Gurpinar Guler[64], C. Isik, O. Kara, A. Kayis Topaksu, Y. Komurcu, G. Onengut, K. Ozdemir[65], B. Tali[66], U.G. Tok, E. Uslan, I.S. Zorbakir

**Middle East Technical University, Physics Department, Ankara, Turkey**
M. Yalvac[67]

**Bogazici University, Istanbul, Turkey**
B. Akgun, I.O. Atakisi[68], E. Gülmez, M. Kaya[69], O. Kaya[70], M.A. Sarkisla[71], S. Tekten[72]

**Istanbul Technical University, Istanbul, Turkey**
A. Cakir, K. Cankocak[63,73], S. Sen[74]

**Istanbul University, Istanbul, Turkey**
O. Aydilek[75], B. Hacisahinoglu, I. Hos[76], B. Kaynak, S. Ozkorucuklu, O. Potok, H. Sert, C. Simsek, C. Zorbilmez

**Yildiz Technical University, Istanbul, Turkey**
S. Cerci, C. Dozen[77], B. Isildak[78], E. Simsek, D. Sunar Cerci, T. Yetkin[77]

**Institute for Scintillation Materials of National Academy of Science of Ukraine, Kharkiv, Ukraine**
A. Boyaryntsev, O. Dadazhanova, B. Grynyov

**National Science Centre, Kharkiv Institute of Physics and Technology, Kharkiv, Ukraine**
L. Levchuk

**University of Bristol, Bristol, United Kingdom**
J.J. Brooke, A. Bundock, F. Bury, E. Clement, D. Cussans, D. Dharmender, H. Flacher, J. Goldstein, H.F. Heath, M.-L. Holmberg, L. Kreczko, S. Paramesvaran, L. Robertshaw, M.S. Sanjrani[42], J. Segal, V.J. Smith

**Rutherford Appleton Laboratory, Didcot, United Kingdom**
A.H. Ball, K.W. Bell, A. Belyaev[79], C. Brew, R.M. Brown, D.J.A. Cockerill, A. Elliot, K.V. Ellis, J. Gajownik, K. Harder, S. Harper, J. Linacre, K. Manolopoulos, M. Moallemi, D.M. Newbold, E. Olaiya, D. Petyt, T. Reis, A.R. Sahasransu, G. Salvi, T. Schuh, C.H. Shepherd-Themistocleous, I.R. Tomalin, K.C. Whalen, T. Williams

**Imperial College, London, United Kingdom**
I. Andreou, R. Bainbridge, P. Bloch, O. Buchmuller, C.A. Carrillo Montoya, D. Colling, J.S. Dancu, I. Das, P. Dauncey, G. Davies, M. Della Negra, S. Fayer, G. Fedi, G. Hall, H.R. Hoorani, A. Howard, G. Iles, C.R. Knight, P. Krueper, J. Langford, K.H. Law, J. León Holgado, E. Leutgeb, L. Lyons, A.-M. Magnan, B. Maier, S. Mallios, A. Mastronikolis, M. Mieskolainen, J. Nash[80], M. Pesaresi, P.B. Pradeep, B.C. Radburn-Smith, A. Richards, A. Rose, L. Russell, K. Savva, C. Seez, R. Shukla, A. Tapper, K. Uchida, G.P. Uttley, T. Virdee[29], M. Vojinovic, N. Wardle, D. Winterbottom

**Brunel University, Uxbridge, United Kingdom**
J.E. Cole, A. Khan, P. Kyberd, I.D. Reid

**Baylor University, Waco, Texas, USA**
S. Abdullin, A. Brinkerhoff, E. Collins, M.R. Darwish, J. Dittmann,

K. Hatakeyama, V. Hegde, J. Hiltbrand, B. McMaster, J. Samudio, S. Sawant, C. Sutantawibul, J. Wilson

**Bethel University, St. Paul, Minnesota, USA**
J.M. Hogan[81]

**Catholic University of America, Washington, DC, USA**
R. Bartek, A. Dominguez, S. Raj, A.E. Simsek, S.S. Yu

**The University of Alabama, Tuscaloosa, Alabama, USA**
B. Bam, A. Buchot Perraguin, S. Campbell, R. Chudasama, S.I. Cooper, C. Crovella, G. Fidalgo, S.V. Gleyzer, A. Khukhunaishvili, K. Matchev, E. Pearson, C.U. Perez, P. Rumerio[82], E. Usai, R. Yi

**Boston University, Boston, Massachusetts, USA**
S. Cholak, G. De Castro, Z. Demiragli, C. Erice, C. Fangmeier, C. Fernandez Madrazo, E. Fontanesi, J. Fulcher, F. Golf, S. Jeon, J. O'Cain, I. Reed, J. Rohlf, K. Salyer, D. Sperka, D. Spitzbart, I. Suarez, A. Tsatsos, E. Wurtz, A.G. Zecchinelli

**Brown University, Providence, Rhode Island, USA**
G. Barone, G. Benelli, D. Cutts, S. Ellis, L. Gouskos, M. Hadley, U. Heintz, K.W. Ho, T. Kwon, L. Lambrecht, G. Landsberg, K.T. Lau, J. Luo, S. Mondal, J. Roloff, T. Russell, S. Sagir[83], X. Shen, M. Stamenkovic, N. Venkatasubramanian

**University of California, Davis, Davis, California, USA**
S. Abbott, B. Barton, R. Breedon, H. Cai, M. Calderon De La Barca Sanchez, E. Cannaert, M. Chertok, M. Citron, J. Conway, P.T. Cox, R. Erbacher, O. Kukral, G. Mocellin, S. Ostrom, I. Salazar Segovia, J.S. Tafoya Vargas, W. Wei, S. Yoo

**University of California, Los Angeles, California, USA**
K. Adamidis, M. Bachtis, D. Campos, R. Cousins, A. Datta, G. Flores Avila, J. Hauser, M. Ignatenko, M.A. Iqbal, T. Lam, Y.f. Lo, E. Manca, A. Nunez Del Prado, D. Saltzberg, V. Valuev

**University of California, Riverside, Riverside, California, USA**
R. Clare, J.W. Gary, G. Hanson

**University of California, San Diego, La Jolla, California, USA**
A. Aportela, A. Arora, J.G. Branson, S. Cittolin, S. Cooperstein, B. D'Anzi, D. Diaz, J. Duarte, L. Giannini, Y. Gu, J. Guiang, V. Krutelyov, R. Lee, J. Letts, H. Li, M. Masciovecchio, F. Mokhtar, S. Mukherjee, M. Pieri, D. Primosch, M. Quinnan, V. Sharma, M. Tadel, E. Vourliotis, F. Würthwein, A. Yagil, Z. Zhao

**University of California, Santa Barbara - Department of Physics, Santa Barbara, California, USA**
A. Barzdukas, L. Brennan, C. Campagnari, S. Carron Montero[84], K. Downham, C. Grieco, M.M. Hussain, J. Incandela, M.W.K. Lai, A.J. Li, P. Masterson, J. Richman, S.N. Santpur, U. Sarica, R. Schmitz, F. Setti, J. Sheplock, D. Stuart, T.Á. Vámi, X. Yan, D. Zhang

**California Institute of Technology, Pasadena, California, USA**
A. Albert, S. Bhattacharya, A. Bornheim, O. Cerri, R. Kansal, J. Mao, H.B. Newman, G. Reales Gutiérrez, T. Sievert, M. Spiropulu, J.R. Vlimant, R.A. Wynne, S. Xie

**Carnegie Mellon University, Pittsburgh, Pennsylvania, USA**
J. Alison, S. An, M. Cremonesi, V. Dutta, E.Y. Ertorer, T. Ferguson, T.A. Gómez Espinosa, A. Harilal, A. Kallil Tharayil, M. Kanemura, C. Liu, P. Meiring, T. Mudholkar, S. Murthy, P. Palit, K. Park, M. Paulini, A. Roberts, A. Sanchez, W. Terrill

**University of Colorado Boulder, Boulder, Colorado, USA**
J.P. Cumalat, W.T. Ford, A. Hart, A. Hassani, S. Kwan, J. Pearkes, C. Savard, N. Schonbeck, K. Stenson, K.A. Ulmer, S.R. Wagner, N. Zipper, D. Zuolo

**Cornell University, Ithaca, New York, USA**
J. Alexander, X. Chen, J. Dickinson, A. Duquette, J. Fan, X. Fan, J. Grassi, S. Hogan, P. Kotamnives, J. Monroy, G. Niendorf, M. Oshiro, J.R. Patterson, A. Ryd, J. Thom, P. Wittich, R. Zou, L. Zygala

**Fermi National Accelerator Laboratory, Batavia, Illinois, USA**
M. Albrow, M. Alyari, O. Amram, G. Apollinari, A. Apresyan, L.A.T. Bauerdick, D. Berry, J. Berryhill, P.C. Bhat, K. Burkett, J.N. Butler, A. Canepa, G.B. Cerati, H.W.K. Cheung, F. Chlebana, C. Cosby, G. Cummings, I. Dutta, V.D. Elvira, J. Freeman, A. Gandrakota, Z. Gecse, L. Gray, D. Green, A. Grummer, S. Grünendahl, D. Guerrero, O. Gutsche, R.M. Harris, T.C. Herwig, J. Hirschauer, B. Jayatilaka, S. Jindariani, M. Johnson, U. Joshi, T. Klijnsma, B. Klima, K.H.M. Kwok, S. Lammel, C. Lee, D. Lincoln, R. Lipton, T. Liu, K. Maeshima, D. Mason, P. McBride, P. Merkel, S. Mrenna, S. Nahn, J. Ngadiuba, D. Noonan, S. Norberg, V. Papadimitriou, N. Pastika, K. Pedro, C. Pena[85], C.E. Perez Lara, F. Ravera, A. Reinsvold Hall[86], L. Ristori, M. Safdari, E. Sexton-Kennedy, N. Smith, A. Soha, L. Spiegel, S. Stoynev, J. Strait, L. Taylor, S. Tkaczyk, N.V. Tran, L. Uplegger, E.W. Vaandering, C. Wang, I. Zoi

**University of Florida, Gainesville, Florida, USA**
C. Aruta, P. Avery, D. Bourilkov, P. Chang, V. Cherepanov, R.D. Field, C. Huh, E. Koenig, M. Kolosova, J. Konigsberg, A. Korytov, N. Menendez, G. Mitselmakher, K. Mohrman, A. Muthirakalayil Madhu, N. Rawal, S. Rosenzweig, V. Sulimov, Y. Takahashi, J. Wang

**Florida State University, Tallahassee, Florida, USA**
T. Adams, A. Al Kadhim, A. Askew, S. Bower, R. Goff, R. Hashmi, R.S. Kim, T. Kolberg, G. Martinez, M. Mazza, H. Prosper, P.R. Prova, R. Yohay

**Florida Institute of Technology, Melbourne, Florida, USA**
B. Alsufyani, S. Butalla, S. Das, M. Hohlmann, M. Lavinsky, E. Yanes

**University of Illinois Chicago, Chicago, Illinois, USA**
M.R. Adams, N. Barnett, A. Baty, C. Bennett, R. Cavanaugh, R. Escobar Franco, O. Evdokimov, C.E. Gerber, H. Gupta, M. Hawksworth, A. Hingrajiya, D.J. Hofman, J.h. Lee, C. Mills, S. Nanda, G. Nigmatkulov, B. Ozek, T. Phan, D. Pilipovic, R. Pradhan, E. Prifti, P. Roy, T. Roy, N. Singh, M.B. Tonjes, N. Varelas, M.A. Wadud, J. Yoo

**The University of Iowa, Iowa City, Iowa, USA**
M. Alhusseini, D. Blend, K. Dilsiz[87], O.K. Köseyan, A. Mestvirishvili[88], O. Neogi, H. Ogul[89], Y. Onel, A. Penzo, C. Snyder, E. Tiras[90]

**Johns Hopkins University, Baltimore, Maryland, USA**

B. Blumenfeld, J. Davis, A.V. Gritsan, L. Kang, S. Kyriacou, P. Maksimovic, M. Roguljic, S. Sekhar, M.V. Srivastav, M. Swartz

**The University of Kansas, Lawrence, Kansas, USA**
A. Abreu, L.F. Alcerro Alcerro, J. Anguiano, S. Arteaga Escatel, P. Baringer, A. Bean, Z. Flowers, D. Grove, J. King, G. Krintiras, M. Lazarovits, C. Le Mahieu, J. Marquez, M. Murray, M. Nickel, S. Popescu[91], C. Rogan, C. Royon, S. Rudrabhatla, S. Sanders, C. Smith, G. Wilson

**Kansas State University, Manhattan, Kansas, USA**
B. Allmond, N. Islam, A. Ivanov, K. Kaadze, Y. Maravin, J. Natoli, G.G. Reddy, D. Roy, G. Sorrentino

**University of Maryland, College Park, Maryland, USA**
A. Baden, A. Belloni, J. Bistany-riebman, S.C. Eno, N.J. Hadley, S. Jabeen, R.G. Kellogg, T. Koeth, B. Kronheim, S. Lascio, P. Major, A.C. Mignerey, C. Palmer, C. Papageorgakis, M.M. Paranjpe, E. Popova[92], A. Shevelev, L. Zhang

**Massachusetts Institute of Technology, Cambridge, Massachusetts, USA**
C. Baldenegro Barrera, H. Bossi, S. Bright-Thonney, I.A. Cali, Y.c. Chen, P.c. Chou, M. D'Alfonso, J. Eysermans, C. Freer, G. Gomez-Ceballos, M. Goncharov, G. Grosso, P. Harris, D. Hoang, G.M. Innocenti, D. Kovalskyi, J. Krupa, L. Lavezzo, Y.-J. Lee, K. Long, C. Mcginn, A. Novak, M.I. Park, C. Paus, C. Reissel, C. Roland, G. Roland, S. Rothman, T.a. Sheng, G.S.F. Stephans, D. Walter, Z. Wang, B. Wyslouch, T. J. Yang

**University of Minnesota, Minneapolis, Minnesota, USA**
B. Crossman, W.J. Jackson, C. Kapsiak, M. Krohn, D. Mahon, J. Mans, B. Marzocchi, R. Rusack, O. Sancar, R. Saradhy, N. Strobbe

**University of Nebraska-Lincoln, Lincoln, Nebraska, USA**
K. Bloom, D.R. Claes, G. Haza, J. Hossain, C. Joo, I. Kravchenko, A. Rohilla, J.E. Siado, W. Tabb, A. Vagnerini, A. Wightman, F. Yan

**State University of New York at Buffalo, Buffalo, New York, USA**
H. Bandyopadhyay, L. Hay, H.w. Hsia, I. Iashvili, A. Kalogeropoulos, A. Kharchilava, A. Mandal, M. Morris, D. Nguyen, S. Rappoccio, H. Rejeb Sfar, A. Williams, P. Young, D. Yu

**Northeastern University, Boston, Massachusetts, USA**
G. Alverson, E. Barberis, J. Bonilla, B. Bylsma, M. Campana, J. Dervan, Y. Haddad, Y. Han, I. Israr, A. Krishna, M. Lu, N. Manganelli, R. Mccarthy, D.M. Morse, T. Orimoto, A. Parker, L. Skinnari, C.S. Thoreson, E. Tsai, D. Wood

**Northwestern University, Evanston, Illinois, USA**
S. Dittmer, K.A. Hahn, Y. Liu, M. Mcginnis, Y. Miao, D.G. Monk, M.H. Schmitt, A. Taliercio, M. Velasco, J. Wang

**University of Notre Dame, Notre Dame, Indiana, USA**
G. Agarwal, R. Band, R. Bucci, S. Castells, A. Das, A. Ehnis, R. Goldouzian, M. Hildreth, K. Hurtado Anampa, T. Ivanov, C. Jessop, A. Karneyeu, K. Lannon, J. Lawrence, N. Loukas, L. Lutton, J. Mariano, N. Marinelli, I. Mcalister, T. McCauley, C. Mcgrady, C. Moore, Y. Musienko[23], H. Nelson, M. Osherson,

A. Piccinelli, R. Ruchti, A. Townsend, Y. Wan, M. Wayne, H. Yockey

**The Ohio State University, Columbus, Ohio, USA**
A. Basnet, M. Carrigan, R. De Los Santos, L.S. Durkin, C. Hill, M. Joyce, M. Nunez Ornelas, D.A. Wenzl, B.L. Winer, B. R. Yates

**Princeton University, Princeton, New Jersey, USA**
H. Bouchamaoui, P. Das, G. Dezoort, P. Elmer, A. Frankenthal, M. Galli, B. Greenberg, N. Haubrich, K. Kennedy, G. Kopp, Y. Lai, D. Lange, A. Loeliger, D. Marlow, I. Ojalvo, J. Olsen, F. Simpson, D. Stickland, C. Tully

**University of Puerto Rico, Mayaguez, Puerto Rico, USA**
S. Malik, R. Sharma

**Purdue University, West Lafayette, Indiana, USA**
S. Chandra, R. Chawla, A. Gu, L. Gutay, M. Jones, A.W. Jung, D. Kondratyev, M. Liu, G. Negro, N. Neumeister, G. Paspalaki, S. Piperov, N.R. Saha, J.F. Schulte, F. Wang, A. Wildridge, W. Xie, Y. Yao, Y. Zhong

**Purdue University Northwest, Hammond, Indiana, USA**
N. Parashar, A. Pathak, E. Shumka

**Rice University, Houston, Texas, USA**
D. Acosta, A. Agrawal, C. Arbour, T. Carnahan, K.M. Ecklund, S. Freed, P. Gardner, F.J.M. Geurts, T. Huang, I. Krommydas, N. Lewis, W. Li, J. Lin, O. Miguel Colin, B.P. Padley, R. Redjimi, J. Rotter, M. Wulansatiti, E. Yigitbasi, Y. Zhang

**University of Rochester, Rochester, New York, USA**
O. Bessidskaia Bylund, A. Bodek, P. de Barbaro[†], R. Demina, A. Garcia-Bellido, H.S. Hare, O. Hindrichs, N. Parmar, P. Parygin[92], H. Seo, R. Taus

**Rutgers, The State University of New Jersey, Piscataway, New Jersey, USA**
B. Chiarito, J.P. Chou, S.V. Clark, S. Donnelly, D. Gadkari, Y. Gershtein, E. Halkiadakis, C. Houghton, D. Jaroslawski, A. Kobert, S. Konstantinou, I. Laflotte, A. Lath, J. Martins, M. Perez Prada, B. Rand, J. Reichert, P. Saha, S. Salur, S. Schnetzer, S. Somalwar, R. Stone, S.A. Thayil, S. Thomas, J. Vora

**University of Tennessee, Knoxville, Tennessee, USA**
D. Ally, A.G. Delannoy, S. Fiorendi, J. Harris, T. Holmes, A.R. Kanuganti, N. Karunarathna, J. Lawless, L. Lee, E. Nibigira, B. Skipworth, S. Spanier

**Texas A&M University, College Station, Texas, USA**
D. Aebi, M. Ahmad, T. Akhter, K. Androsov, A. Bolshov, O. Bouhali[93], A. Cagnotta, V. D'Amante, R. Eusebi, P. Flanagan, J. Gilmore, Y. Guo, T. Kamon, S. Luo, R. Mueller, A. Safonov

**Texas Tech University, Lubbock, Texas, USA**
N. Akchurin, J. Damgov, Y. Feng, N. Gogate, Y. Kazhykarim, K. Lamichhane, S.W. Lee, C. Madrid, A. Mankel, T. Peltola, I. Volobouev

**Vanderbilt University, Nashville, Tennessee, USA**
E. Appelt, Y. Chen, S. Greene, A. Gurrola, W. Johns, R. Kunnawalkam Elayavalli, A. Melo, D. Rathjens, F. Romeo, P. Sheldon, S. Tuo, J. Velkovska, J. Viinikainen, J. Zhang

**University of Virginia, Charlottesville, Virginia, USA**
B. Cardwell, H. Chung, B. Cox, J. Hakala, G. Hamilton Ilha Machado, R. Hirosky, M. Jose, A. Ledovskoy, C. Mantilla, C. Neu, C. Ramón Álvarez

**Wayne State University, Detroit, Michigan, USA**
S. Bhattacharya, P.E. Karchin

**University of Wisconsin - Madison, Madison, Wisconsin, USA**
A. Aravind, S. Banerjee, K. Black, T. Bose, E. Chavez, S. Dasu, P. Everaerts, C. Galloni, H. He, M. Herndon, A. Herve, C.K. Koraka, S. Lomte, R. Loveless, A. Mallampalli, A. Mohammadi, S. Mondal, T. Nelson, G. Parida, L. Pétré, D. Pinna, A. Savin, V. Shang, V. Sharma, W.H. Smith, D. Teague, H.F. Tsoi, W. Vetens, A. Warden

**Authors affiliated with an international laboratory covered by a cooperation agreement with CERN**
S. Afanasiev, V. Alexakhin, Yu. Andreev, T. Aushev, D. Budkouski, R. Chistov[94], M. Danilov[94], T. Dimova[94], A. Ershov[94], S. Gninenko, I. Gorbunov, A. Gribushin[94], A. Kamenev, V. Karjavine, M. Kirsanov, V. Klyukhin[94], O. Kodolova[95], V. Korenkov, I. Korsakov, A. Kozyrev[94], N. Krasnikov, A. Lanev, A. Malakhov, V. Matveev[94], A. Nikitenko[96,95], V. Palichik, V. Perelygin, S. Petrushanko[94], S. Polikarpov[94], O. Radchenko[94], M. Savina, V. Shalaev, S. Shmatov, S. Shulha, Y. Skovpen[94], K. Slizhevskiy, V. Smirnov, O. Teryaev, I. Tlisova[94], A. Toropin, N. Voytishin, B.S. Yuldashev[†97], A. Zarubin, I. Zhizhin

**Authors affiliated with an institute formerly covered by a cooperation agreement with CERN**
E. Boos, V. Bunichev, M. Dubinin[85], V. Savrin, A. Snigirev, L. Dudko, K. Ivanov, V. Kim[23], V. Murzin, V. Oreshkin, D. Sosnov

†: Deceased
[1]Also at Yerevan State University, Yerevan, Armenia
[2]Also at TU Wien, Vienna, Austria
[3]Also at Ghent University, Ghent, Belgium
[4]Also at Universidade do Estado do Rio de Janeiro, Rio de Janeiro, Brazil
[5]Also at FACAMP - Faculdades de Campinas, Sao Paulo, Brazil
[6]Also at Universidade Estadual de Campinas, Campinas, Brazil
[7]Also at Federal University of Rio Grande do Sul, Porto Alegre, Brazil
[8]Also at The University of the State of Amazonas, Manaus, Brazil
[9]Also at University of Chinese Academy of Sciences, Beijing, China
[10]Also at China Center of Advanced Science and Technology, Beijing, China
[11]Also at University of Chinese Academy of Sciences, Beijing, China
[12]Also at School of Physics, Zhengzhou University, Zhengzhou, China
[13]Now at Henan Normal University, Xinxiang, China
[14]Also at University of Shanghai for Science and Technology, Shanghai, China
[15]Now at The University of Iowa, Iowa City, Iowa, USA
[16]Also at Center for High Energy Physics, Peking University, Beijing, China
[17]Also at Helwan University, Cairo, Egypt
[18]Now at Zewail City of Science and Technology, Zewail, Egypt
[19]Also at British University in Egypt, Cairo, Egypt
[20]Also at Purdue University, West Lafayette, Indiana, USA
[21]Also at Université de Haute Alsace, Mulhouse, France
[22]Also at Tbilisi State University, Tbilisi, Georgia

[23]Also at an institute formerly covered by a cooperation agreement with CERN
[24]Also at University of Hamburg, Hamburg, Germany
[25]Also at RWTH Aachen University, III. Physikalisches Institut A, Aachen, Germany
[26]Also at Bergische University Wuppertal (BUW), Wuppertal, Germany
[27]Also at Brandenburg University of Technology, Cottbus, Germany
[28]Also at Forschungszentrum Jülich, Juelich, Germany
[29]Also at CERN, European Organization for Nuclear Research, Geneva, Switzerland
[30]Also at HUN-REN ATOMKI - Institute of Nuclear Research, Debrecen, Hungary
[31]Now at Universitatea Babes-Bolyai - Facultatea de Fizica, Cluj-Napoca, Romania
[32]Also at MTA-ELTE Lendület CMS Particle and Nuclear Physics Group, Eötvös Loránd University, Budapest, Hungary
[33]Also at HUN-REN Wigner Research Centre for Physics, Budapest, Hungary
[34]Also at Physics Department, Faculty of Science, Assiut University, Assiut, Egypt
[35]Also at The University of Kansas, Lawrence, Kansas, USA
[36]Also at Punjab Agricultural University, Ludhiana, India
[37]Also at University of Hyderabad, Hyderabad, India
[38]Also at Indian Institute of Science (IISc), Bangalore, India
[39]Also at University of Visva-Bharati, Santiniketan, India
[40]Also at IIT Bhubaneswar, Bhubaneswar, India
[41]Also at Institute of Physics, Bhubaneswar, India
[42]Also at Deutsches Elektronen-Synchrotron, Hamburg, Germany
[43]Also at Isfahan University of Technology, Isfahan, Iran
[44]Also at Sharif University of Technology, Tehran, Iran
[45]Also at Department of Physics, University of Science and Technology of Mazandaran, Behshahr, Iran
[46]Also at Department of Physics, Faculty of Science, Arak University, ARAK, Iran
[47]Also at Italian National Agency for New Technologies, Energy and Sustainable Economic Development, Bologna, Italy
[48]Also at Centro Siciliano di Fisica Nucleare e di Struttura Della Materia, Catania, Italy
[49]Also at Università degli Studi Guglielmo Marconi, Roma, Italy
[50]Also at Scuola Superiore Meridionale, Università di Napoli 'Federico II', Napoli, Italy
[51]Also at Fermi National Accelerator Laboratory, Batavia, Illinois, USA
[52]Also at Lulea University of Technology, Lulea, Sweden
[53]Also at Consiglio Nazionale delle Ricerche - Istituto Officina dei Materiali, Perugia, Italy
[54]Also at UPES - University of Petroleum and Energy Studies, Dehradun, India
[55]Also at Institut de Physique des 2 Infinis de Lyon (IP2I ), Villeurbanne, France
[56]Also at Department of Applied Physics, Faculty of Science and Technology, Universiti Kebangsaan Malaysia, Bangi, Malaysia
[57]Also at Trincomalee Campus, Eastern University, Sri Lanka, Nilaveli, Sri Lanka
[58]Also at Saegis Campus, Nugegoda, Sri Lanka
[59]Also at National and Kapodistrian University of Athens, Athens, Greece
[60]Also at Ecole Polytechnique Fédérale Lausanne, Lausanne, Switzerland
[61]Also at Universität Zürich, Zurich, Switzerland
[62]Also at Stefan Meyer Institute for Subatomic Physics, Vienna, Austria
[63]Also at Near East University, Research Center of Experimental Health Science, Mersin, Turkey
[64]Also at Konya Technical University, Konya, Turkey
[65]Also at Izmir Bakircay University, Izmir, Turkey
[66]Also at Adiyaman University, Adiyaman, Turkey

[67]Also at Bozok Universitetesi Rektörlügü, Yozgat, Turkey
[68]Also at Istanbul Sabahattin Zaim University, Istanbul, Turkey
[69]Also at Marmara University, Istanbul, Turkey
[70]Also at Milli Savunma University, Istanbul, Turkey
[71]Also at Informatics and Information Security Research Center, Gebze/Kocaeli, Turkey
[72]Also at Kafkas University, Kars, Turkey
[73]Now at Istanbul Okan University, Istanbul, Turkey
[74]Also at Hacettepe University, Ankara, Turkey
[75]Also at Erzincan Binali Yildirim University, Erzincan, Turkey
[76]Also at Istanbul University - Cerrahpasa, Faculty of Engineering, Istanbul, Turkey
[77]Also at Istinye University, Istanbul, Turkey
[78]Also at Yildiz Technical University, Istanbul, Turkey
[79]Also at School of Physics and Astronomy, University of Southampton, Southampton, United Kingdom
[80]Also at Monash University, Faculty of Science, Clayton, Australia
[81]Also at Bethel University, St. Paul, Minnesota, USA
[82]Also at Università di Torino, Torino, Italy
[83]Also at Karamanoğlu Mehmetbey University, Karaman, Turkey
[84]Also at California Lutheran University;, Thousand Oaks, California, USA
[85]Also at California Institute of Technology, Pasadena, California, USA
[86]Also at United States Naval Academy, Annapolis, Maryland, USA
[87]Also at Bingol University, Bingol, Turkey
[88]Also at Georgian Technical University, Tbilisi, Georgia
[89]Also at Sinop University, Sinop, Turkey
[90]Also at Erciyes University, Kayseri, Turkey
[91]Also at Horia Hulubei National Institute of Physics and Nuclear Engineering (IFIN-HH), Bucharest, Romania
[92]Now at another institute formerly covered by a cooperation agreement with CERN
[93]Also at Hamad Bin Khalifa University (HBKU), Doha, Qatar
[94]Also at another institute formerly covered by a cooperation agreement with CERN
[95]Also at Yerevan Physics Institute, Yerevan, Armenia
[96]Also at Imperial College, London, United Kingdom
[97]Also at Institute of Nuclear Physics of the Uzbekistan Academy of Sciences, Tashkent, Uzbekistan